Reconstruction of atmospheric CO_2 and climate of the middle Eocene based on fossil plants from the Messel Formation

Dissertation
zur Erlangung des Grades eines Doktors der Naturwissenschaften

der Geowissenschaftlichen Fakultät
der Eberhard-Karls-Universität Tübingen

vorgelegt von
Michaela Grein
aus Tübingen

2010

Tag der mündlichen Prüfung:	20. September 2010
Dekan:	Prof. Dr. Peter Grathwohl
1. Berichterstatter:	Priv.-Doz. Dr. Anita Roth-Nebelsick
2. Berichterstatter:	Priv.-Doz. Dr. Volker Wilde

In der Wissenschaft gleichen
wir alle nur den Kindern,
die am Rande des Wissens
hie und da einen Kiesel aufheben,
während sich der weite Ozean des Unbekannten
vor unseren Augen erstreckt.

Isaac Newton (1643-1727),
engl. Physiker, Mathematiker u. Astronom

Zusammenfassung

Der globale Klimawandel entwickelt sich zur größten Herausforderung für die Menschheit im 21. Jahrhundert. Will man abschätzen, wie sich zukünftige Klimaveränderungen auf die belebte Umwelt - und somit auch auf uns - auswirken könnten, muss man zunächst wissen, wie sich das Klima in der Erdgeschichte entwickelte und welche Konsequenzen sich daraus für die Paläoumwelt ergaben.

Der Einfluss von Treibhausgasen auf die Entwicklung des globalen Klimas erregt seit langem die Aufmerksamkeit von Forschern auf der ganzen Welt. Seit dem Beginn der Messungen am Mauna Loa (Hawaii/USA) im Jahr 1959 ist der atmosphärische Kohlenstoffdioxidgehalt (C_a) von etwa 316 auf etwa 387 ppm im Jahr 2009 gestiegen. Verschiedene Proxies und geochemische Modelle wurden angewandt um das Paläoklima und den paläo-C_a zu rekonstruieren. Diese liefern zum Teil widersprüchliche Ergebnisse. Da Kohlenstoffdioxid (CO_2) die Grundlage der pflanzlichen Fotosynthese ist, sind Pflanzen sehr gute Klimaindikatoren und liefern aussagekräftige Informationen zu Temperatur und C_a. Bei vielen Arten sinkt mit zunehmendem C_a die Anzahl der Stomata (Poren auf der Blattoberfläche, die dem Gasaustausch dienen), was diese zu einem weiteren vielversprechenden Proxy für die Paläoklimatologie macht.

In dieser Dissertation wird mit fossilem Pflanzenmaterial aus der mittleren Messelformation der Grube Messel nahe Darmstadt (Hessen, Deutschland) der C_a im mittleren Eozän rekonstruiert. Für diese Rekonstruktion wird ein neuartiger mechanistisch-theoretischer Ansatz angewandt, der die Reaktion der Stomatadichte auf den sich verändernden C_a quantitativ darstellt. Das Modell verbindet 1) den biochemischen Prozess der Fotosynthese von C_3-Pflanzen, 2) den physikalischen Prozess der Diffusion, i. e. die Bewegung der CO_2-Moleküle in das Blatt hinein und der Wassermoleküle aus dem Blatt heraus durch die geöffneten Stomata und 3) einen Optimierungsansatz, der sich mit dem Problem der Landpflanzen beschäftigt, ihre Stomata so einzustellen, dass sie maximale CO_2-Aufnahme für die Fotosynthese bei minimalem Wasserverlust durch stomatäre Transpiration erreichen. Diese drei Untermodelle beinhalten auch Daten zur Paläoumwelt (Temperatur, Wasserverfügbarkeit, Windgeschwindigkeit und Luftfeuchtigkeit), Blattanatomie und Stoma-Geometrie (wie Tiefe, Länge und Breite der Stomapore und Dicke des Assimilationsgewebes). Um Kurven für die Stomatadichte als Funktion von C_a berechnen zu können, müssen verschiedene biochemische Parameter von heute lebenden Verwandten übernommen werden. Die notwendigen Paläoklimadaten werden mittels Blattrandanalyse und Koexistenzansatz rekonstruiert. Um aussagekräftige Ergebnisse zu erzielen, werden für die C_a-Berechnungen zwei Pflanzenarten aus unterschiedlichen Familien ausgewählt.

Die Berechnungen zum Paläoklima der mitteleozänen Grube Messel deuten auf ein warm-feuchtes Klima hin mit einer durchschnittlichen Jahrestemperatur um 22 °C (bis $\sim$24 °C) und bis zu 2540 mm durchschnittlichem Jahresniederschlag ohne ausgedehnte Trockenperioden. Die mittlere relative Luftfeuchtigkeit war mit bis zu 77 % ebenfalls recht hoch. Die kombinierten Ergebnisse der beiden ausgewählten Pflanzenarten weisen auf einen atmosphärischen CO_2-Gehalt zwischen etwa 700 und 840 ppm im mittleren Eozän von Messel hin.

Summary

Global climate change has become one of the largest challenges for humans in the 21^{st} century. In order to estimate future climate change and possible consequences for the living environment - and thus for our own - we need a profound knowledge about climate changes in former times of Earth history and its consequences for the palaeoenvironment.

The influence of greenhouse gases on the development of global climate has attracted the attention of scientists all over the world. Since the beginning of carbon dioxide monitoring at Mauna Loa (Hawaii/USA) in 1959, the atmospheric carbon dioxide concentration (C_a) has increased from approximately 316 to about 387 ppm in 2009. Various proxies and geochemical models have been applied in order to reconstruct palaeoclimate and palaeo-C_a, partially providing conflicting results. Since carbon dioxide (CO_2) is the substrate of plant photosynthesis, plants are suitable climate indicators providing accurate information about temperature and C_a. In many species, the frequency of stomata (pores on the leaf surface used for gaseous exchange) decreases with increasing C_a and, thus, stomatal frequency is another promising proxy in palaeoclimatology.

In this dissertation, fossil plant material from the Middle Messel Formation excavated in the Messel Pit near Darmstadt (Hesse, Germany) is used to reconstruct C_a in the middle Eocene. For this reconstruction, a novel mechanistic-theoretical approach is applied providing a quantitative derivation of the stomatal density response to varying C_a. The model couples: 1) the biochemical process of C_3-photosynthesis, 2) the physical process of diffusion describing the movement of water molecules out of and carbon dioxide molecules into the leaf through opened stomata, and 3) an optimisation principle solving the problem of land plants to adjust their stomata in such a way that they reach maximum CO_2 uptake for photosynthesis at minimum water loss via stomatal transpiration. These three sub-models also include palaeoenvironmental data (temperature, water availability, wind velocity and atmospheric humidity), leaf anatomy and stoma geometry (such as depth, length and width of stomatal porus and thickness of assimilation tissue). In order to calculate curves of stomatal density as a function of C_a, various biochemical parameters have to be borrowed from extant representatives. The necessary palaeoclimate data are reconstructed using Leaf Margin Analysis and the Coexistence Approach. In order to obtain significant results, two species in different plant families are selected for C_a-calculations.

Palaeoclimate calculations for the middle Eocene Messel Pit indicate a warm and humid climate with a mean annual temperature probably around 22 °C (up to $\sim$24 °C), up to 2540 mm mean annual precipitation and the absence of extended periods of drought. Mean relative air humidity is reconstructed as rather high too, up to 77 %. The combined results of the two selected plant taxa indicate values for atmospheric CO_2 between approximately 700 and 840 ppm for the middle Eocene of Messel.

Ich versichere, dass ich bei der Anfertigung der vorliegenden Arbeit lediglich die angegebenen Hilfsmittel benutzt habe.

Tübingen, September 2010

This thesis is based on the following publications:

Konrad, W., Roth-Nebelsick, A., Grein, M. (2008). Modelling of stomatal density response to atmospheric CO_2. *Journal of Theoretical Biology* 253: 638-658.

Grein, M., Utescher, T., Wilde, V., Roth-Nebelsick, A.: Reconstruction of the middle Eocene climate of Messel using palaeobotanical data. *Neues Jahrbuch für Geologie und Paläontologie, Abhandlungen.* (accepted for publication)

Grein, M., Roth-Nebelsick, A., Wilde, V.: Carbon isotope composition of middle Eocene leaves. (submitted to *Palaeodiversity*)

Grein, M., Roth-Nebelsick, A., Konrad, W., Wilde, V., Utescher, T.: Reconstruction of atmospheric CO_2 during the middle Eocene by application of a gas exchange model to fossil plants. (submitted to *Geology*)

Contents

1 Introduction

1.1 Scope of the thesis

The global climate system consists of five components comprising the biosphere, the hydrosphere, the cryosphere, the atmosphere and the land surface. These components respond to numerous kinds of so-called external forcing such as plate tectonic activity, volcanism, changing orbital parameters, changing sun intensity and insolation quality. The most rapidly changing and unstable component in the interactive global climate system is the atmosphere. Its main components nitrogen (N_2), oxygen (O_2) and argon (Ar) hardly interact with incoming solar radiation and do not interact with the infrared radiation emitted by the Earth. In contrast, atmospheric trace gases have an essential influence on global climate. Among trace-gases, so-called greenhouse gases such as carbon dioxide (CO_2), methane (CH_4), nitrous oxide (N_2O), water vapour (H_2O) and ozone (O_3) absorb and emit infrared radiation emitted by the Earth's surface, the atmosphere and clouds. Heat is thereby trapped within the atmosphere leading to an increase of the Earth's surface temperature, a process which is called the natural greenhouse effect (Baede et al., 2001).

Although humans (like all other living organisms) have always influenced their environment, the impact of human activities has increased rapidly since the beginning of the Industrial Revolution. In the last two centuries, this so-called anthropogenic forcing (for example the production of greenhouse gases and aerosols by industrial and agricultural activities) has become another factor capable of influencing the climate system. The role of atmospheric carbon dioxide (CO_2) - along with water vapour the most important greenhouse gas in the atmosphere - has attracted considerable scientific attention. In the industrial era, the amount of atmospheric CO_2 has increased by about 35 % as a consequence of human activities such as deforestation and the burning of fossil fuels (Le Treut et al., 2007). Since the start of scientific monitoring at Mauna Loa (Hawaii/USA) in 1959, atmospheric CO_2 has increased from 316 to the present level of 387 ppm (Tans, 2010). This alarming development has generated extensive studies on the coupling of CO_2 and global climate change (e. g. Lindzen, 1997; Idso, 1998; Hansen et al., 2005; 2008). Indeed, future scenarios in changes of global sea level, sea surface temperature and global mean temperature summarized and published in the reports of the Intergovernmental Panel on Climate Change (IPCC, 2001; 2007) are a cause for concern. It seems that global climate change is one of the largest challenges for humans in the 21^{st} century. In order to understand present climate change and thus make predictions concerning future developments and their consequences, it is imperative to understand the development of global climate during Earth history, the factors triggering climate change and possible consequences for the environment.

The biosphere is one of the major components of the global climate system. Green plants strongly influence the composition of the atmosphere by storing large amounts of carbon from carbon dioxide (Baede et al., 2001). Since CO_2 is the substrate for photosynthesis, green plants are a suitable source of proxy data for global carbon cycle and past climates. During the biochemical process of photosynthesis, plants draw CO_2 from the atmosphere and water from the soil and produce organic matter under the release of oxygen to the atmosphere if enough nutrients, CO_2, water and energy (sunlight) are available. The movement of gaseous H_2O and CO_2 into and out of the leaf is governed by the physical process of diffusion. As the saturation of water inside the leaf is nearly 100 % and the concentration of CO_2 inside the leaf is lower than the ambient concentration, H_2O moves out and CO_2 moves into the leaf using the same gateway: stomata, tiny pores on the leaf surface (Taiz & Zeiger, 2006). This causes a dilemma, as plants try to maximize carbon uptake for photosynthesis and thus open their stomata as much as possible. This results, however, in an increased water loss by stomatal transpiration. Consequently, plants optimize their gaseous exchange in such a way that they reach maximum carbon uptake at simultaneously minimal water loss (e. g. Konrad et al., 2008). Under changing environmental conditions, plants adapt their stomatal conductance for example to varying CO_2 levels, irradiance, temperature, air humidity and soil moisture (Farquhar et al., 1982; Farquhar & Sharkey, 1982; Ehleringer & Cerling, 1995). The qualitative and quantitative effects of these variations on plants are an important topic for both carbon cycle and climate research (e. g. Ehleringer & Cerling, 1995; Beerling & Woodward, 1997; Beerling & Royer, 2002).

Changes in global climate occurred throughout many periods of Earth history and the early to middle Palaeogene represents a crucial geological period in which "greenhouse" conditions prevailed (Zachos et al., 1994; Greenwood & Wing, 1995; Wilf et al., 1998; Gingerich, 2006; Jahren, 2007; Bohaty et al., 2009; Hollis et al., 2009). After the Early Eocene Climatic Optimum (EECO), climatic conditions deteriorated as is indicated by deep sea temperatures derived from isotope records (Fig. 1.1). This decline was accompanied by a number of floral and faunal changes (for example Zachos et al., 2001; Francis & Poole, 2002; Prothero et al., 2003 and citations therein; Dupont-Nivet et al., 2007).

Since atmospheric CO_2 (C_a) is an important greenhouse gas, changes in C_a were largely credited for the development of global temperatures during the Palaeogene and the Neogene (Raymo, 1991; Berner & Kothavala, 2001; Crowley & Berner, 2001; Royer, 2006). Data obtained from antarctic ice cores indeed indicate a tight coupling between C_a and temperature for the past 740.000 years (Petit et al., 1999; Epica Community Members, 2004). It is dabatable, however, whether this tight coupling between C_a and climate was also valid throughout other time periods. For example, Pagani et al. (1999) suggest a decoupling of climate and C_a for the Miocene whereas results of Kürschner et al. (2008) indicate a coupling of C_a and temperature during the Miocene. The question whether or not C_a was high during the Palaeocene/Eocene and if it decreased simultaneously during global cooling is an important problem since the time interval from the Eocene to the Oligocene represents an exceptionally period of Earth´s history.

A complete picture of the underlying processes is considered significant for our

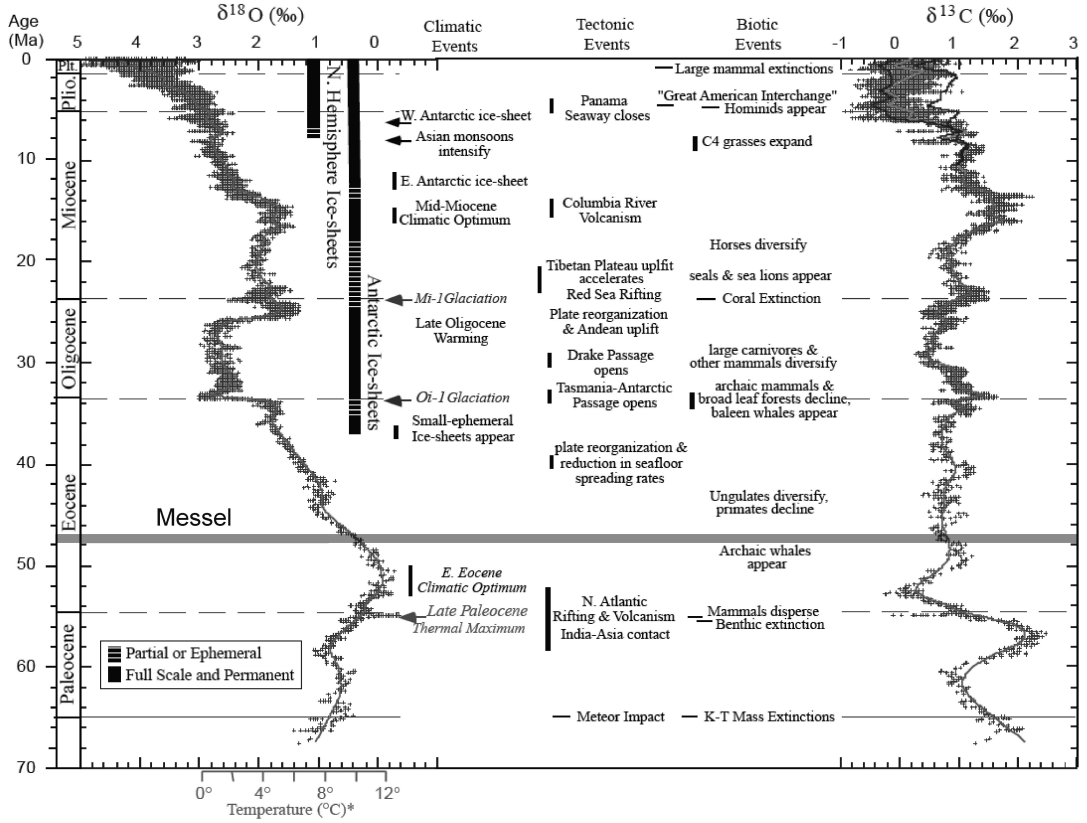

Figure 1.1: Overview of important Cenozoic climatic, tectonic and biotic events and global deep-sea oxygen and carbon isotope records derived from bottom-dwelling, deep-sea foraminifera. The numerical age of the Messel sediments was determined by Mertz & Renne (2005) to approximately 47-48 Ma (grey horizontal rectancle) with an age of ∼47 Ma for the top of the sediments and hence for the fossils excavated today. (modified, after Zachos et al., 2001)

understanding of global climate (Pagani et al., 2005). Numerous techniques have been applied in order to obtain C_a levels of the Palaeogene as carbon and boron isotopes e. g. of pedogenic carbonates and other palaeosols, foraminiferal shells or alkenones from Haptophyte algae (Ekart et al., 1999; Pearson & Palmer, 2000; Demicco et al., 2003; Yapp, 2004; Pagani et al., 2005; Lowenstein & Demicco, 2006; Bohaty et al., 2009) or geochemical models (Tajika, 1998; Berner & Kothavala, 2001; Wallmann, 2001; Rothman, 2002). Results of these techniques, however, provide partially conflicting results. Some C_a records suggest that C_a was higher during the Eocene compared to the present-day level (Ekart et al., 1999; Berner & Kothavala, 2001; Rothman, 2002; Yapp, 2004; Lowenstein & Demicco, 2006, Bohaty et al., 2009) whereas the results of Pearson & Palmer (2000) indicate high C_a levels during the Palaeocene and early Eocene (up to 3600 ppm) but with an erratic decline during the middle Eocene (down to 340 ppm), culminating at ∼46 Ma at about 2500 ppm. Demicco et al. (2003) re-calculated the C_a record of Pearson & Palmer (2000) by using additional factors (such as the

ionic composition of seawater) with resulting C_a values a little lower ranging between 100 and 2500 ppm. The results of Pagani et al. (2005) indicate high but fluctuating C_a values from approximately 600 to 2200 ppmv during the middle and late Eocene. Recently, Pearson et al. (2009) found a reduction in C_a at the Eocene/Oligocene boundary. This decline followed a sharp recovery in the early Oligocene and again, a subsequent gradual decline.

Results of geochemical modelling indicate C_a values for the Eocene (between 40 and 50 Ma) about 2.1 to 3.2 times the modern level (Berner & Kothavala, 2001) and about 1.7 to 2.1 times at $\sim$47 Ma (Rothman, 2002).

DeConto & Pollard (2003) who simulated the growth of the East Antarctic ice sheet by using a circulation model provided indirect evidence of a C_a decrease as triggering agent for global cooling during the Eocene/Oligocene transition. According to their results, a decrease in Cenozoic C_a is necessary to allow for the rapid glaciation of Antarctica at the Eocene/Oligocene boundary. At any rate, further simulations indicate a crucial role of vegetation climate feedback during glaciation (Thorn & DeConto, 2006). Tripati et al. (2005) also suggested a coupling between the greenhouse-icehouse transition and polar ice sheet growth to C_a. It is, however, likely that other factors influenced the climate development of the Eocene time period e. g. precessional forcing (Thrasher & Sloan, 2009; Warnaar et al., 2009; Zeebe et al., 2009). In summary, the results of most studies indicate high C_a during the Eocene greenhouse period.

Another promising proxy for the evolution of C_a is the stomatal density (SD, number of stomata per leaf area) of land plants. Woodward (1987) observed a decrease in stomatal densities of sub-recent plant material of herbarium collections with increasing C_a. This discovery introduced stomatal frequency as a C_a-sensor into palaeoclimatological sciences. A direct explanation for the decrease of SD with increasing C_a (and vice versa) is that the plant adjusts its epidermal gas permeability to changing C_a (Woodward, 1987). This means that under high C_a less stomata are necessary to obtain the same amount of C_a for photosynthesis.

Observations on extant plants show that the SD(C_a)-response is strongly species-specific (e. g. Woodward & Bazzaz, 1988; Beerling & Chaloner, 1992; Beerling & Kelly, 1997). This leads to the conclusion that fossil plants can only provide for reliable reconstructions of C_a if they have living representatives whose SD(C_a)-response can be documented and used as calibration basis (for example Royer, 2001; Beerling & Royer, 2002). The common technique for calibrating the stomatal frequency of fossil species is therefore to collect data concerning the C_a response of extant plants from herbarium material and/or greenhouse experiments under controlled C_a levels (Kürschner, 1996; Royer, 2001; Beerling & Royer, 2002; Roth-Nebelsick, 2005). An empirical "transfer function" is then fitted to the data which serves as base for calculating C_a from the fossil stomatal data. Utilizing the approach becomes increasingly difficult with the increasing age of the considered time interval. This is due to the fact that the number of still extant taxa decreases with increasing age. "Living fossils" such as the gymnosperms *Gingko biloba* and *Metasequoia glyptostroboides* are thus obviously conducive as a supplier of SD(C_a)-data.

By using stomatal indices of fossil material of *Gingko biloba* and *Metasequoia glyptostroboides* from various locations, Royer et al. (2001) presented C_a data from the late Palaeocene, early Eocene and the middle Miocene. These C_a data are in the range of $\sim$300 to 450 ppmv. Only one data point shows a higher value of about 800 ppmv at $\sim$55 Ma. Thus, the stomatal proxy data of *Gingko biloba* and *Metasequoia glyptostroboides* strongly contradict the other C_a reconstructions mentioned before. McElwain (1998) determined leaf stomatal data of Lauraceae species from the middle Eocene. The fossil material showed significantly lower stomatal frequencies than leaves from early post-industrial herbarium material which developed under ambient C_a (between 286 and 310 ppm). Since a calibration curve was not available, palaeo-C_a was extrapolated based on extant taxa. Results indicate C_a values for the middle Eocene about 1.4 to 3 times the pre-industrial level. Stomatal frequencies of *Eotrigonobalanus furcinervis* (Fagaceae) and *Laurophyllum acutimontanum* (Lauraceae) also indicate that C_a during the Eocene was higher than during the Oligocene and early Miocene (Roth-Nebelsick et al., 2004). Beerling et al. (2009) applied new statistical transfer functions to the stomatal frequencies of fossil *Gingko biloba* and *Metasequoia glyptostroboides* from the datasets of Royer et al. (2001) and Retallack (2002). Their median reconstructed C_a-values indicate C_a-levels during the Palaeogene (58-54 Ma) of typically 450 to 700 ppm.

In summary, most studies indicate that C_a levels during the Eocene were considerably higher than the ambient level followed by a decline towards the Oligocene. The results of Royer et al. (2001) based on "living fossils" yield, however, values for C_a close to the present level. Other studies based on stomatal frequency of Eocene plants indicate that C_a was higher during this time. Since results about fossil C_a obtained by stomatal data are usually only acknowledged to be quantitative reconstructions if based on a transfer function achieved with extant representatives, the results of Royer et al. (2001) are considered to be more reliable. The current technique of transfer function based reconstructions, however, hampers further investigations on additional plant taxa from the Eocene as it requires an extant representative. Thus, for time intervals older than the Miocene the method of empirical transfer curves is restricted to the very few species which represent "living fossils". Furthermore, it is debatable whether or not the phenotypical (short-term) response of plants to changing C_a observed on herbarium sheets and during greenhouse experiments does, in fact, reflect the evolutionary (long-term) response of plants to their environment.

1.2 Objectives of the thesis

The main object of this thesis is the modelling of atmospheric CO_2 in the middle Eocene based on stomatal data of fossil leaf material but without accessing empirical "transfer functions" generated from the stomatal response of extant representatives grown under experimental greenhouse conditions or from herbarium collections. For this purpose, a mechanistic-theoretical approach was developed which allows for CO_2-reconstructions based on stomatal data of fossil plant species even when there is no nearest living relative or direct descendant available (see **Section 3.1**: Konrad et al. (2008), *Modelling of stomatal density response to atmospheric CO_2*). This novel

approach calculates curves of stomatal density as a function of atmospheric carbon dioxide concentration and consists of three submodels:

Submodel 1 the biochemical process of C_3-photosynthesis after the assimilation model of Farquhar et al. (1980; 2001)

Submodel 2 the physical process of diffusion describing the movement of water- and carbon dioxide molecules into and out of the leaf through open stomata described by Fick's first law of diffusion

Submodel 3 an optimisation principle concerning water availability and gaseous exchange which deals with the problem of land plants to adjust their stomata in such a way that they reach maximum CO_2 uptake for photosynthesis at minimum water loss via stomatal transpiration.

Most land plants are confronted with the problem that water vapour and CO_2 use the same gateways (stomata) for entering and leaving the leaf. As the waxy leaf cuticle is a very effective barrier to water movement, nearly all leaf transpiration results from diffusion of water vapour through opened stomata. Unfortunately, the concentration gradient for CO_2 uptake is clearly smaller than the concentration gradient that drives stomatal transpiration and, thus, water loss (Taiz & Zeiger, 2006). Therefore, opening of stomata to decrease the stomatal resistance and to allow higher CO_2 uptake is unavoidably accompanied by an increase in water loss via stomatal transpiration. If the water supply is not limited, plants are able to afford some what more water loss for CO_2 uptake for photosynthesis. In habitats with limited water supply, plants have to keep water loss as low as possible. In general, it is assumed that plants solve this functional dilemma by optimizing stomatal conductance in order to gain maximized CO_2 uptake and minimized stomatal transpiration (Cowan & Farquhar, 1977; Konrad et al., 2008). For doing this plants have two options:

I) In a *short-term response*, plants can adapt stomatal conductance to environmental conditions by opening and closing stomata resulting in changes of the stomatal pore area. This adaptation can be diurnal or even seasonal (Hari et al., 1986; Mäkelä et al., 1996) and defines the phenotypical response of plants which displays the actual observed SD(C_a) response. Here, the area of the stomatal aperture is adjusted to short-term variations of environmental traits such as temperature, atmospheric humidity, wind speed, insolation and C_a.

II) In a *long-term response*, plants can adapt stomatal conductance by changing the number of stomata per area (stomatal density) or modifying the stomata geometry such as width, length and depth of the stomatal pore. As morphological modifications require a long time for realisation, this option reflects the evolutionary response of stomatal density to long-term variations in C_a. For the reconstruction of atmospheric CO_2 from fossil SD only the *long-term, evolutionary response* is of interest (Konrad et al., 2008).

For the modelling of stomatal density as a function of C_a, numerous parameters are required (Fig. 1.2) which can be summarized in four groups:

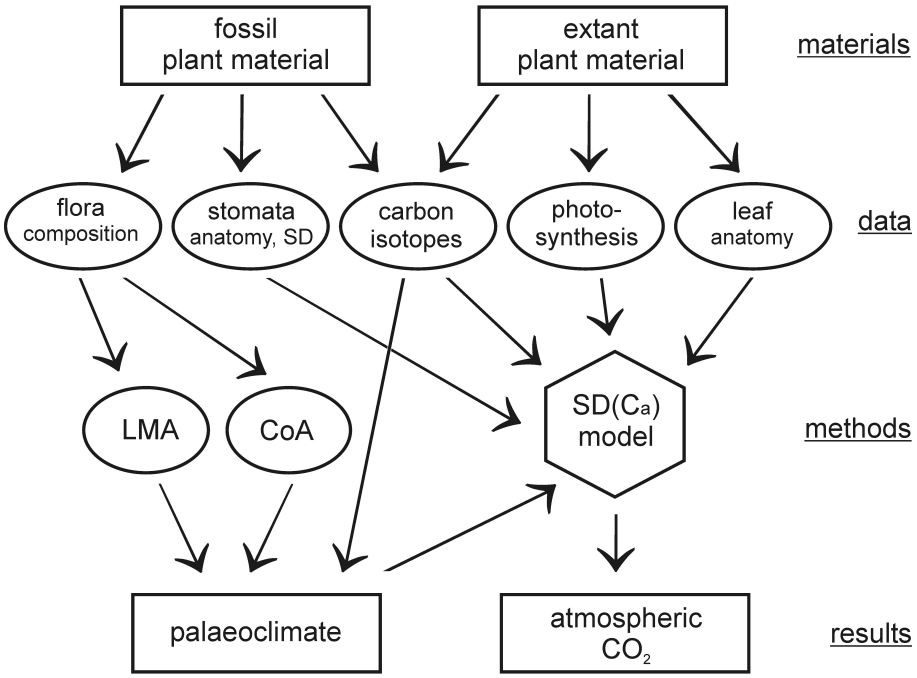

Figure 1.2: Working schedule of the presented thesis showing connections between used materials, obtained data, applied methods and received results. SD = Stomatal density, LMA = Leaf Margin Analysis, CoA = Coexistence Approach, SD(C_a) model = mechanistic model after Konrad et al. (2008). (drawing by M. Grein)

Group 1 palaeoenvironmental parameters (temperature, wind velocity, atmospheric humidity) obtained from Leaf Margin Analysis and the Coexistence Approach (**Section 3.2**: *Reconstruction of the middle Eocene climate of Messel using palaeobotanical data*)

Group 2 information about water availability which can be estimated from the c_i/c_a-ratio obtained from the carbon isotope signal of leaves (**Section 3.3**: *Carbon isotope composition of middle Eocene leaves*)

Group 3 anatomical and morphological parameters (thickness, tortuosity and porosity of assimilation tissue, leaf length, depth, length and width of stomatal porus and stomatal density) obtained from fossil and extant leaves (**Section 1.3.3**)

Group 4 photosynthetical data (Michaelis-Menten constants, CO_2 compensation point, maximum RuBP-saturated rate of carboxylation, mitochondrial respiration rate) obtained from extant plants (**Section 1.3.3**)

1.3 Materials

1.3.1 The Messel Pit

The fossil taphocoenosis of the Messel Pit (Middle Messel Formation) proved to be especially suited for collecting stomatal data as it provides a large number of almost complete well-preserved leaves lacking extended fragmentation. The sediments of the Messel Formation deposited in a freshwater lake whose remains are known today as "Messel Pit" situated near Darmstadt, federal state of Hesse in Germany (Fig. 1.3). The Messel Pit represents a UNESCO World Heritage Site and it is a famous source for numerous well-preserved fossil material as fish, birds, mammals, amphibians, reptiles, insects and plants (e. g. Engelhardt, 1922; Sturm, 1971; 1978; Collinson, 1982; Schaarschmidt, 1984; Franzen, 1985; Collinson, 1988; Wilde, 1989; Neubert, 1999; Mayr, 2000; Wilde & Süss, 2001; Wedmann et al., 2007). The "Messel Pit" as it is known today is the result of intense mining operations between 1870 and 1974 (Schaal & Schneider, 1995) where most of the Upper Messel Formation and parts of the Middle Messel Formation had been removed by mining.

The world-famous "oil-shale" of Messel belongs to a series of isolated occurrences of Palaeogene deposits on the "Sprendlinger Horst" forming the northern extension of the Odenwald (Felder et al., 2001). The presence of massive volcanoclastic deposits provides evidence that the overlying lake sediments have been deposited within a maar structure which was formed by one or more phreatomagmatic eruptions (Schulz et al., 2002; Lenz et al., 2007, and citations therein). The Messel "oil-shale" corresponds to the Middle Messel Formation and consists of finely laminated and highly bituminous shales which developed during a predominantly stable meromictic phase of the maar lake that formed after the eruptions and during water filling. The age of the lapilli tuff sequence underlying the maar sediments of Lake Messel was dated to 47.8 Ma $\pm$ 0.2 myr by Mertz & Renne (2005) with an age of approximately 47 Ma for the top of the sedimentation and hence also for the fossils excavated today. This is an exceptionally exact dating for terrestrial fossil materials. The sedimentation of the bituminous shales lasted $\sim$1 million years (Schulz et al., 2002; Mertz & Renne, 2005). The Middle Messel Formation spans therefore a limited time interval of the middle Eocene situated rather close to the C_a peak of Pearson & Palmer (2000) at about 46 Ma. Furthermore, Messel is close to the thermal and mammalian species-diversity maximum of the early middle Eocene (Blondel, 2001).

1.3.2 Fossil & extant leaf material

In this thesis, species of the Lauraceae (laurel family) and Myrtaceae (myrtle family) were chosen for C_a reconstruction as they represent frequent elements in the leaf taphocoenosis of Messel.

The laurel family (Lauraceae) consists of approximately 50 described genera and more than 2500 species with a mainly pantropical distribution (Christophel & Rowett, 1996) but also occurring in Macaronesia and the Mediterranean region (e. g. Rodríguez-Sánchez et al., 2009). In the fossil record, this family is found

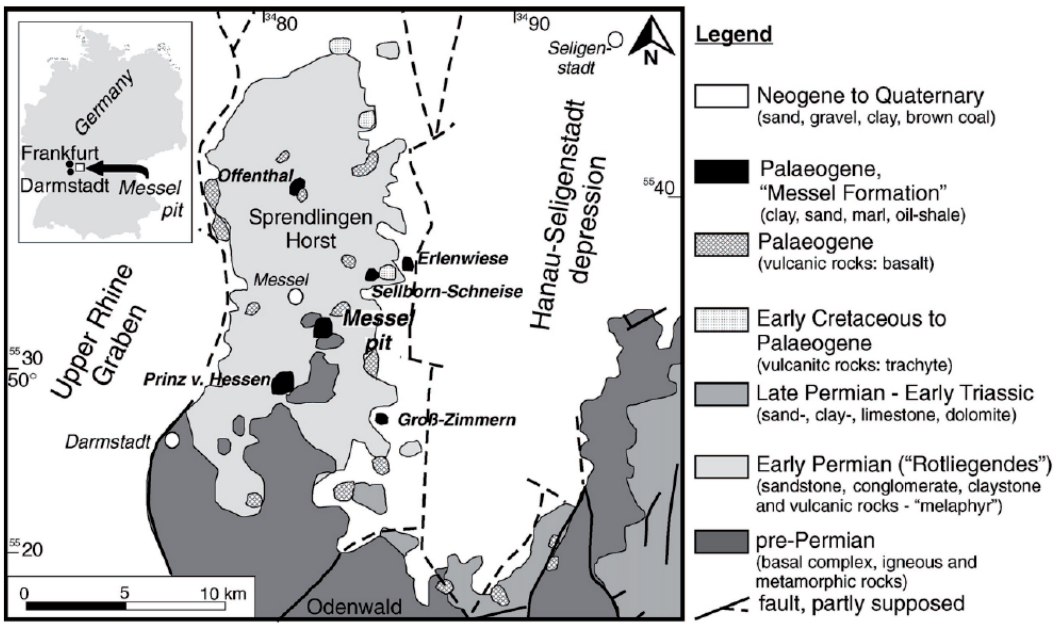

Figure 1.3: Geological map showing the location of the Messel Pit Fossil Site including Palaeogene sites nearby. (from Lenz et al., 2007, modified after Harms 1999)

from the Cretaceous onward (e. g. Upchurch & Dilcher, 1990; Taylor et al., 2009, and citations therein). Familiar representatives in the Lauraceae are species such as bay laurel (*Laurus nobilis*), camphor tree (*Cinnamomum camphora*), cinnamon (*Cinnamomum verum*) and avocado (*Persea americana*).

The myrtle family (Myrtaceae) consists of approximately 100 extant genera with 3000 species and is also known from the Cretaceous onward. Today, these evergreen trees or shrubs are found principally in Australia and tropical America (Taylor et al., 2009), but are also distributed in Mediterranean regions (e. g. Tognetti et al., 2000). Well-known representatives in the Myrtaceae are species such as eucalyptus (*Eucalyptus* sp.), piment (*Pimenta dioica*), guave (*Psidium guajava*) and cloves (*Syzygium aromaticum*).

Leaves of the extant Lauraceae and Myrtaceae considered in this thesis are fairly similar with regard to tissue composition. All investigated species grow as evergreen, sclerophylleous shrubs or trees and have broad, more or less leathery, entire margined and hypostomatic leaves. The mesophyll is dorsiventral and clearly separated in spongy and palisade parenychyma (Fig. 1.4).

Fossil leaf material

Laurophyllum lanigeroides (ENGELHARDT 1922) WILDE 1989 (Plate 1) is a fossil Lauraceae representing a frequent element of the Messel flora. Leaves of *Laurophyllum lanigeroides* are broad, entire margined and up to 11 cm long. Leaf

shape is very variable and can be narrow ovate to lanceolate, sometimes elliptic to narrow elliptic with a more or less straight primary vein. Secondary veins are eucamptodromous in most cases but sometimes even cladodromous. The stomatal distribution is hypostomatic with paracytic stomatal complexes.

Daphnogene crebrigranosa (STURM 1971) WILDE 1989 (Plate 2) is another Lauraceae from Messel. Its leaves are broad and entire margined with a length of up to 9 cm. Leaf shape can be narrow ovate to lanceolate or elliptic to narrow elliptic with three primary veins (acrodromous). Just a few secondary veins leave the middle primary vein in the upper part of the lamina. Unfortunately, the exact determination of stomata and consequently the reliable determination of stomatal density was hampered by the granulate cuticle surface of *Daphnogene crebrigranosa*. Therefore, this species was just used for the analysis of the carbon-isotopic signal without further use in CO_2-calculation so far.

As is common in Lauraceae (Bandulska, 1926; Hill, 1986; Christophel et al., 1996; Christophel & Rowett, 1996; Carpenter et al., 2007) the stomata of *Laurophyllum lanigeroides* and *Daphnogene crebrigranosa* are sunken in the epidermis which means that guard cells are sunken below overarching subsidiary cells (Fig. 1.5). Taxonomic affinities and detailed morphological and anatomical descriptions of *Laurophyllum lanigeroides* and *Daphnogene crebrigranosa* are presented and discussed in the monograph of Wilde (1989) and in Sturm (1971).

Rhodomyrtophyllum sinuatum (BANDULSKA 1923) WALTHER ex MAI & WALTHER 1985 (Plate 3) is a fossil Myrtaceae. It has broad, entire margined leaves which are up to 9 cm long. Leaf shape can be narrow elliptic to oblong obovate with brochidodromeous secondary veins. Stomata are brachyparacytic to laterocytic (Glinka & Walther, 2003) or "incomplete cyclocytic" (Wilde, 1989) and the size of stomata varies. A small number of giant stomata is existent. This variability in stomatal size and sometimes even in shape is typical for nearly all Myrtaceae (Glinka & Walther, 2003). For taxonomic affinities and detailed morphological and anatomical descriptions of *Rhodomyrtophyllum sinuatum* see Wilde (1989) and Glinka & Walther (2003).

The investigated fossil leaves are stored in the palaeobotanical collection of the Senckenberg Forschungsinstitut und Naturmuseum (Frankfurt am Main/Germany).

Extant leaf material

Several parameters that cannot be provided by fossil plants have to be determined by using extant material. The required data can either be taken from the relevant literature or have to be derived from leaf cross sections. Unfortunately, the convincing identification of a nearest living relative species may be quite difficult for Eocene species (Wilde, 1989). There is no available reliable determination of a nearest living relative for the three considered species from Messel, except the family level. Therefore in order to obtain reliable results, representatives in the Lauraceae and Myrtaceae showing anatomical, morphological and/or ecological similarities to the fossil species were investigated. After profound studies on fresh and historical (herbarium) leaf material, the following genera were considered as most suitable: *Laurus*

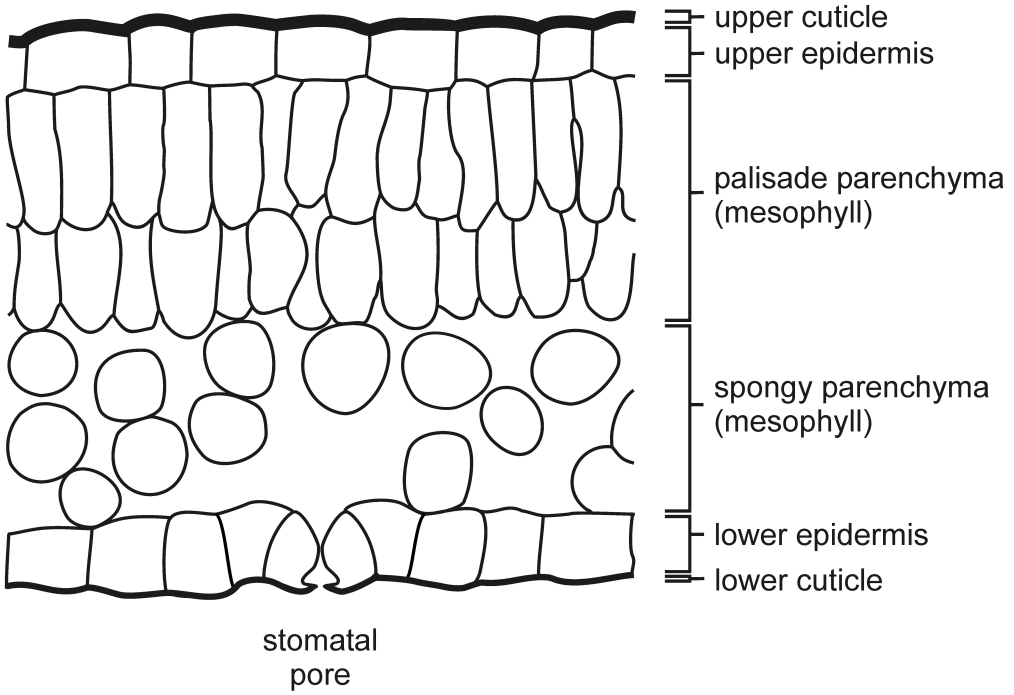

Figure 1.4: Schematic leaf cross section through a hypostomatic leaf showing the typical kinds of tissue as is upper and lower epidermis with overlying waxy cuticle, the mesophyll consisting of palisade parenchyma and spongy parenchyma and a stomatal pore in the lower epidermis. (drawing by M. Grein)

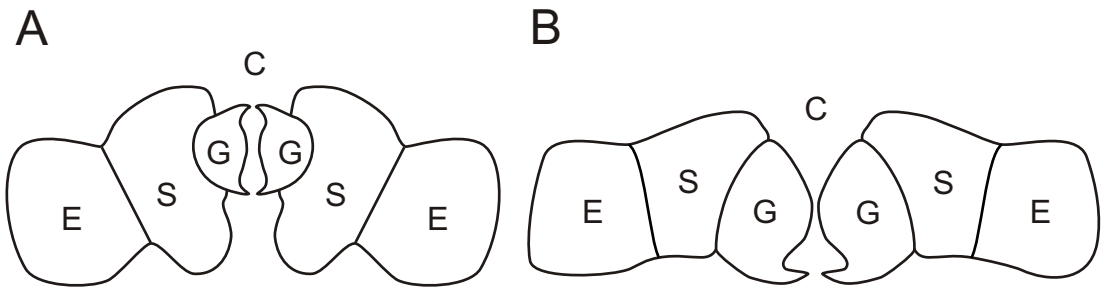

Figure 1.5: Simplified, schematic cross sections through stomata with guard cells (G), subsidiary cells (S), epidermal cells (E) and substomatal cavity (C). A) sunken stomate of a typical Lauraceae, B) stomate of a typical Myrtaceae. (drawing by M. Grein)

sp., *Ocotea* sp., *Cryptocarya* sp. and *Cinnamomum* sp. in the Lauraceae and *Psidium* sp., *Syzygium* sp. and *Eugenia* sp. in the Myrtaceae. Fresh plant material was provided by the botanical gardens of Tübingen, Berlin-Dahlem, Munich and Heidelberg (all Germany). Herbarium specimens were obtained from the State Museum of Natural History (Stuttgart).

1.3.3 Sampling

In order to obtain the required anatomical and morphological information, cuticle slides, epidermal impressions and leaf cross sections were produced.

As the SD varies significantly over a single leaf (Poole et al., 1996; 2000) cuticle preparations were produced from three defined regions of the lamina (base, center, apex). The cumulative mean method after Beerling & Royer (2002) was used to determine the number of leaves per taxon that are required to obtain a stable signal of SD. In total, 999 counts were performed on 75 fossil leaves of *L. lanigeroides*, *D. crebrigranosa* and *R. sinuatum* with at least 20 leaves per species. As to extant leaf material, five leaves per species were analyzed. Samples for producing leaf cross section were taken from the central area of the leaf blade. Historical leaves (from herbarium collections) were sampled by producing epidermal impressions, a gentle sampling method that prevents destruction. Cuticle slides, leaf cross sections and epidermal impressions were digitalized using a light microscope (Leica DM 2500 M) with an adapted digital camera (Leica DFC 320) and an image processing software (Leica IM 500). They were produced as follows:

Procedure of cuticle preparation

1. Tissue samples of about 5 x 5 mm size were cut out of the leaf blade.
2. In order to remove adhering sediment, samples were treated with hydrofluoric acid (HF, 48 %) followed by washing with water.
3. For maceration, samples were subsequently put in Schulze Solution which is crystalline potassium chlorate ($KClO_3$) and nitric acid (HNO_3, 65 %) in ratio about 1:1.
4. After maceration samples were neutralized in ammonia solution ($NH_3 + H_2O$, 32 %) followed by washing with clear water as soon as the cuticles had removed from the mesophyll.
5. The cuticles were then stained with safranin and washed with water again.
6. Finally, cuticles were embedded in glycerine jelly and mounted on microscope slides.

As to fresh leaf material, there was no treatment with HF. For isotopic measurements, only preparation steps one to four were performed on the fossil samples followed by drying in an oven. SEM images were produced with a LEO-1450 VP SEM located in the SEM/EDX Laboratory of the Institute for Geosciences (University

of Tübingen). For SEM photography, preparation steps one to five were performed on the fossil samples. Fresh leaf material was photographed without any further chemical preparation.

Procedure of leaf cross section preparation

1. Tissue samples (about 5 x 5 mm size) from the central region between margin and midrip were cut out of the lamina.
2. Each sample was embedded with low pressure into a notch cut in a small dice consisting of commercial glycerine soap.
3. Afterwards cross sections of about 10 - 30 μm thickness were cut with a microtome and directly put into clear water.
4. As soon as the soap had dissolved, cross sections were stained with safranin and astra blue.
5. Finally, the cross sections were embedded in glycerine jelly and mounted on microscope slides.

Production of epidermal impressions

1. A large drop of "Marabu Fixogum Rubber Cement" (a mounting adhesive that remains elastic) was applied to the leaf surface.
2. After full hardening, the peel was carefully removed with a pair of tweezers.
3. For processing, the edges of the peel were cut off with a razor blade or a scalpel to obtain a flat sample.
4. Finally, the impression peels were put on microscope slides.

Photosynthetical data

Photosynthesis is a central component of the SD(C_a)-model. In order to calculate curves of stomatal density as a function of C_a, various biochemical parameters have to be borrowed from extant Lauraceae and Myrtaceae. For this purpose, typical ranges for extant Lauraceae, Myrtaceae, tropical forest species and sclerophylleous shrubs were estimated and derived from different authors (e. g. Wullschleger, 1993; Reich et al., 1998; Niinemets et al., 2005; Kosugi & Matsuo, 2006; Funk, 2008; Cai et al., 2009) and citations therein.

In order to complete the available data, gas exchange measurements were carried out in summer 2009 in the Botanical Garden of Tübingen. These measurements were performed on potted plants using a portable gas analyzer (LCi Ultra Compact Photosynthesis Measurement System, ADC BioScientific Ltd.). Measurements on stomatal conductance were carried out before noon on fully expanded leaves under ambient conditions.

1.4 Procedure of CO_2-modelling & Synopsis

Numerous parameters have to be inserted into the model in order to model the stomatal density as a function of C_a. In the following, the procedure of CO_2-modelling including the results obtained from palaeoclimatic calculations, carbon isotope analysis and mechanistic modelling are summarized. These correspond to three publications included in this dissertation.

The required environmental data can be reconstructed by using several approaches developed for palaeoclimate reconstructions based on terrestrial plant material (see **Section 3.2**: *Reconstruction of the middle Eocene climate of Messel using palaeobotanical data*). Here, two different approaches were used for reconstructing the Messel climate:

The first approach, *Leaf Margin Analysis* (LMA), is a well known approach dealing with the distinct correlation of leaf margin characters in woody dicotyledonous leaves and mean annual temperature (Bailey & Sinnott, 1915; 1916; Wolfe, 1979; Spicer & Parrish, 1986; Parrish & Spicer, 1988; Wing & Greenwood, 1993; Wilf, 1997; Jacobs, 2002; Greenwood et al., 2004; Traiser et al., 2005; Royer & Wilf, 2006; Yang et al., 2007). In this thesis, LMA is based on descriptions and images of STURM (1971) and WILDE (1989), the latter providing a modern overview of the Messel leaf assemblage containing systematic descriptions of 60 dicotyledonous angiosperm leaf types. 53 of them were regarded as woody and were used for LMA. Aquatic plants, plants with insecure leaf margin type and herbs were excluded. Three equations obtained from extant floras in N-, M- and S-America (Wilf, 1997), East Asia (Wing & Greenwood, 1993) and Europe were used (Traiser et al., 2005).

The second method for palaeoclimate reconstruction, the *Coexistence Approach* (CA), uses the climatic tolerances of nearest living relatives (NLR). The CA is based on a calibration dataset containing climatic requirements of over 800 Cenozoic plant taxa that have modern relatives (Mosbrugger & Utescher, 1997). Although the CA has been already applied successfully to Asian and European plant taphocoenoses from the Cenozoic (Mosbrugger & Utescher, 1997; Bruch, 1998; Pross et al., 1998; Utescher et al., 2000; Ivanov et al., 2002; Kvaček et al., 2002; Liang et al., 2003; Uhl et al., 2003; Roth-Nebelsick et al., 2004; Mosbrugger et al., 2005; Utescher et al., 2009), most of these studies are restricted to floras of Miocene and Pliocene age. Mosbrugger & Utescher (1997) expected the CA to produce the best results for plant taphocoenoses of Oligocene age or younger since the identification of a NLR becomes more difficult with increasing age of the fossil. As to Eocene taxa, plant remains can frequently only be reliably identified to the family level and, moreover, their climatic requirements may have changed with time.

Most studies describe the climate of Messel as more or less consistently warm and moist, subtropical to tropical (Schaarschmidt, 1988; Wilde, 1989 and citations therein; 2005; Wilde & Micklich, 2007). Wilde (1989) suggested a paratropical climate for the middle Eocene of Messel with a MAT of clearly above 20 °C and a mean temperature of the coldest month clearly above 10 °C. The latter is also confirmed by the presence of crocodiles in the fossil record of Messel indicating mean

temperatures of the coldest month between 10 °C and 15 °C (Berg, 1964). Wilde (1989) also suggested that precipitation might have been relatively high, possibly with seasonal fluctuations but without extended periods of drought. In fact, many general statements about the climate prevailing in the surroundings of Lake Messel have been made, but no quantitative calculations have been carried out so far.

The results obtained with CA and LMA indicate a mean annual temperature up to ~24 °C, likely around 22 °C with the mean temperature of the coldest month clearly ranging above 10 °C. Mean annual precipitation rates reached values of 2540 mm and mean relative air humidity reached 77 % at most. In spite of some uncertainties caused by the comparison on family level and potential changes in the climatic limitations of the respective families, previous suggestions of a comparatively warm and humid, frost-free climate for the middle Eocene of Messel are confirmed.

Further information about the environment and water availability can be obtained from the isotopic composition of the fossil leaves (see **Section 3.3**: *Carbon isotope composition of middle Eocene leaves*). Since the ratio of leaf-internal to ambient carbon dioxide concentration (c_i/c_a) provides information about the ecophysiological situation (e. g. water balance) of a certain species and hence information about prevailing palaeoclimate conditions this parameter was determined as well. Furthermore, the c_i/c_a-ratio served as control-parameter in the mechanistic model allowing for estimations concerning the reliability of the calculated C_a. In this thesis, the δ^{13}C-derived c_i/c_a-ratio was determined from three fossil species from the Messel Pit: *Laurophyllum lanigeroides*, *Daphnogene crebrigranosa* (both Lauraceae) and *Rhodomyrtophyllum sinuatum* (Myrtaceae). Results show that mean δ^{13}C values of the three fossil plant species are situated in the range typically for modern C_3 plants which is approximately $\delta^{13}C = -36$ to -22 ‰ (e. g. Farquhar et al., 1989; O'Leary 1995; Cerling et al., 2004; Kingston & Harrison 2007; and citations therein). Intra-leaf analysis indicates slight δ^{13}C variations across the leaves. These variations, however, are not significant and much lower than the inter-leaf variability within a species. The fossil c_i/c_a-ratios calculated from the measured δ^{13}C values varied from mean 0.78 to 0.87 and are consequently comparably high, indicating a relatively small stomatal limitation to assimilation rate and non-conservative water use (e. g. Ishida et al., 1996; González-Rodríguez et al., 2001). Thus, δ^{13}C data reflect the warm and humid climate that prevailed during the middle Eocene of Messel.

Finally, the palaeoenvironmental, anatomical/morphological and photosynthetical parameters were inserted into the SD(C_a)-model (see **Section 3.4**: *Reconstruction of atmospheric CO_2 during the middle Eocene by application of a gas exchange model to fossil plants*). C_a-modelling was performed using a MAPLE-sheet (versions 12 and 13). By varying a certain parameter within a range realistic for a species (or family respectively) possible ranges for C_a were calculated. Ideally, ranges of the considered species overlap in a certain interval representing the likely C_a. Reliability of the ranges was estimated by considering control parameters (here: assimilation rate and the c_i/c_a-ratio) which were calculated in the MAPLE-sheet under a given C_a. Results were compared to actual measurements and literature data. In order to validate results of palaeoatmospheric CO_2 modelling, the model was used to "recon-

struct" extant C_a with extant representatives of the same families as the fossil ones. Calculations with extant *Cinnamomum camphora* (Lauraceae) and *Psidium littorale* (Myrtaceae) resulted in an overlapping interval between 350 to 393 ppm which is in good agreement to direct CO_2 measurements on Mauna Loa, Hawaii, providing a C_a of about 382 ppm in 2006 (Tans, 2010). The fossil CO_2 ranges of *Laurophyllum lanigeroides* and *Rhodomyrtophyllum sinuatum* range from 563 to 1098 ppm. The overlapping interval from 703 to 836 ppm indicates CO_2 concentrations in the middle Eocene which were substantially higher than the extant level. As global climate was still warm when the Messel sediments developed and the oceans were almost ice-free (Greenwood et al., 2010) a C_a range above 700 ppm is in good agreement with results of models on Antarctic glaciations that require a CO_2 concentration of less than 750 ppm for the onset of ice sheet formation.

1.5 Concluding remarks & future research

The combined results obtained in this PhD Thesis indicate levels of C_a between 700 and 840 ppm for the middle Eocene of Messel. This corresponds well to other studies investigating this time interval. Nevertheless, this range for palaeo-CO_2 results from mechanistic modelling performed on just two plant species in two different plant families.

Thus, one aspect of future research should be an increase of the number of species investigated in order to corroborate or even narrow down the C_a-interval. Possible candidates may be *Ampelopsis* sp. in the Vitaceae and some representatives in the Juglandaceae, the latter representing very frequent elements in the fossil plant taphocoenosis of Messel. Up to now, the analysis of Juglandaceae was hampered by difficulties in preparing cuticle slides since the cuticle of certain Juglandaceae is very fragile and decomposes during chemical preparation (Wilde, pers. comm.). One possibility of avoiding these difficulties in chemical preparation may be epifluorescence microscopy where no chemical treatment is necessary. Unfortunately, the application of epifluorescence is not suitable for certain species for example for the Lauraceae *Daphnogene crebrigranosa* because its oil bodies prevent the proper identification of stomata almost completely.

Another aspect of future research can be the mechanistic modelling of the SD(C_a)-response of fossil species originating from other taphocoenoses in the middle Eocene of Germany for example some sites of the Geiseltal (Central Germany), Helmstedt (Northern Germany) and Eckfeld (Western Germany). Additionally, species of late Eocene fossil sites of the Weißelster Basin (Central Germany) could be investigated.

This PhD thesis validates the mechanistic approach after Konrad et al. (2008) for reconstructing palaeoatmospheric CO_2 using fossil leaf material. In contrast to approaches basing on transfer functions obtained from an extant living relative, this novel approach bases on environmental, biochemical and anatomical information and is, thus, also applicable even when there is no direct modern extant representative available.

2 References

Baede, A. P. M., Ahlonsou, E., Ding, Y. & Schimel, D. (2001): The Climate System: an Overview. – In: Climate Change 2001: The Scientific Basis. Contribution of Working Group I to the Third Assessment Report of the Intergovernmental Panel on Climate Change; edited by Houghton, J. T., Ding, Y., Griggs, D. J., Noguer, M., van der Linden, P. J., Dai, X., Maskell, K. and Johnson, C. A., Cambridge University Press, Cambridge, United Kingdom and New York, NY, USA., pp. 85-98.

Bailey, I. W. & Sinnott, E. W. (1915): A botanical index of Cretaceous and Tertiary climates. *Science* 41, 831-834.

Bailey, I. W. & Sinnott, E. W. (1916): The climatic distribution of certain types of Angiosperm leaves. A*merican Journal of Botany* 3, 24-39.

Bandulska, H. (1926): On the cuticles of some fossil and recent Lauraceae. *Journal of the Linnean Society of London (Botany)* 47, 383-425.

Beerling, D. J. & Chaloner, W. G. (1992): Stomatal density as an indicator of atmospheric CO_2 concentration. *The Holocene* 2, 71-78.

Beerling, D. J. & Kelly, C. K. (1997): Stomatal density responses of temperate woodland plants over the past seven decades of CO_2 increase: A comparison of Salisbury (1927) with contemporary data. *American Journal of Botany* 84, 1572-1583.

Beerling, D. J. & Royer, D. L. (2002): Reading a CO_2 signal from fossil stomata. *New Phytologist* 153, 387-397.

Beerling, D. J. & Woodward, F. I. (1997): Changes in land plant function over the Phanerozoic: reconstructions based on the fossil record. *Botanical Journal of the Linnean Society* 124, 137-153.

Beerling, D. J., Fox, A. & Anderson, C. W. (2009): Quantitative uncertainty analyses of ancient atmospheric CO_2 estimates from fossil leaves. *American Journal of Science* 309, 775-787.

Berg, D. E. (1964): Krokodile als Klimazeugen. *Geologische Rundschau* 54, 328-333.

Berner, R. A. & Kothavala, Z. (2001): GEOCARB III: a revised model of atmospheric CO_2 over Phanerozoic time. *American Journal of Science* 301, 182-204.

Blondel, C. (2001): The Eocene-Oligocene ungulates from Western Europe and their environment. *Palaeogeography, Palaeoclimatology, Palaeoecology* 168, 125-139.

Bohaty, S. M., Zachos, J. C., Florindo, F. & Delaney, M. L. (2009): Coupled greenhouse warming and deep-sea acidification in the middle Eocene. *Paleoceanography* 24, PA2207, doi: 10.1029/2008PA001676.

Bruch, A. A. (1998): Palynologische Untersuchungen im Oligozän Sloweniens - Paläo-Umwelt und Paläoklima im Ostalpenraum. - *Tübinger Mikropaläontologische Mitteilungen* 18, 1-193.

Cai, Z.-Q., Schnitzer, S. A. & Bongers, F. (2009): Seasonal differences in leaf-level physiology give lianas a competitive advantage over trees in a tropical seasonal forest. *Oecologia* 161, 25-33.

Carpenter, R. J., Jordan, G. J. & Hill, R.S. (2007): A toothed Lauraceae leaf from the Early Eocene of Tasmania, Australia. *International Journal of Plant Sciences* 168, 1191-1198.

Cerling T. E., Hart, J. A. & Hart, T. B. (2004): Stable isotope ecology in the Ituri Forest. *Oecologia* 138, 5-12.

Christophel, D. C. & Rowett, A. I. (1996): Leaf and cuticle atlas of Australian leafy Lauraceae. *Flora of Australia Supplementary Series* 6, 1-217; Australian Biological Resources Study, Canberra.

Christophel, D. C., Kerrigan, R. & Rowett, A.I. (1996): The use of cuticular features in the taxonomy of the Lauraceae. *Annals of the Missouri Botanical Garden* 83, 419-432.

Collinson, M. E. (1982): A preliminary report on the Senckenberg-Museum collection of fruits and seeds from Messel bei Darmstadt. C*ourier Forschungsinstitut Senckenberg* 56, 49-57.

Collinson, M. E. (1988): The special significance of the Middle Eocene fruit and seed flora from Messel, West Germany. *Courier Forschungsinstitut Senckenberg* 107, 187-197.

Cowan, I. R. & Farquhar, G. D. (1977): Stomatal function in relation to leaf metabolism and environment. *Symposium of the Society for Experimental Biology* 31, 471-505.

Crowley, T. J. & Berner, R. A. (2001): CO_2 and climate change. *Science* 292, 870-872.

DeConto, R. M. & Pollard, D. (2003): Rapid Cenozoic glaciation of Antarctica induced by declining atmospheric CO_2. *Nature* 421, 245-249.

Demicco, R. V., Lowenstein, T. K. & Hardie, L. A. (2003): Atmospheric pCO_2 since 60 Ma from records of seawater pH, calcium, and primary carbonate mineralogy. *Geology* 31, 793-796.

Dupont-Nivet, G., Krijgsman, W., Langereis, C. G., Abels, H. A., Dai, S. & Fang, X. (2007): Tibetan plateau aridification linked to global cooling at the Eocene-Oligocene transition. *Nature* 445, 635-638.

Ehleringer, J. R. & Cerling, T. E. (1995): Atmospheric CO_2 and the ratio of intercellular to ambient CO_2 concentrations in plants. *Tree Physiology* 15, 105-111.

Ekart, D. D., Cerling, T. E., Montañez, I. P. & Tabor, N. J. (1999): A 400 million year carbon isotope record of pedogenic carbonate: Implications for paleoatmospheric carbon dioxide. *American Journal of Science* 299, 805-827.

Engelhardt, H. (1922): Die alttertiäre Flora von Messel bei Darmstadt. *Abhandlungen der Hessischen Geologischen Landesanstalt zu Darmstadt* 7, 17-128.

Epica Community Members (2004): Eight glacial cycles from an Antarctic ice core. *Nature* 429, 623-628.

Farquhar, G. D. & Sharkey T. D. (1982): Stomatal Conductance And Photosynthesis. *Annual Review of Plant Physiology* 33, 317-345.

Farquhar, G. D., Ehleringer, J. R. & Hubick, K. T. (1989): Carbon isotope discrimination and photosynthesis. *Annual Review of Plant Physiology and Plant Molecular Biology* 40, 503-537.

Farquhar, G. D., O´Leary, M. H. & Berry, J. A. (1982): On the relationship between carbon isotope discrimination and intercellular carbon dioxide concentration in leaves. *Australian Journal of Plant Physiology* 9, 121-137.

Farquhar, G. D., Von Caemmerer, S. & Berry, J. A. (1980): A biochemical model of photosynthetic CO_2 assimilation in leaves of C_3-species. *Planta* 149, 78-90.

Farquhar, G. D., Von Caemmerer, S. & Berry, J. A. (2001): Models of Photosynthesis. *Plant Physiology* 125, 42-45.

Felder, M., Harms, F.-J. & Liebig, V. (2001): Lithologische Beschreibung der Forschungsbohrungen Groß-Zimmern, Prinz von Hessen und Offenthal sowie zweier Lagerstättenbohrungen bei Eppertshausen (Sprendlinger Horst, Eozän, Messel-Formation, Süd-Hessen). *Geologisches Jahrbuch Hessen* 128, 29-82.

Francis, J. E. & Poole, I. (2002): Cretaceous and early Tertiary climates of Antarctica: Evidence from fossil wood. *Palaeogeography, Palaeoclimatology, Palaeoecology* 182, 47-64.

Franzen, J. L. (1985): Exceptional preservation of Eocene vertebrates in the lake deposit of Grube Messel (West Germany). *Philosophical Transactions of the Royal Society London, B* 311, 181-186.

Funk, J. L. (2008): Differences in plasticity between invasive and native plants from a low resource environment. *Journal of Ecology* 96, 1162-1173.

Gingerich, P. D. (2006): Environment and evolution through the Paleocene-Eocene thermal maximum. *Trends in Ecology and Evolution* 21, 246-253.

Glinka, U. & Walther, H. (2003): *Rhodomyrtophyllum reticulosum* (ROSSM.) KNOBLOCH & Z. Kvaček – ein bedeutendes eozänes Florenelement im Tertiär Mitteleuropas. *Feddes Repertorium* 114, 30-55.

González-Rodríguez, A. M., Morales, D. & Jiménez, M. S. (2001): Gas exchange characteristics of a Canarian laurel forest tree species (*Laurus azorica*) in relation to environmental conditions and leaf canopy position. *Tree Physiology* 21, 1039-1045.

Greenwood, D. R. & Wing, S. L. (1995): Eocene continental climates and latitudinal temperature gradients. *Geology* 23, 1044-1048.

Greenwood, D. R., Basinger, J. F. & Smith, R. Y. (2010): How wet was the Arctic Eocene rain forest? Estimates of precipitation from Paleogene Arctic macrofloras. *Geology* 38, 15-18.

Greenwood, D. R., Wilf, P., Wing, S. L. & Christophel, D. C. (2004): Paleotemperature estimation using leaf-margin analysis: Is Australia different? *Palaios* 19, 129-142.

Hansen, J., Sato, M., Kharecha, P., Beerling, D., Berner, R., Masson-Delmotte, V., Pagani, M., Raymo, M., Royer, D. L. & Zachos, J. C. (2008): Target Atmospheric CO_2: Where should humanity aim? *The Open Atmospheric Science Journal* 2, 217-231.

Hansen, J., Sato, M., Ruedy, R., Nazarenko, L., Lacis, A., Schmidt, G. A., Russell, G., Aleinov, I., Bauer, M., Bauer, S., Bell, N., Cairns, B., Canuto, V., Chandler, M., Cheng, Y., Del Genio, A., Faluvegi, G., Fleming, E., Friend, A., Hall, T., Jackman, C., Kelley, M., Kiang, N., Koch, D., Lean, J., Lerner, J., Lo, K., Menon, S., Miller, R., Minnis, P., Novakov, T., Oinas, V., Perlwitz, J., Perlwitz, J., Rind, D., Romanou, A., Shindell, D., Stone, P., Sun, S., Tausnev, N., Thresher, D., Wielicki, B., Wong, T., Yao, M. & Zhang, S. (2005): Efficacy of climate forcings. *Journal of Geophysical Research* 110, D18104, doi:18110.11029/12005JD005776.

Hari, P., Mäkelä, A., Korpilahti, E. & Holmberg, M. (1986): Optimal control of gas exchange. *Tree Physiology* 2, 169-175.

Harms, F.-J. (1999): Karte zur Verbreitung der Messel-Formation/Faltblatt Welterbe Grube Messel. - Map, back side with comment; with contrib. of Wallner, H., Jacoby, W. R., Hessisches Landesamt für Bodenforschung, Wiesbaden.

Hill, R. S. (1986): Lauraceous leaves from the Eocene of Nerriga, New South Wales. *Alcheringa* 10, 327-351.

Hollis, C. J., Handley, L., Crouch, E. M., Morgans, H. E. G., Baker, J. A., Creech, J., Collins, K. S., Gibbs, S. J., Huber, M., Schouten, S., Zachos, J. C. & Pancost, R. D. (2009): Tropical sea temperatures in the high-latitude South Pacific during the Eocene. *Geology* 37, 99-102.

Idso, S. B. (1998): CO_2-induced global warming: a skeptic's view of potential climate change. *Climate Research* 10, 69-82.

IPCC (2001): Climate Change 2001: The Scientific Basis. *Contribution of Working Group I to the Third Assessment Report of the Intergovernmental Panel*

on Climate Change, 881 pp., Cambridge University Press, Cambridge, United Kingdom and New York, NY, USA.

IPCC (2007): Climate Change 2007: The Physical Science Basis. *Contribution of Working Group I to the Fourth Assessment Report of the Intergovernmental Panel on Climate Change*, 996 pp., Cambridge University Press, Cambridge, United Kingdom and New York, NY, USA.

Ishida, A., Toma, T., Matsumoto, Y., Yap, S. K. & Maruyama, Y. (1996): Diurnal changes in leaf gas exchange characteristics in the uppermost canopy of a rain forest tree, *Dryobalanops aromatica* Gaertn. f. *Tree Physiology* 16, 779-785.

Ivanov, D., Ashraf, A. R., Mosbrugger, V. & Palamarev, E. (2002): Palynological evidence for Miocene climate change in the Forecarpathian Basin (Central Paratethys, NW Bulgaria). *Palaeogeography, Palaeoclimatology, Palaeoecology* 178, 19-37.

Jacobs, B. F. (2002): Estimation of low-latitude paleoclimates using fossil angiosperm leaves: examples from the Miocene Tugen Hills, Kenya. *Paleobiology* 28, 399-421.

Jahren, A. H. (2007): The arctic forest of the Middle Eocene. *Annual Review of Earth and Planetary Sciences* 35, 509-540.

Kürschner, W. M., Kvaček, Z. & Dilcher, D. L. (2008): The impact of Miocene atmospheric carbon dioxide fluctuations on climate and the evolution of terrestrial ecosystems. *Proceedings of the National Academy of Sciences of the United States of America* 105, 449-453.

Kürschner, W. M. (1996): Leaf stomata as biosensors of palaeoatmospheric CO_2 levels. PhD Thesis, Laboratory of Palaeobotany and Palynology, Utrecht University.

Kingston, J. D. & Harrison, T. (2007): Isotopic dietary reconstructions of Pliocene herbivores at Laetoli: Implications for early hominin paleoecology. *Palaeogeography, Palaeoclimatology, Palaeoecology* 243, 272-306.

Konrad, W., Roth-Nebelsick, A. & Grein, M. (2008): Modelling of stomatal density response to atmospheric CO_2. *Journal of Theoretical Biology* 253, 638-658.

Kosugi, Y. & Matsuo, N. (2006): Seasonal fluctuations and temperature dependence of leaf gas exchange parameters of co-occuring evergreen and deciduous trees in a temperate broad-leaved forest. *Tree Physiology* 26, 1173-1184.

Kvaček, Z., Velitzelos, D. & Velitzelos, E. (2002): Late Miocene flora of Vegora, Macedonia, N. Greece. University of Athens. 175 pp.; Athens (Korali Publications).

Le Treut, H., Somerville, R., Cubasch, U., Ding, Y., Mauritzen, C., Mokssit, A., Peterson, T. & Prather, M. (2007): Historical Overview of Climate Change. - In: Climate Change 2007: The Physical Science Basis.

Contribution of Working Group I to the Fourth Assessment Report of the Intergovernmental Panel on Climate Change; edited by Solomon, S., Qin, D., Manning, M., Chen, Z., Marquis, M., Averyt, K. B., Tignor, M. and Miller, H. L., Cambridge University Press, Cambridge, United Kingdom and New York, NY, USA.

Lenz, O. K., Wilde, V., Riegel, W. (2007): Recolonization of a Middle Eocene volcanic site: quantitative palynology of the initial phase of the maar lake of Messel (Germany). *Review of Palaeobotany and Palynology* 145, 217-242.

Liang, M.-M., Bruch, A. A., Collinson, M., Mosbrugger, V., Li, C.-S., Sun, Q.-G. & Hilton, J. (2003): Testing the climatic estimates from different palaeobotanical methods: an example from the Middle Miocene Shangwang Flora of China. *Palaeogeography, Palaeoclimatology, Palaeoecology* 198, 279-301.

Lindzen, R. S. (1997): Can increasing carbon dioxide cause climate change? *Proceedings of the National Academy of Sciences of the United States of America* 94, 8335-8342.

Lowenstein, T.K. & Demicco, R.V. (2006): Elevated Eocene atmospheric CO_2 and its subsequent decline. *Science* 313, 1928.

Mäkelä, A., Berninger, F. & Hari, P. (1996): Optimal control of gas exchange during drought: Theoretical Analysis. *Annals of Botany* 77, 461-467.

Mayr, G. (2000): Tiny hoopoe-like birds from the middle Eocene of Messel (Germany). *The Auk* 117, 964-970.

McElwain, J. C. (1998): Do fossil plants signal palaeoatmospheric CO_2 concentration in the geological past? *Philosophical Transactions of the Royal Society of London B* 353, 83-96.

Mertz, D. F. & Renne, P. R. (2005): A numerical age for the Messel fossil deposit (UNESCO World Heritage Site) derived from $^{40}Ar/^{39}Ar$ dating on a basaltic rock fragment. *Courier Forschungsinstitut Senckenberg* 255, 67-75.

Mosbrugger, V. & Utescher, T. (1997): The coexistence approach - a method for quantitative reconstructions of Tertiary terrestrial paleoclimate data using plant fossils. *Palaeogeography, Palaeoclimatology, Palaeoecology* 134, 61-86.

Mosbrugger, V., Utescher, T. & Dilcher, D. L. (2005): Cenozoic continental climatic evolution of Central Europe. *Proceedings of the National Academy of Sciences of the United States of America* 102, 14964-14969.

Neubert, E. (1999): The Mollusca of the Eocene Lake of Messel. *Courier Forschungsinstitut Senckenberg* 216, 167-181.

Niinemets, Ü., Cescatti, A., Rodeghiero, M. & Tosens, T. (2005): Leaf internal diffusion conductance limits photosynthesis more strongly in older leaves of Mediterranean evergreen broad-leaved species. *Plant, Cell and Environment* 28, 1552-1566.

O'Leary, M. H. (1995): Environmental effects on carbon isotope fractionation in terrestrial plants,. - In: Wada, E., Yoneyama, T., Minigawa, M., Ando, T. & Fry, B. D. (eds.): *Stable Isotopes in the Biosphere*, 78-91; Kyoto (Kyoto University Press).

Pagani, M., Arthur, M. A. & Freeman, K. H. (1999): Miocene evolution of atmospheric carbon dioxide. *Paleoceanography* 14, 273-292.

Pagani, M., Zachos, J. C., Freeman, K. H., Tipple, B. & Bohaty, S. (2005): Marked decline in atmospheric carbon dioxide concentrations during the Paleogene. *Science* 309, 600-603.

Parrish, J. T. & Spicer, R. A. (1988): Late Cretaceous terrestrial vegetation: a near-polar temperature curve. *Geology* 16, 22-25.

Pearson, P. N. & Palmer, M. R. (2000): Atmospheric carbon dioxide concentrations over the past 60 million years. *Nature* 406, 695-699.

Pearson, P. N., Foster, G. L. & Wade, B. S. (2009): Atmospheric carbon dioxide through the Eocene-Oligocene climate transition. *Nature* 461, 1110-1114.

Petit, J. R., Jouzel, J., Raynaud, D., Barkov, N. I., barnola, J.-M., Basile, I., Bender, M., Chappellaz, J., Davis, M., Delaygue, G., Delmotte, M., Kotlyakov, V. M., Legrand, M., Lipenkov, V. Y., Lorius, C., Pepin, L., Ritz, C., Saltzman, E. & Stievenard, M. (1999): Climate and atmospheric history of the past 420000 years from the Vostock ice core, Antarctica. *Nature* 399, 429-436.

Poole, I., Lawson, T., Weyers, J. D. B. & Raven, J. A. (2000): Effect of elevated CO_2 on the stomatal distribution and leaf physiology of *Alnus glutinosa*. *New Phytologist* 145, 511-521.

Poole, I., Weyers, J. D. B., Lawson, T. & Raven, J. A. (1996): Variations in stomatal density and index: implications for paleoclimatic reconstructions. *Plant, Cell and Environment* 19, 705-712.

Pross, J., Bruch, A. A. & Kvaček, Z. (1998): Paläoklima-Rekonstruktionen für den Mittleren Rupelton (Unter-Oligozän) des Mainzer Beckens auf der Basis mikro- und makrobotanischer Befunde. *Mainzer geowissenschaftliche Mitteilungen* 27, 79-92.

Prothero, D. R., Ivany, L. C. & Nesbitt, E. A. (2003): From greenhouse to icehouse: the marine Eocene-Oligocene transition. 541 pp., New York (Columbia University Press).

Raymo, M.E. (1991): Geochemical evidence supporting Chamberlin, T. C. ´s theory of glaciation. *Geology* 19, 344-347.

Reich, P. B., Walters, M. B., Ellsworth, D.S., Vose, J. M., Volin, J. C., Gresham, C. & Bowman, W. D. (1998): Relationships of leaf dark respiration to leaf nitrogen, specific leaf area and leaf life-span: a test across biomes and functional groups. *Oecologia* 114, 471-482.

Retallack, G. J. (2002): Carbon dioxide and climate over the past 300 Myr. *Philosophical Transactions of the Royal Society of London Series A* 360, 659-673.

Rodríguez-Sánchez, F., Guzmán, B., Valido, A., Vargas, P. & Arroyo, J. (2009): Late Neogene history of the laurel tree (*Laurus* L., Lauraceae) based on phylogeographical analyses of Mediterranean and Macaronesian populations. *Journal of Biogeography* 36, 1270-1281.

Rothman, D. H. (2002): Atmospheric carbon dioxide levels for the last 500 million years. *Proceedings of the National Academy of Sciences of the United States of America* 99, 4167-4171.

Roth-Nebelsick, A., Utescher, T., Mosbrugger, V., Diester-Haass, L. & Walther, H. (2004): Changes in atmospheric CO_2 concentrations and climate from the Late Eocene to Early Miocene: palaeobotanical reconstruction based on fossil floras from Saxony, Germany. *Palaeogeography, Palaeoclimatology, Palaeoecology* 205, 43-67.

Roth-Nebelsick, A. (2005): Reconstructing atmospheric carbon dioxide with stomata: possibilities and limitiations of a botanical pCO_2-sensor. *Trees - Structure and Function* 19, 251-265.

Royer, D. L. & Wilf, P. (2006): Why do toothed leaves correlate with cold climates? Gas exchange at leaf margins provide new insights into a classic paleotemperature proxy. *International Journal of Plant Sciences* 167, 11-18.

Royer, D. L., Wing, S. L., Beerling, D. J., Jolley, D. W., Koch, P. L., Hickey, L. J. & Berner, R. A. (2001): Paleobotanical evidence for near present-day levels of atmospheric CO_2 during part of the Tertiary. *Science* 292, 2310-2313.

Royer, D. L. (2001): Stomatal density and stomatal index as indicators of paleoatmospheric CO_2 concentration. *Review of Palaeobotany and Palynology* 114, 1-28.

Royer, D. L. (2006): CO_2-forced climate thresholds during the Phanerozoic. *Geochimica et Cosmochimica Acta* 70, 5665-5675.

Schaal, S. & Schneider, U. (1995): Chronik der Grube Messel. Kempkes, Gladenbach.

Schaarschmidt, F. (1984): Flowers from the Eocene oil-shale of Messel: a preliminary report. *Annals of the Missouri Botanical Garden* 71, 599-606.

Schaarschmidt, F. (1988): Der Wald, fossile Pflanzen als Zeugen eines warmen Klimas. – In: Messel - Ein Schaufenster in die Geschichte der Erde und des Lebens; edited by Schaal, S. and Ziegler, W., pp. 27-52, Waldemar Kramer, Frankfurt am Main.

Schulz, R., Harms, F.-J. & Felder, M. (2002): Die Forschungsbohrung Messel 2001: Ein Beitrag zur Entschlüsselung der Genese einer Ölschieferlagerstätte. *Zeitschrift für Angewandte Geologie* 4, 9-17.

Spicer, R. A. & Parrish, J. T. (1986): Paleobotanical evidence for cool North Polar climates in middle Cretaceous (Albian-Cenomanian) time. *Geology* 14, 703-706.

Sturm, M. (1971): Die eozäne Flora von Messel bei Darmstadt. I. Lauraceae. *Palaeontographica B* 134, 1-60.

Sturm, M. (1978): Maw contents of an Eocene horse (*Propalaeotherium*) out of the oil shale of Messel near Darmstadt. *Courier Forschungsinstitut Senckenberg* 30, 120-122.

Taiz, L. & Zeiger, E. (2006): Plant Physiology. 4th ed., 700 pp., Sinauer Associates, Sunderland, Massachusetts.

Tajika, E. (1998): Climate change during the last 150 million years: reconstruction from a carbon cycle model. *Earth and Planetary Sciences Letters* 160, 695-707.

Tans, P. (2010): Mauna Loa CO_2 annual mean data. National Oceanic & Atmospheric Administration (NOAA)/ Earth System Research Laboratory (ESRL); (www.esrl.noaa.gov/gmd/ccgg/trends/); Access Date: 25th May 2010.

Taylor, E. L., Taylor, T. N. & Krings, M. (2009): Paleobotany. The biology and evolution of fossil plants. 2nd ed., 1230 pp., Academic Press, Oxford.

Thorn, V. C., DeConto, R. (2006): Antarctic climate at the Eocene/Oligocene boundary - climate model sensitivity to high latitude vegetation type and comparisons with the palaeobotanical record. *Palaeogeography, Palaeoclimatology, Palaeoecology* 231, 134-157.

Thrasher, B. L. & Sloan, L. C. (2009): Carbon dioxide and the early Eocene climate of western North America. *Geology* 37, 807-810.

Tognetti, R., Minnocci, A., Penuelas, J., Raschi, A. & Jones, M. B. (2000): Comparative field water relations of three Mediterranean shrub species co-occurring at a natural CO_2 vent. *Journal of Experimental Botany* 51, 1135-1146.

Traiser, C., Klotz, S., Uhl, D. & Mosbrugger, V. (2005): Environmental signals from leaves - a physiognomic analysis of European vegetation. *New Phytologist* 166, 465-484.

Tripati, A., Backman, J., Elderfield, H. & Ferretti, P. (2005): Eocene bipolar glaciation associated with global carbon cycle changes. *Nature* 436, 341-346.

Uhl, D., Mosbrugger, V., Bruch, A. A. & Utescher, T. (2003): Reconstructing palaeotemperatures using leaf floras - case studies for a comparison of leaf margin analysis and the coexistence approach. *Review of Palaeobotany and Palynology* 126, 49-64.

Upchurch, G. R., Jr. & Dilcher, D. L. (1990): Cenomanian angiosperm leaf megafossils, Dakota Formation, Rose Creek locality, Jefferson County, southeastern Nebraska. *U.S. Geological Survey Bulletin* 1915, 1-52.

Utescher, T., Ivanov, D., Harzhauser, M., Bozukov, V., Ashraf, A. R., Rolf, C., Urbat, M. & Mosbrugger, V. (2009): Cyclic climate and vegetation change in the late Miocene of Western Bulgaria. *Palaeogeography, Palaeoclimatology, Palaeoecology* 272, 99-114.

Utescher, T., Mosbrugger, V. & Ashraf, A. R. (2000): Terrestrial climate evolution in Northwest Germany over the last 25 million years. *Palaios* 15, 430-449.

Wallmann, K. (2001): Controls on the Cretaceous and Cenozoic evolution of seawater composition, atmospheric CO_2 and climate. *Geochimica et Cosmochimica Acta* 65, 3005-3025.

Warnaar, J., Bijl, P. K., Huber, M., Sloan, L., Brinkhuis, H., Röhl, U., Sriver, R. & Visscher, H. (2009): Orbitally forced climate changes in the Tasman sector during the Middle Eocene. *Palaeogeography, Palaeoclimatology, Palaeoecology* 280, 361-370.

Wedmann, S., Bradler, S. & Rust, J. (2007): The first fossil leaf insect: 47 million years of specialized cryptic morphology and behaviour. *Proceedings of the National Academy of Sciences of the United States of America* 104, 565-569.

Wilde, V. & Micklich, N. (2007): Lebensraum Messel-See. Der See und seine Uferzonen. – In: Messel - Schätze der Urzeit (Begleitbuch zur Ausstellung "Messel on Tour"); edited by Gruber, G. and Micklich, N., 52-55 pp., Hessisches Landesmuseum Darmstadt (Theiss).

Wilde, V. & Süss, H. (2001): First wood with anatomically preserved details from the Middle Eocene oilshale of Messel (Hesse, Germany). *Acta Palaeobotanica* 41, 133-139.

Wilde, V. (1989): Untersuchungen zur Systematik der Blattreste aus dem Mitteleozän der Grube Messel bei Darmstadt (Hessen, Bundesrepublik Deutschland). *Courier Forschungsinstitut Senckenberg* 115, 1-213.

Wilde, V. (2005): The green Eocene. The diverse flora of a paratropical climate. *Vernissage UNESCO World Heritage Series* 21, 14-19.

Wilf, P., Wing, S. L., Greenwood, D. R. & Greenwood, C. L. (1998): Using fossil leaves as paleoprecipitation indicators: An Eocene example. *Geology* 26, 203-206.

Wilf, P. (1997): When are leaves good thermometers? A new case for Leaf Margin Analysis. *Paleobiology* 23, 373-390.

Wing, S. L. & Greenwood, D. R. (1993): Fossils and fossil climate: the case for equable continental interiors in the Eocene. *Philosophical Transactions of the Royal Society of London B* 341, 243-252.

Wolfe, J. A. (1979): Temperature parameters of humid to mesic forests of eastern Asia and their relation to forests of other regions of the Northern Hemisphere and Australasia. *U.S. Geological Survey Professional Paper* 1106, 1-37.

Woodward, F. I. & Bazzaz, F. A. (1988): The responses of stomatal density to CO_2 partial pressure. *Journal of Experimental Botany* 39, 1771-1781.

Woodward, F. I. (1987): Stomatal numbers are sensitive to increases in CO_2 concentration from pre-industrial levels. *Nature* 327, 617-618.

Wullschleger, S. D. (1993): Biochemical limitations to carbon assimilation in C_3 plants - a retrospectve analysis of the A/C_i curves from 109 species. *Journal of Experimental Botany* 44, 907-920.

Yang, J., Wang, Y. F., Spicer, R. A., Mosbrugger, V., Li, C. S. & Sun, Q. G. (2007): Climatic reconstruction at the Miocene Shanwang basin, China, using leaf margin analysis, CLAMP, Coexistence approach, and overlapping distribution analysis. *American Journal of Botany* 94, 599-608.

Yapp, C. J. (2004): $Fe(CO_3)OH$ in goethite from a mid-latitude North American Oxisol: Estimate of atmospheric CO_2 concentration in the Early Eocene "climatic optimum". *Geochimica et Cosmochimica Acta* 68, 935-947.

Zachos, J. C., Pagani, M., Sloan, L., Thomas, E. & Billups, K. (2001): Trends, rhythms, and aberrations in global climate 65 Ma to present. *Science* 292, 686-693.

Zachos, J. C., Stott, L. D. & Lohmann, K. C. (1994): Evolution of early Cenozoic marine temperatures. *Paleoceanography* 9, 353-387.

Zeebe, R. E., Zachos, J. C. & Dickens, G. R. (2009): Carbon dioxide forcing alone insufficient to explain Palaeocene-Eocene Thermal Maximum warming. *Nature Geoscience* 2, 576-580.

3 Publications

3.1 Konrad, W., Roth-Nebelsick, A., Grein, M. (2008)**: Modelling of stomatal density response to atmospheric CO_2. - Journal of Theoretical Biology 253: 638-658.**

Journal of Theoretical Biology 253 (2008) 638–658

Contents lists available at ScienceDirect

Journal of Theoretical Biology

journal homepage: www.elsevier.com/locate/yjtbi

Modelling of stomatal density response to atmospheric CO_2

W. Konrad *, A. Roth-Nebelsick, M. Grein

Institute for Geosciences, University of Tübingen, Sigwartstrasse 10, D-72076 Tübingen, Germany

ARTICLE INFO

Article history:
Received 2 August 2007
Received in revised form
11 March 2008
Accepted 27 March 2008
Available online 6 April 2008

Keywords:
Palaeoclimate
Gas exchange
Fossil plants
Stomatal conductance
Photosynthesis

ABSTRACT

Stomatal density tends to vary inversely with changes in atmospheric CO_2 concentration (C_a). This phenomenon is of significance due to: (i) the current anthropogenic rise in C_a and its impact on vegetation, and (ii) the potential applicability for reconstructing palaeoatmospheric C_a by using fossil plant remains. It is generally assumed that the inverse change of stomatal density with C_a represents an adaptation of epidermal gas conductance to varying C_a. Reconstruction of fossil C_a by using stomatal density is usually based on empirical curves which are obtained by greenhouse experiments or the study of herbarium material. In this contribution, a model describing the stomatal density response to changes in C_a is introduced. It is based on the diffusion of water vapour and CO_2, photosynthesis and an optimisation principle concerning gas exchange and water availability. The model considers both aspects of stomatal conductance: degree of stomatal aperture and stomatal density. It is shown that stomatal aperture and stomatal density response can be separated with stomatal aperture representing a short-term response and stomatal density a long-term response. The model also demonstrates how the stomatal density response to C_a is modulated by environmental factors. This in turn implies that reliable reconstructions of ancient C_a require additional information concerning temperature and humidity of the considered sites. Finally, a sensitivity analysis was carried out for the relationship between stomatal density and C_a in order to identify critical parameters (= small parameter changes lead to significant changes of the results). Stomatal pore geometry (pore size and depth) represents a critical parameter. In palaeoclimatic studies, pore geometry should therefore also be considered.

1. Introduction

Numerous studies have shown that stomatal densities vary inversely with changing atmospheric CO_2 (termed as C_a throughout the rest of this text). This has been demonstrated by observations on herbarium material (Woodward, 1987; Penuelas and Matamala, 1990; van de Water et al., 1994; Beerling and Kelly, 1997; Kouwenberg et al., 2003; Garcia-Amorena et al., 2006), greenhouse experiments (Woodward and Bazzazz, 1988; Kürschner et al., 1998; Royer et al., 2001; Teng et al., 2006) and palaeobotanical studies (Kürschner, 1996; Royer, 2001; Beerling and Royer, 2002; McElwain et al., 2002). Since stomata represent the gateways for gas exchange and are therefore involved in a plant's reaction to rising C_a level, stomatal responses to C_a are of general interest (Tricker et al., 2005). Furthermore, C_a-induced changes of stomatal density appear to represent a valuable proxy for palaeoatmospheric C_a. In various studies, stomatal density was used for reconstructing ancient C_a (Kürschner et al., 1996; Royer et al., 2001; Beerling, 2002; McElwain et al., 2002; Kürschner et al., 2008).

It is assumed that the reason for the $v(C_a)$-response is due to the adaptation of the epidermal permeability which is dependent on stomatal density and stomatal architecture (i.e. pore area and pore depth) to changing C_a-level (Woodward, 1987). This is reasonable since an increase in C_a increases the diffusional CO_2 flux into the leaf under a given stomatal conductance and CO_2 gradient. Perception of the C_a-signal was shown for *Arabidopsis thaliana* to occur in mature leaves, with the HIC gene being involved (Lake et al., 2001, 2002). If C_a increases, a plant can decrease its stomatal density while maintaining the required CO_2 influx. This is advantageous since stomata represent sites of water loss and construction expenses can be saved. It is therefore to be expected that adaptations of stomatal density to C_a are of selective value for a plant lineage. The current technique for reconstructing past CO_2 is based on empirically established transfer functions. The stomatal density (termed v in the following) of extant material grown under different C_a concentrations—herbarium material or potted plants grown in greenhouses—is obtained and a function is fitted to the data points (Beerling and Royer, 2002). Since the $v(C_a)$-response is species specific, a transfer function has to be established for each

* Corresponding author. Tel.: +49 7071 2973561.
E-mail addresses: wilfried.konrad@uni-tuebingen.de (W. Konrad), anita.roth@uni-tuebingen.de (A. Roth-Nebelsick), michaela.grein@t-online.de (M. Grein).

0022-5193/$ - see front matter © 2008 Elsevier Ltd. All rights reserved.
doi:10.1016/j.jtbi.2008.03.032

considered species. v is influenced by various environmental factors (temperature, humidity), the stomatal index (the number of stomata in relation to the number of epidermis cells) is therefore often applied as a surrogate parameter which shows less variation (Beerling et al., 1998; Poole and Kürschner, 1999).

There are, however, also reports about unchanging stomatal frequency under increasing C_a. For example, in two studies which were performed within the framework of FACE (free-air enrichment) experiments, no stable and/or significant decreases of stomatal density under elevated C_a could be observed (Reid et al., 2003; Tricker et al., 2005). On some occasions, stomatal density is even reported to increase with elevated C_a (Lawson et al., 2002). Since a decrease in stomatal conductance due to decreasing stomatal aperture under elevated CO_2 is almost always observed in experiments (Medlyn et al., 2001; Ainsworth and Long, 2005), it was suggested by the authors that C_a-induced changes of stomatal density require an evolutionary process (Reid et al., 2003; Tricker et al., 2005). This is consistent with results of a literature survey which indicate that the frequency of taxa which show an inverse change of stomatal density with C_a increases with increasing age of the material (fossil > subfossil > Herbarium > Recent material) (Royer, 2001). The empirical method of producing transfer functions makes no use of the assumed underlying biological mechanism of adaptation of the total epidermal conductance to C_a. An approach was devised by Wynn (2003) who applied the process of gas diffusion through the epidermis (and thus through the stomata) as basis for the curve fitting which is completed by obtaining empirical parameters from measured data.

In order to fully explore the $v(C_a)$-responses it is indispensable to consider the process of photosynthesis since both transpiration and assimilation are affected by stomatal conductance and therefore by stomatal density. A mechanistic model of the $v(C_a)$-response would be desirable, because: (i) ecophysiological aspects of the $v(C_a)$-response could be explored, (ii) the tacitly assumed evolutionary optimisation process of the response in the case of fossil material could be described (the current $v(C_a)$-response data represent phenotypic reactions and it is not clear whether they are valid for responses on the evolutionary level) and (iii) sensitivity analyses would be possible which provide insight into the reliability of the approach, identify critical parameters and supply a meaningful error margin. In this contribution, it will be attempted to model the $v(C_a)$-response by coupling diffusion and photosynthesis. The approach is completed by including an optimisation principle which introduces an interrelationship between gas exchange and the availability of water. Finally, the model will be applied to *Ginkgo biloba*. This species was used repeatedly for reconstructing ancient C_a levels and various data sets are therefore available (Sun et al., 2003; Royer et al., 2001).

2. The model

2.1. Diffusion of water vapour and carbon dioxide

The movement of water vapour and carbon dioxide into and out of plants is governed by the process of diffusion, described by Fick's first law:

$$\mathbf{j} = -S \operatorname{grad} c \tag{1}$$

In the following, c stands either for the concentration w of water vapour or the concentration C of carbon dioxide. The Diffusion equation (also known as Fick's second law) is derived from applying the principle of mass conservation to Fick's first law. It reads as

$$\Sigma = \frac{\partial c}{\partial t} + \operatorname{div}(S \operatorname{grad} c) \tag{2}$$

If the source (or sink) term $\Sigma = \Sigma(x, y, z, t, c)$ is independent of c and if the effective conductance $S = S(x, y, z)$ and appropriate boundary conditions for c are prescribed, the diffusion Eq. (2) has exactly one solution for the concentration $c = c(x, y, z, t)$ of water vapour or carbon dioxide. Once $c = c(x, y, z, t)$ is calculated the flux $\mathbf{j}(x, y, z, t)$ follows from (1).

It is impossible to solve (2) in all generality for realistic conditions, because the complex network of voids and channels which form the intercellular air space implies very complex boundary conditions for (2). If, however, we claim that c and $\mathbf{j}$ shall be correct only down to dimensions of a few diameters of a typical cell, we can employ approximations which lead to symmetries that allow for drastic simplifications in (2) and (1). In that case, we can apply (i) the porous medium approach and assume that (ii) the effective conductance S remains constant within the functionally different tissue layers of a plant leaf. We may furthermore assume (iii) stationary conditions. These approximations are discussed in Appendix A.1.

After applying the various approximations, the differential equation (2) simplifies to

$$\Sigma = S\left(\frac{\partial^2 c}{\partial x^2} + \frac{\partial^2 c}{\partial y^2} + \frac{\partial^2 c}{\partial z^2}\right) \tag{3}$$

The source (or sink) term Σ (if present) and the concentration c are functions of the coordinates (x, y, z). Leaves are flat objects whose lateral dimensions (several centimeters) are about a factor 10^4 greater than stomatal radii (a few micrometers). This implies, together with the layered structure of leaves:

(i) The general direction of the diffusional flux is perpendicular to the leaf plane, i.e. parallel to the x-axis, if we orient the coordinate system such that the y- and z-axes are parallel to the leaf plane.
(ii) In the coordinate system defined in (i) all quantities appearing in Eqs. (3) and (1) depend only on the coordinate x, but not on y or z.

Then the three-dimensional partial differential equation (3) reduces to a one-dimensional ordinary differential equation for $c(x)$

$$\Sigma(x) = S\frac{\mathrm{d}^2 c(x)}{\mathrm{d}x^2} \tag{4}$$

which has to be solved separately for each layer involved in gas diffusion: assimilation layer (*as*), stomatal layer (*sl*) and boundary layer (*bl*). Fick's first law (1) simplifies then to

$$j(x) = -S\frac{\mathrm{d}c}{\mathrm{d}x}(x) \tag{5}$$

where the flux j is directed parallel to the x-axis.

2.2. Sources and sinks

Within boundary layer and stomatal layer we may assume $\Sigma(x) = 0$, both for CO_2- and H_2O-molecules. With respect to sources and sinks within the assimilation layer, the following simplification was applied. The plane which is located near the upper boundary of the assimilation layer and parallel to the leaf surface (the broken line, denoted c_i in Fig. 1) serves as (idealised) source of water vapour and as sink for carbon dioxide molecules. Within the assimilation layer (as depicted in Fig. 1) holds $\Sigma(x) = 0$.

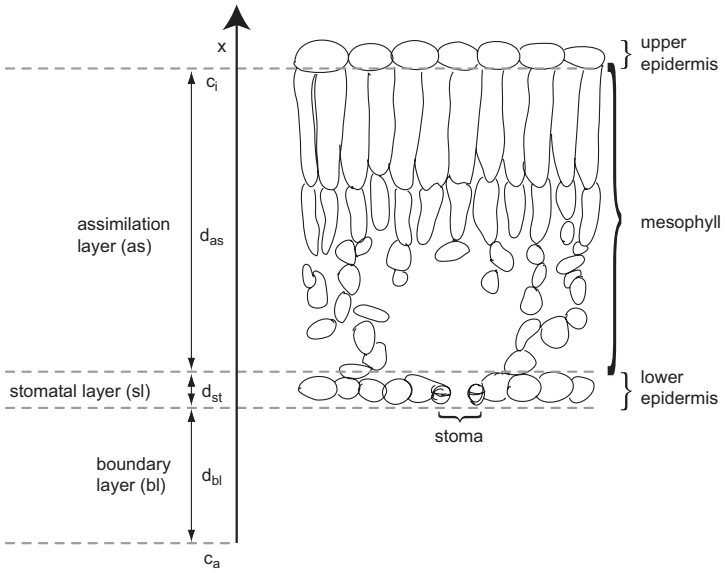

Fig. 1. Schematic cross section through a leaf (based on a drawing by Birgit Binder, Tübingen). The picture shows the different layers of a typical angiosperm leaf and their representation within the model. The assimilation layer (*as*) represents the mesophyll and the stomatal layer (*sl*) includes epidermis and stomata. The boundary layer (*bl*) located at the (lower) leaf surface is also considered in the model. c_a denotes either the atmospheric CO_2 concentration C_a or the atmospheric humidity w_a. c_i refers to C_i and w_i, the internal CO_2 and H_2O concentrations. d_{as}, d_{st} and d_{bl}: thickness of assimilation layer, stomatal layer and boundary layer, respectively.

In this case Eq. (4) becomes *very* simple

$$0 = S\frac{\mathrm{d}^2 c}{\mathrm{d}x^2}(x) \tag{6}$$

with the readily obtained solutions

$$c_{as}(x) = a_{as}x + b_{as} \quad c_{st}(x) = a_{st}x + b_{st} \quad c_{bl}(x) = a_{bl}x + b_{bl} \tag{7}$$

and, from Eq. (5),

$$j_{as}(x) = -S_{as}a_{as} \quad j_{st}(x) = -S_{st}\,a_{st} \quad j_{bl}(x) = -S_{bl}\,a_{bl} \tag{8}$$

where it is understood that positive fluxes j_k ($k = as, sl, bl$) flow parallel, negative fluxes antiparallel to the x-axis (c.f. Fig. 1). The a_k and b_k are arbitrary constants. Their values are calculated from requiring: (i) that the c_k and j_k (from Eqs. (7) and (8)) are continuous at the planes separating adjacent boundary layers, and, (ii) that c_{bl} and c_{as} attain the values c_a and c_i, respectively, at the lower and upper boundary of the region depicted in Fig. 1.

The effective conductances S_k differ from layer to layer. They are defined in analogy to (A.2) as

$$S_{as} := D\frac{n_{as}}{\tau_{as}^2} \tag{9}$$

and similar expressions for (*sl*) and (*bl*). D denotes either D_{H_2O} or D_{CO_2}.

Applying the continuity conditions we find: (i) that the flux does *not* depend explicitly on x, and, (ii) that $j_{as} = j_{st} = j_{bl} =: j$. It is given as

$$j = \frac{D(c_i - c_a)}{\left(\dfrac{d_{bl}\tau_{bl}^2}{n_{bl}} + \dfrac{d_{st}\tau_{st}^2}{n_{st}} + \dfrac{d_{as}\tau_{as}^2}{n_{as}}\right)} \tag{10}$$

The quantities in (10) can be specified more explicitly (c.f. Fig. 1):

- *Boundary layer*: Obviously, porosity and tortuosity attain the very simple values

$$n_{bl} = 1 \quad \text{and} \quad \tau_{bl} = 1 \tag{11}$$

d_{bl} depends (see Nobel, 1999) on the wind velocity u_{wind} and a typical leaf length l according to the empirical formula (m and s denote the units meter and second, respectively)

$$d_{bl} = 4 \times 10^{-3}\,\frac{m}{\sqrt{s}}\sqrt{\frac{l}{u_{wind}}} \tag{12}$$

- *Stomatal layer*: The porosity of the stomatal layer can be expressed in terms of the cross-sectional area of a stoma a_{st} and the stomatal density v as

$$n_{st} = a_{st}v \tag{13}$$

Since the stomatal channels are straight openings we find for their tortuosity

$$\tau_{st} = 1 \tag{14}$$

d_{st} is a combination of the geometrical thickness d_{st}^{geom} and a correction $\sqrt{a_{st}/\pi}$ which is due to the fact that the surfaces of constant CO_2 and H_2O concentration bulge out from the stomata into boundary layer and intercellular airspace (see Nobel, 1999). Thus,

$$d_{st} = d_{st}^{geom} + \sqrt{a_{st}/\pi} \tag{15}$$

In the following, the model will be developed by using v and not the stomatal index which is preferred in most empirical approaches. The reason for this is simply that v has a direct relationship to gas exchange and not the stomatal index.

- *Assimilation layer*: Values for porosity, tortuosity and thickness of the layer should be obtained by measurements from specimen. Typical values are of the order of $n_{as} \approx 0.35$, $\tau_{as} \approx 1.571$ and $d_{as} \approx 200\,\mu\mathrm{m}$.

Insertion of expressions (11), (13) and (14) into Eq. (10) results in a somewhat simplified, intermediate version of (10)

$$j = \frac{va_{st}D(c_a - c_i)}{\left[d_{bl} + d_{as}\frac{\tau_{as}^2}{n_{as}}\right]va_{st} + d_{st}} \tag{16}$$

Writing down expression (16) separately for water vapour ($c_i = w_i$, $c_a = w_a$ and $D = D_{H_2O}$) and carbon dioxide ($c_i = C_i$, $c_a = C_a$ and $D = D_{CO_2}$) results in

$$j_{H_2O} = \frac{va_{st}D_{H_2O}}{\left[d_{bl} + d_{as}\frac{\tau_{as}^2}{n_{as}}\right]va_{st} + d_{st}} \times (w_a - w_i) \tag{17}$$

and

$$j_{CO_2} = \frac{va_{st}D_{CO_2}}{\left[d_{bl} + d_{as}\frac{\tau_{as}^2}{n_{as}}\right]va_{st} + d_{st}} \times (C_a - C_i) \tag{18}$$

where d_{bl} and d_{st} are as given in (12) and (15), respectively. To keep notation simple we define the first factor on the right-hand side of (18) as the total conductance with respect to CO_2

$$g = \frac{va_{st}D_{CO_2}}{\left[d_{bl} + d_{as}\frac{\tau_{as}^2}{n_{as}}\right]va_{st} + d_{st}} \tag{19}$$

Employing the definition $a := D_{H_2O}/D_{CO_2}$ the total conductance with respect to H_2O (i.e. the first factor on the right-hand side of (17)) becomes ag.

Since we restrict our model to stationary conditions all carbon dioxide molecules entering the plant become eventually assimilated, hence $j_{CO_2} = A$ where A denotes the assimilation rate. Eq. (18) can now be rewritten in the more compact form

$$A = g(C_a - C_i) \tag{20}$$

Stationary conditions imply also $-j_{H_2O} = E$, with E representing the transpiration rate. The minus sign in front of j_{H_2O} ensures that E attains positive values. Because w_i is defined as the water vapour concentration around the transpiring mesophyll cells it equals w_{sat}, the saturation value of water vapour concentration in air (equivalent to 100% relative humidity). This depends on temperature T (see Appendix B.3). Inserting expression (19), $a = D_{H_2O}/D_{CO_2}$ and the equality $w_i = w_{sat}$ into (17) we find

$$E = ag(w_{sat} - w_a) \tag{21}$$

In contrast to (21), expression (20) represents only an intermediate result: it relates—in analogy to (21)—A to C_i. C_i, however, does not attain a fixed value as is the case with w_{sat}. It is rather coupled to A by a second relation expressing the intensity of photosynthesis. In other words, C_i has to be known in order to calculate A (Katul et al., 2000). This will be further discussed in the following section.

2.3. Coupling of diffusion and assimilation model

We use the Farquhar model of assimilation (see Farquhar et al., 1980, 2001):

$$A = \left(1 - \frac{\Gamma}{C_i}\right)\min\{W_c, W_j\} - R_d \tag{22}$$

with

$$W_c := V_{max}\frac{C_i}{C_i + K_c\left(1 + \frac{p_o}{K_o}\right)}$$

$$W_j := \left(\frac{2}{9}J\right)\frac{C_i}{C_i + \frac{7}{3}\Gamma}$$

where

$$J := \frac{Q_2 + J_{max} - \sqrt{(Q_2 + J_{max})^2 - 4\Theta_{PSII}Q_2J_{max}}}{2\Theta_{PSII}}$$

and

$$Q_2 := Q\alpha_l\Phi_{PSII,max}\beta \tag{23}$$

The expression $\min\{W_c, W_j\}$ denotes the smaller of W_c and W_j for given values of C_i and J. The variables used in (22) are listed in Table 1. Defining

$$q = \begin{cases} V_{max} & \text{if } W_c < W_j \\ \frac{2}{9}J & \text{if } W_c > W_j \end{cases} \tag{24}$$

and

$$K = \begin{cases} K_c\left(1 + \frac{p_o}{K_o}\right) & \text{if } W_c < W_j \\ \frac{7}{3}\Gamma & \text{if } W_c > W_j \end{cases} \tag{25}$$

expression (22) can be written in the more compact form

$$A = q\frac{C_i - \Gamma}{C_i + K} - R_d \tag{26}$$

Most of the variables defining photosynthesis depend on the leaf temperature T (measured in Kelvin). In order to quantify their temperature dependence we use the parametrisations given by Bernacchi et al. (2003) (see Appendix B.1).

We resume now the discussion of expression (20) from the end of Section 2.2. Having derived now a second relation between A and C_i we can use (20) and (26) to eliminate C_i from the function representing A. Equating expressions (20) and (26) leads to a quadratic equation for C_i with solution

$$C_i = \frac{1}{2g}\{g(C_a - K) - (q - R_d) \pm \sqrt{[g(C_a - K) - (q - R_d)]^2 + 4g(gKC_a + q\Gamma + KR_d)}\} \tag{27}$$

Since the solution with the minus sign in front of the root symbol leads to negative concentrations C_i we discard it. Employing the meaningful solution to eliminate C_i from Eq. (20) in favour of C_a and g we arrive at the following expression for the

Table 1
Parameters defining photosynthesis

Symbol	Unit	Quantity
A	μmol/m²/s	Assimilation rate per leaf area
J	μmol/m²/s	Rate of electron transport
J_{max}	μmol/m²/s	Maximum rate of electron transport
K_o	mmol/mol	Michaelis–Menten constant of oxygenation
K_c	μmol/mol	Michaelis–Menten constant of carboxylation
p_o	mmol/mol	Partial pressure of oxygen
Q	μmol/m²/s	Photosynthetic photon flux density
R_d	μmol/m²/s	Mitochondrial respiration rate in the light
V_{max}	μmol/m²/s	Maximum RuBP-saturated rate of carboxylation
W_c	μmol/m²/s	Rubisco limited rate of carboxylation
W_j	μmol/m²/s	RuBP-limited rate of carboxylation
α_l	–	Total leaf absorbance
β	–	Fraction of absorbed quanta reaching PSII
Γ	μmol/mol	CO_2-compensation point in the absence of dark respiration
Θ_{PSII}	–	Convexity term for electron transport rates
$\Phi_{PSII,max}$	–	Maximum dark-adapted quantum yield of PSII

assimilation rate:

$$A = \tfrac{1}{2}\{g(C_a + K) + (q - R_d) - \sqrt{[g(C_a - K) - (q - R_d)]^2 + 4g(gKC_a + q\Gamma + KR_d)}\} \tag{28}$$

2.4. Derivation of stomatal conductance from the optimisation principle

If the assimilation rate A is known, expression (28) can be solved for g which leads—in connection with definition (19)—to the desired relationship between v and C_a. In general, however, A is *not* known independently from (28). The information which is necessary to calculate $v(C_a)$ can, however, be supplied by an optimisation principle acting on the gas exchange described in Eqs. (21) and (28).

In habitats where water supply is not unlimited, it is imperative for plants to maximise assimilation while keeping the amount of transpired water low. It is generally assumed that stomata behave in an optimal way in order to maximise carbon gain while minimising transpiration (Cowan and Farquhar, 1977). Hari et al. (1986) and Mäkelä et al. (1996) suggested that plants optimise assimilation and transpiration in a way that takes into account diurnal or even seasonal changes of environmental conditions. An optimisation principle considering these aspects was successfully applied to stands of Scots Pine by Berninger et al. (1996) and *Pinus sylvestris* by Aalto and Juurola (2002). The rationale behind this optimisation scheme is that optimal behaviour has to take into account the availability of water (a plant cannot use more water in a certain time period than is available during this time period) and the influence of parameters like humidity, temperature and irradiance. Formally, such a behaviour can be expressed by the statements

$$\int_{\Delta t} A(t)\,\mathrm{d}t = \text{maximum} \tag{29}$$

and

$$\int_{\Delta t} E(t)\,\mathrm{d}t = W_0 \tag{30}$$

which have to be obeyed simultaneously (Mäkelä et al., 1996). Δt represents a reasonable time span (like one day or one season) and W_0 denotes the water supply (per leaf area) available during this time span. Furthermore, the parameters w_a, q, Γ, K and g appearing in expressions (21) and (28) for E and A depend either explicitly on time t, or implicitly via the time-dependent temperature $T(t)$.

Since a plant can regulate its stomatal conductance by adjusting stomatal density v or stomatal area a_{st} (or both) we consider the total conductance g which encompasses both effects (see Eq. (19)) as the variable whose temporal behaviour is to be calculated from the optimisation procedure. The time dependence of the quantities w_a, q, Γ and K are, however, assumed to be explicitly or implicitly prescribed.

In order to calculate the conductance $g(t)$ which maximises $\int_{\Delta t} A(t)\,\mathrm{d}t$ under the constraint $\int_{\Delta t} E(t)\,\mathrm{d}t = W_0$ we apply the method of Lagrangian multipliers (from the Calculus of Variation of Mathematical Physics, see e.g. Arfken, 1970, for slightly different formulations leading to the same results see Cowan, 1977; Cowan and Farquhar, 1977; Farquhar et al., 2002; Buckley et al., 2002; Mäkelä et al., 1996; Berninger et al., 1996). The optimisation procedure starts with forming the expression

$$\begin{aligned} L &= A - \lambda E \\ &= \frac{1}{2g}\{g(C_a + K) + (q - R_d) \\ &\quad - \sqrt{[g(C_a - K) - (q - R_d)]^2 + 4g(gKC_a + q\Gamma + KR_d)}\} \\ &\quad - \lambda a g(w_{sat} - w_a) \end{aligned} \tag{31}$$

where the second version emerges from substitution of A and E by expressions (28) and (21). (In mathematical terminology, the arbitrary constant λ is called the Lagrangian multiplier and $\int_{\Delta t} E(t)\,\mathrm{d}t = W_0$ is the constraint of the problem.) Then we calculate

$$\frac{\mathrm{d}}{\mathrm{d}t}\frac{\partial L}{\partial \dot{g}} = \frac{\partial L}{\partial g} \tag{32}$$

where $\dot{g} \equiv \mathrm{d}g/\mathrm{d}t$. The last equation constitutes an ordinary differential equation of second order for the conductance $g(t)$. Once the conductance $g(t)$ is known, the Lagrangian multiplier λ can—in principle—be calculated by evaluating the constraint $\int_{\Delta t} E(g(t))\,\mathrm{d}t = W_0$.

Inspection of expressions (28) and (21) shows that both A and E depend on g but neither of them depends on $\dot{g}$. Hence, Eq. (32) reduces to

$$0 = \frac{\partial L}{\partial g} \tag{33}$$

This implies two important simplifications: (i) the differential equation (32) of the generic case reduces to a mere algebraic equation for $g(t)$, and (ii) in order to solve Eq. (33) for $g(t)$ the time dependencies of the quantities w_a, q, Γ and K need not to be known explicitly.

Applying the optimisation scheme to Eq. (31) results in

$$\begin{aligned} g = \frac{1}{(C_a + K)^2}\Bigg\{ &\sqrt{\frac{q(K + \Gamma)[C_a(q - R_d) - (q\Gamma + KR_d)]}{[C_a + K - \lambda a(w_{sat} - w_a)]\lambda a(w_{sat} - w_a)}} \\ &\times [C_a + K - 2\lambda a(w_{sat} - w_a)] \\ &+ (q - R_d)C_a - (q\Gamma + KR_d) - q(K + \Gamma)\Bigg\} \end{aligned} \tag{34}$$

If the time-dependencies of insolation $Q(t)$, temperature $T(t)$ and atmospheric water vapour concentration $w_a(t)$ are explicitly known the constant λ (on which g depends) can be expressed in terms of the amount of water W_0 available during the time span Δt by inserting expression (34) into (21) and integrating the result according to (30). Since the photosynthetic parameters q, R_d, K and Γ vary via $T(t)$ also with time t, it is usually impossible to perform the integration in (30). From expression (30) it is, however, clear that λ is connected with water availability. The behaviour of $g(\lambda)$ (see Fig. 2) suggests that λ represents—at least in a loose sense—the "cost of water": small values of λ are related to high values of the optimum conductance g which indicates that high transpiration values are tolerable. This implies in turn that water is easily (without high costs) supplied. g is lower for higher values of λ, meaning that the necessity to avoid transpiration is more severe. In other words, water is more expensive.

It is possible to express λ in terms of quantities characterising the soil on which the tree grows and the hydraulic properties of its water transport system between roots and leaves. This is done in Appendix C.

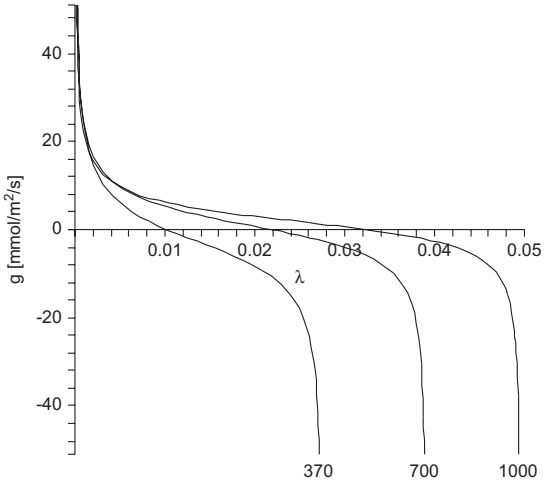

Fig. 2. Optimum conductance g as a function of the Lagrangian multiplier λ for $C_a = 370$, 700 and 1000 μmol/mol. Only values of λ between the pole at $\lambda = 0$ (common to the three curves) and their zeros (where the curves intersect the λ-axis) are meaningful since only they lead to positive values of the conductance g. The acceptable range of λ increases with the atmospheric CO_2 concentration C_a.

The optimum assimilation rate A related to g follows from substitution of expression (34) into Eq. (28)

$$A = \frac{1}{(C_a + K)}\left\{C_a(q - R_d) - (q\Gamma + KR_d) - \sqrt{\frac{q(K+\Gamma)[C_a(q-R_d) - (q\Gamma + KR_d)]\lambda a(w_{sat} - w_a)}{(C_a + K - \lambda a(w_{sat} - w_a))}}\right\} \tag{35}$$

2.5. Relation between stomatal density and atmospheric CO_2

In order to obtain the desired $v(C_a)$-relationship, we insert (15) into (19) and solve for v

$$v = \frac{1}{a_{st}}\left(\frac{\left[d_{st}^{geom} + \sqrt{\frac{a_{st}}{\pi}}\right]g}{D_{CO_2} - \left[d_{bl} + d_{as}\frac{\tau_{as}^2}{n_{as}}\right]g}\right) \tag{36}$$

Then we substitute expression (12)

$$d_{bl} = 4 \times 10^{-3}\frac{m}{\sqrt{s}}\sqrt{\frac{l}{u_{wind}}}$$

and $g(C_a)$ from (34). The result is quite complex and the complexity increases if the temperature dependencies of the various parameters are included (see appendix).

In order to use (36) to exploit fossil values of v as a proxy for palaeoatmospheric C_a it is necessary to realise that two different time scales are involved in (36) which correspond to the two different options a plant has to regulate stomatal conductance $g(t)$: A plant can (i) open and close its stomata or it can (ii) create additional stomata, discard existing ones, and/or modify the dimensions of the stomatal pores (i.e. d_{st}^{geom}, w_{st}, h_{st}). Since the second option is related to morphological modifications, its realisation requires more time and expenditure than the first one. Hence, it is plausible to assume that (i) variations of stomatal aperture a_{st} are caused by the diurnal variations of temperature, insolation, atmospheric humidity and wind speed and by short-term variations of C_a while (ii) variations of v are due to long-term variations of the atmospheric CO_2-concentration. The time-scales of both variations differ by three orders of magnitude, i.e. they can be treated as being effectively independent of one another.

If we want ro reconstruct palaeoatmospheric CO_2 from fossil stomatal density we are interested only in the long-term variations of v. Hence, we have to separate both effects. This can be achieved as follows. The maximum stomatal area a_{st}^{max} corresponds to the maximum conductance g_{max} which may be temporarily realised if the partially interacting quantities solar insolation, temperature and humidity attain favourable values. Under such conditions relation (36) takes the form

$$v = \frac{1}{a_{st}^{max}}\left(\frac{\left[d_{st}^{geom} + \sqrt{\frac{a_{st}^{max}}{\pi}}\right]g_{max}}{D_{CO_2} - \left[d_{bl} + d_{as}\frac{\tau_{as}^2}{n_{as}}\right]g_{max}}\right) \tag{37}$$

with

$$d_{bl} = 4 \times 10^{-3}\frac{m}{\sqrt{s}}\sqrt{\frac{l}{u_{wind}}}$$

Principally, the (short-term) maximum conductance g_{max} and the time t_{max} when it occurs can be calculated from Eq. (34), provided the diurnal variations of insolation, temperature and humidity (resp. $Q(t)$, $T(t)$ and $w_{rel}(t)$, where $w_{rel} = w_a/w_{sat}$) are known (e.g. as illustrated by Fig. 5). Because the diurnal variation of g involves a much shorter time-scale than changes in stomatal density caused by changes in the atmospheric CO_2-concentration, C_a can be held constant when t_{max} is calculated. In principle, this can be done by first solving $dg/dt = 0$ for $t = t_{max}$ and then inserting t_{max} back into expression (34). The resulting relation $g_{max}(C_a)$ is not dependent on time. Substitution of $g_{max}(C_a)$ into (37) concludes the derivation of $v(C_a)$.

In reality, this course of action is not feasible because g is usually a very complicated function of t. We may, however, proceed as follows (in order to illustrate this procedure we refer to Figs. 3 and 4 which will be properly introduced and discussed in Section 3.2): Fig. 3 depicts the "mountain crests" of the functions $g(t, C_a)$ (upper row of Fig. 4) which represent the functions $g_{max}(C_a)$ used in (37). The curves indicate at what time of

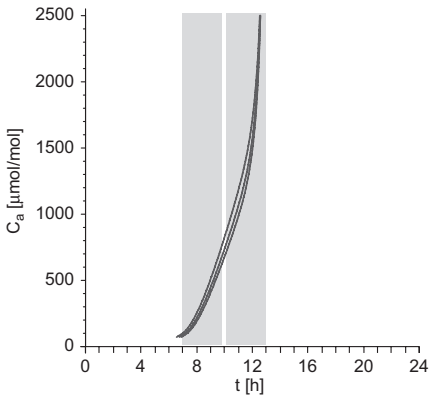

Fig. 3. Projections of the "mountain crests" of the functions $g(t, C_a)$ (upper row of Fig. 4) along the g-axis into the (t, C_a)-plane (corresponding—from right to left—to $\lambda = 0.0005$, 0.001 and 0.002). The curves indicate at what time of day—depending on C_a — the optimum stomatal conductance g attains its maximum value g_{max}. For $C_a \lessapprox 700$ μmol/mol this happens between $t \approx 7$ and 10 h, for $C_a \gtrapprox 700$ μmol/mol at a time between $t \approx 10$ and 13 h. The temporal intervals (grey areas) shown here are the same as in Fig. 5, depicting the diurnal variations of $Q(t)$, $T(t)$ and $w_{rel}(t)$. $t = 0$ and $t = 24$ denote midnight.

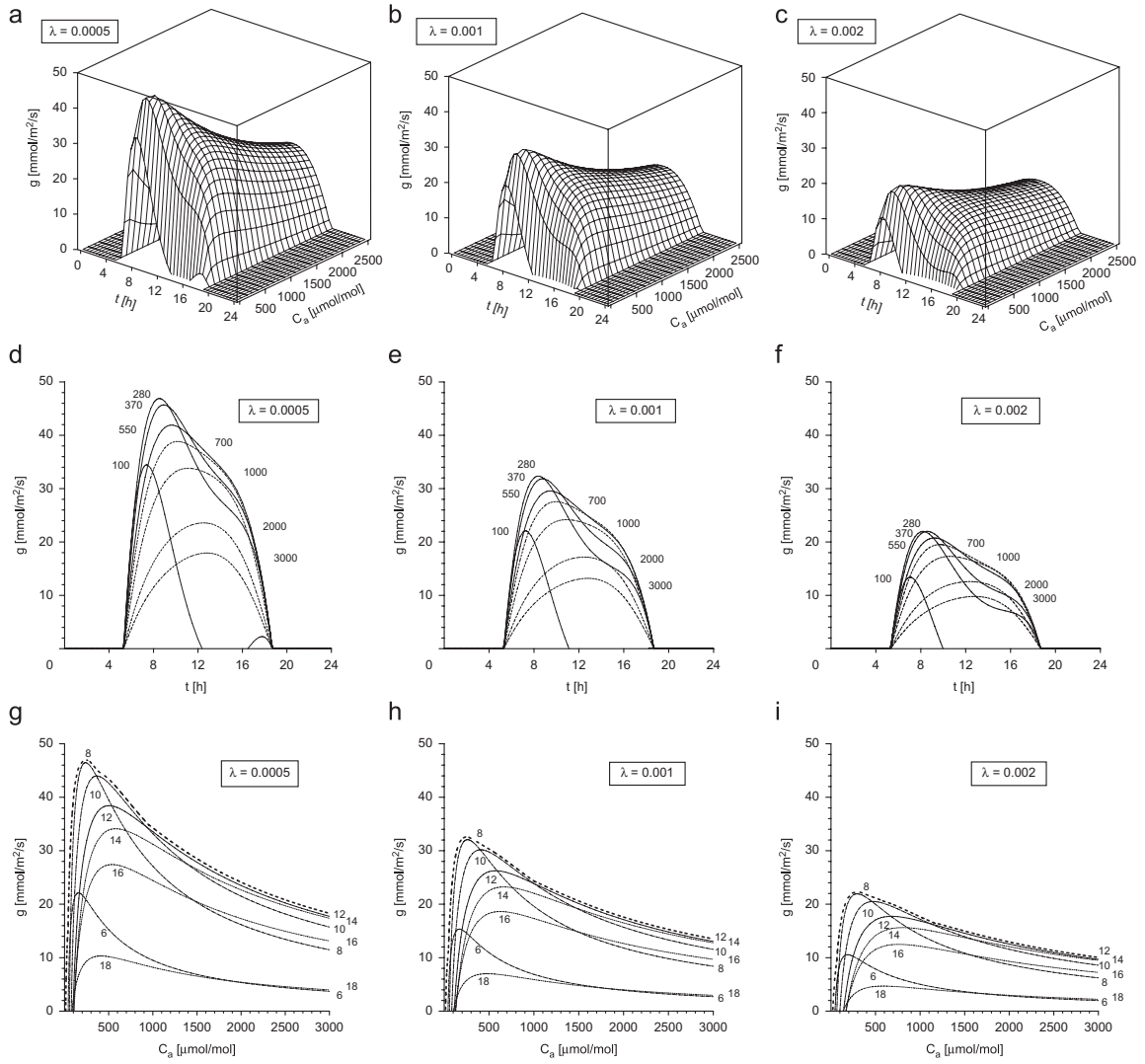

Fig. 4. *Upper row*: Conductance $g(t, C_a)$ as a function of t (diurnal variations) and atmospheric CO_2 concentration C_a for (a) $\lambda = 0.0005$, (b) $\lambda = 0.001$ and (c) $\lambda = 0.002$ (λ represents the cost of water). $g(t, C_a)$ is calculated according to (34) from diurnal variations of $Q(t)$, $T(t)$ and $w_a(t)$ as shown in Fig. 5. C_a is given in units of µmol/mol. $t = 0$ and 24 denote midnight. *Centre row*: Slices through the three-dimensional surfaces $g(t, C_a)$ of the upper row with C_a held constant. Numbers close to the maxima of the curves give C_a in units of µmol/mol (700, 1000, 2000 and 3000 µmol/mol correspond to the broken curves). Obviously, small values of λ (i.e. cheap water) are in favour of high values of optimum conductance g. *Lower row*: Slices through the three-dimensional surfaces $g(t, C_a)$ of the upper row with t held constant. Numbers close to the curves indicate the time of day. The assumption of darkness between 19 h in the evening and 5 h in the morning implies $g = 0$. Broken lines indicate the envelopes around the families of curves. The envelopes represent the functions $g_{max}(C_a)$ used in (37). Geometrically, they can be obtained by projecting the "crests" of the "mountains" of the upper row along the t-axis into the (g, C_a)-plane.

day—depending on C_a—the optimum stomatal conductance g attains its maximum value g_{max}. For $C_a \lessapprox 700$ µmol/mol this happens between $t \approx 7$ and 10 h, for $C_a \gtrapprox 700$ µmol/mol at a time between $t \approx 10$ and 13 h. Comparison of the grey areas in Fig. 3 with their counterparts in Fig. 5 allows to identify combinations of temperature and humidity ranges which correspond approximately to the maximum stomatal conductance. Insertion of these values of T and w_{rel} into (34) produces g_{max} which is then used in expression (37) in order to obtain $v(C_a)$.

Fig. 5 indicates also that maximum stomatal conductance is coupled with a high flux density Q of photosynthetic active photons. Then the first alternative of expressions (24) and (25) is valid, implying, that we need to know only two assimilation parameters explicitly in order to calculate g_{max}, namely $V_{\max,25\,^\circ C}$ and $R_{d,25\,^\circ C}$.

Summarising these results: In order to calculate stomatal density v as a function of atmospheric CO_2 concentration C_a from Eq. (37) we need to know (or estimate) the following parameters:

(i) The assimilation parameters q, R_d, K and Γ.
(ii) The average of the diurnal temperature variation $T(t)$ during the vegetation period.

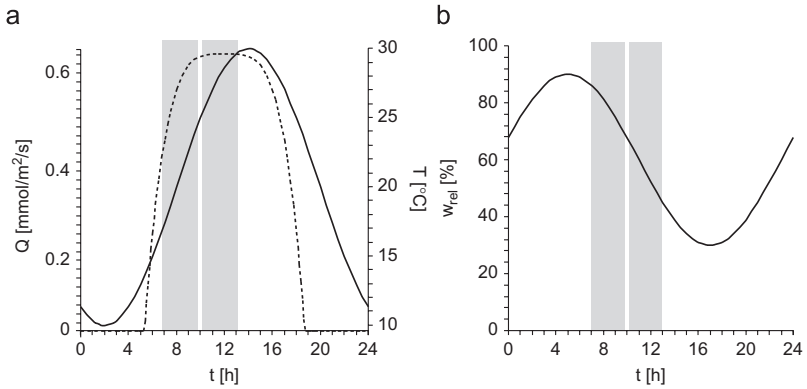

Fig. 5. Diurnal variations used as input functions for the stomatal conductance $g(t, C_a)$ shown in Fig. 4 ($t = 0$ and 24 h denote midnight): (a) photon flux density $Q(t)$ (dotted line) and temperature $T(t)$ (solid line) and (b) relative atmospheric humidity $w_{rel}(t)$. The input functions determine the time dependence of $g(t, C_a)$, either directly or via the temperature dependencies of the assimilation parameters q, R_d, K and Γ which occur in $g(t, C_a)$ (see (24), (25), (B.1) and (B.4)). The temporal intervals (grey areas) shown here are the same as in Fig. 3.

(iii) The average of the diurnal variation of the (relative) atmospheric humidity $w_{rel}(t)$ during the vegetation period.
(iv) The "cost of water" λ during the vegetation period.
(v) The average wind speed u_{wind} during the vegetation period.
(vi) The leaf anatomic parameters: maximum stomatal area a_{st}^{max}, depth of stomatal opening d_{st}^{geom}, thickness of assimilation tissue d_{as}, tortuosity of assimilation tissue τ_{as}, porosity of assimilation tissue n_{as} and average leaf length l (implying—together with u_{wind}—the thickness of the boundary layer d_{bl}).

In order to calculate g_{max} from (34) only the quantities (i)–(iv) are required. The first of these is species specific, the other three describe the environment.

The leaf anatomic parameters in (vi) can be obtained from fossil material. The value of a_{st}^{max}, however, has to be borrowed from extant counterparts by determining the maximum pore opening that is possible. Also the assimilation parameters in (i) have to be taken from an extant representative of the plant under consideration. The environmental parameters in (ii)–(v) are probably the most difficult to obtain because they are part of the climatic scenario one wants to unravel.

3. Exploration of model behaviour

3.1. Model parametrisation with G. biloba

The photosynthetic, environmental and anatomical parameters (and their sources) used to calculate $g(C_a)$-curves (from Eq. (34)) and $v(C_a)$-curves (from Eq. (37)) for *G. biloba* are provided in Table 2.

In the following it will be explained how the photosynthetic quantities and λ, the cost of water, have been obtained from measurements of physiological parameters of an adult *Ginkgo* in the field performed by Overdieck and Strassemeyer, 2005 (see Figs. 6 and 7 and Tables 3 and 4). These measurements were carried out at a temperature of $T = 27.3\,^{\circ}$C and at a relative atmospheric humidity of 50%.

3.1.1. Calculation of q, R_d, K and Γ

In order to calculate q, R_d, K and Γ we apply the method of least squares to Eq. (26)

$$A(C_i) = q\frac{C_i - \Gamma}{C_i + K} - R_d \tag{38}$$

q and K were defined in Eqs. (24) and (25). If the rate of carboxylation is limited by Rubisco activity and not by insolation—which we may assume in our case, see Fig. 5—they are given as $q = V_{max}$ and $K = K_c(1 + p_o/K_o)$. First, we form from Eq. (38) and the six data points $(C_{i,k}, A_k)$ of Table 3 the sum

$$\sigma_A^2 = \sum_k [A(C_{i,k}) - A_k]^2 \tag{39}$$

σ_A^2 constitutes a measure for the deviation of the curve $A(C_i)$ from the data points $(C_{i,k}, A_k)$, $(k = 1 \ldots 6)$. It depends on the four unknown quantities q, R_d, K and Γ. In order to obtain a "best fit" of the curve representing Eq. (38) to the data points, we have to locate the minimum of σ_A^2 ("nonlinear regression"). The minimum is characterised by the value of the quadruple (q, R_d, K, Γ) for which the four partial derivatives of σ_A^2 with respect to q, R_d, K and Γ vanish simultaneously. This system of four equations can be readily solved. Employing the temperature dependencies given by Bernacchi et al. (2003) in expressions (B.1) the solutions are normalised to the temperature $T = 25\,^{\circ}$C. For the results see Table 2. The dotted curve in Fig. 6 represents $A(C_i)$ emerging from reinsertion of the values representing the minimum of (39) into Eq. (38).

3.1.2. Calculation of λ

In order to proceed, we need a numeric value of the Lagrangian multiplier λ which represents the cost of water. As pointed out in Section 2.4, direct integration of Eq. (30) in order to express λ in terms of W_0, the amount of water available during the time Δt, is not possible. The method outlined in Appendix C, the derivation of λ from quantities characterising soil and plant water transport system would require detailed knowledge of the soil parameters and the ground water regime.

Fortunately, a third approach is feasible and successful because (i) Overdieck and Strassemeyer (2005) provide data relating $g_{sH_2O} = ag$ and C_a, and (ii) λ is the only still unknown quantity in expression (34) for $g(C_a)$. Proceeding similarly as above we use nonlinear regression in order to obtain a "best fit" of the curve $g_{sH_2O}(C_a)$ to the six data points $(C_{a,k}, g_{sH_2O,k})$ $(k = 1 \ldots 6)$ given in

Table 2
Photosynthetic, environmental and anatomical parameters used to calculate $v(C_a)$ related to *Ginkgo biloba* and *Quercus petraea* from Eq. (37)

Symbol	*G. biloba*	*Q. petraea*	Unit	Quantity/Source/Remarks
Photosynthetic parameters				
q	4.28	22.6	$\mu mol/m^2/s$	See (26) and (B.1)[a]
R_d	0.11	0.39	$\mu mol/m^2/s$	See (26) and (B.1)[a]
K	205	464	$\mu mol/mol$	See (26) and (B.1)[a]
Γ	43	33	$\mu mol/mol$	See (26) and (B.1)[a]
$V_{max,25\,^\circ C}$	7.34	35.7	–	See (B.1)[a]
$R_{d,25\,^\circ C}$	0.16	0.54	–	See (B.1)[a]
$k_{25\,^\circ C}$	0.48	1	–	See(B.1)[a]
$\gamma_{25\,^\circ C}$	1.37	1	–	See (B.1)[a]
Environmental parameters				
u_{wind}	3	3	m/s	Wind speed[b]
w_{rel}	60	65	%	Relative atmospheric humidity[c]
T	19.07	20	°C	Temperature[c]
λ	1.57×10^{-3}	1.23×10^{-3}	–	"Cost of water"[a]
Anatomical parameters				
d_{st}^{geom}	31.9 ± 3.7	23	μm	Depth of stomatal opening (Fig. 1)[d]
w_{st}^{max}	1.2 ± 0.4	1.4	μm	Maximum width of stomatal opening[d]
h_{st}	13.1 ± 1.7	10.1	μm	Length of stomatal opening[d]
d_{as}	218 ± 32	100	μm	Thickness of assimilation tissue[d]
τ_{as}	1.571	1.571	–	Tortuosity of assimilation tissue[e]
n_{as}	0.35	0.33	–	Porosity of assimilation tissue[e]
l	84 ± 11	54	mm	Average leaf length[d]

Ginkgo biloba: The meaning of the superscripts in the last column is as follows:
[a]Calculated from Table 3.
[b]Rough estimate for Berlin.
[c]Average value for Berlin during growth period.
[d]Own measurements, Copeland (1902), Napp-Zinn (1966).
[e]Rough estimate.
The environmental parameters w_{rel}, T and λ are derived from data in Overdieck and Strassemeyer (2005). The photosynthetic quantities q, R_d, K and Γ refer to $T = 19.07\,^\circ C$. They are calculated from data provided in Overdieck and Strassemeyer (2005) via the expressions due to Bernacchi et al. (2003) as given in (B.1).
Quercus petraea: All data are taken from or derived from data in Kürschner (1996) and Kürschner et al. (1998).

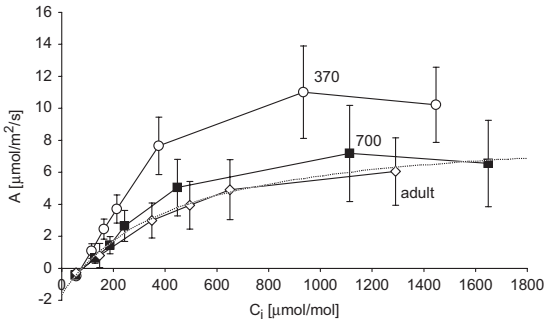

Fig. 6. Calculation of q, R_d, K and Γ from data points included in Figs. 1 and 2 of Overdieck and Strassemeyer (2005). The data are related to three groups of *Ginkgo biloba* plants. Open circles: Saplings grown for 2 years at $C_a \approx 370\,\mu mol/mol$. *Black squares*: Saplings grown for 2 years at $C_a \approx 700\,\mu mol/mol$. *Open squares*: Values of an adult *Ginkgo biloba* growing in the field (Berlin) at $C_a \approx 370\,\mu mol/mol$. The dotted curve represents the function $A(C_i)$ (see (38)). q, R_d, K and Γ were obtained by the least squares method according to (39) from the (C_i, A) data pairs in Table 3.

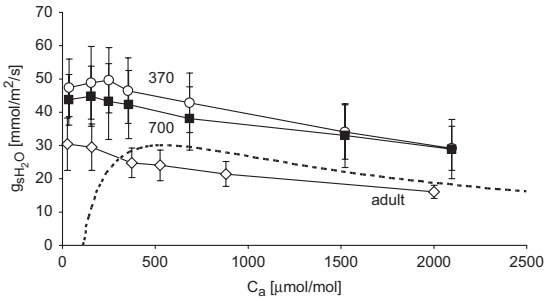

Fig. 7. Calculation of λ from data points included in Figs. 1 and 2 of Overdieck and Strassemeyer, 2005. The data are related to three groups of *Ginkgo biloba* plants. *Open circles*: Saplings grown for 2 years at $C_a \approx 370\,\mu mol/mol$. *Filled diamonds*: Saplings grown for 2 years at $C_a \approx 700\,\mu mol/mol$. *Open squares*: Values of an adult *Ginkgo biloba* growing in the field (Berlin) at $C_a \approx 370\,\mu mol/mol$. The dotted curve represents the function $g_{sH_2O}(C_a)$. λ was obtained by the least squares method (according to (40)) from the $(C_a, g_{s\,H_2O,})$ data pairs of Table 4.

Table 4. Using the relation $g_{s\,H_2O,} = ag$ (with $a = D_{H_2O}/D_{CO_2}$) we start with the expression

$$\sigma_g^2 = \sum_k [ag(C_{a,k}) - g_k]^2 \tag{40}$$

which depends on λ, the only parameter in $g(C_a)$ which is not yet fixed. Calculating a "best fit" of the curve representing Eq. (34) to

Table 3
Data pairs (C_i, A) from Overdieck and Strassemeyer (2005) used to calculate the quantities (q, R_d, K, Γ) via the least squares method

C_i	55.5	145	340	492	647	1287	µmol/mol
A	−0.26	0.81	3.13	3.93	4.9	6.11	$\mu mol/m^2/s$

The data were obtained at a temperature $T = 27.3\,^\circ C$ and a relative atmospheric humidity of 50%.

Table 4
Data points (C_a, g_{sH_2O}) from Overdieck and Strassemeyer (2005) used to calculate the "cost of water" λ via the least squares method

C_a	25	163	375	525	875	2000	μmol/mol
g_{sH_2O}	31	29	25	24	22	17	mmol/m²/s

The data were obtained at a temperature $T = 27.3\,^{\circ}C$ and a relative atmospheric humidity of 50%.

the data points similarly as in Section 3.1.1, the minimum of σ_g^2 is found at $\lambda = 1.57 \times 10^{-3}$. The dotted curve in Fig. 7 represents $g_{sH_2O}(C_a) = ag(C_a)$ obtained from this value for λ (B.1).

3.2. Basic model features

In the following, the basic features of the model are demonstrated. Although these features are in principle species independent we need numerical parameter values in order to illustrate

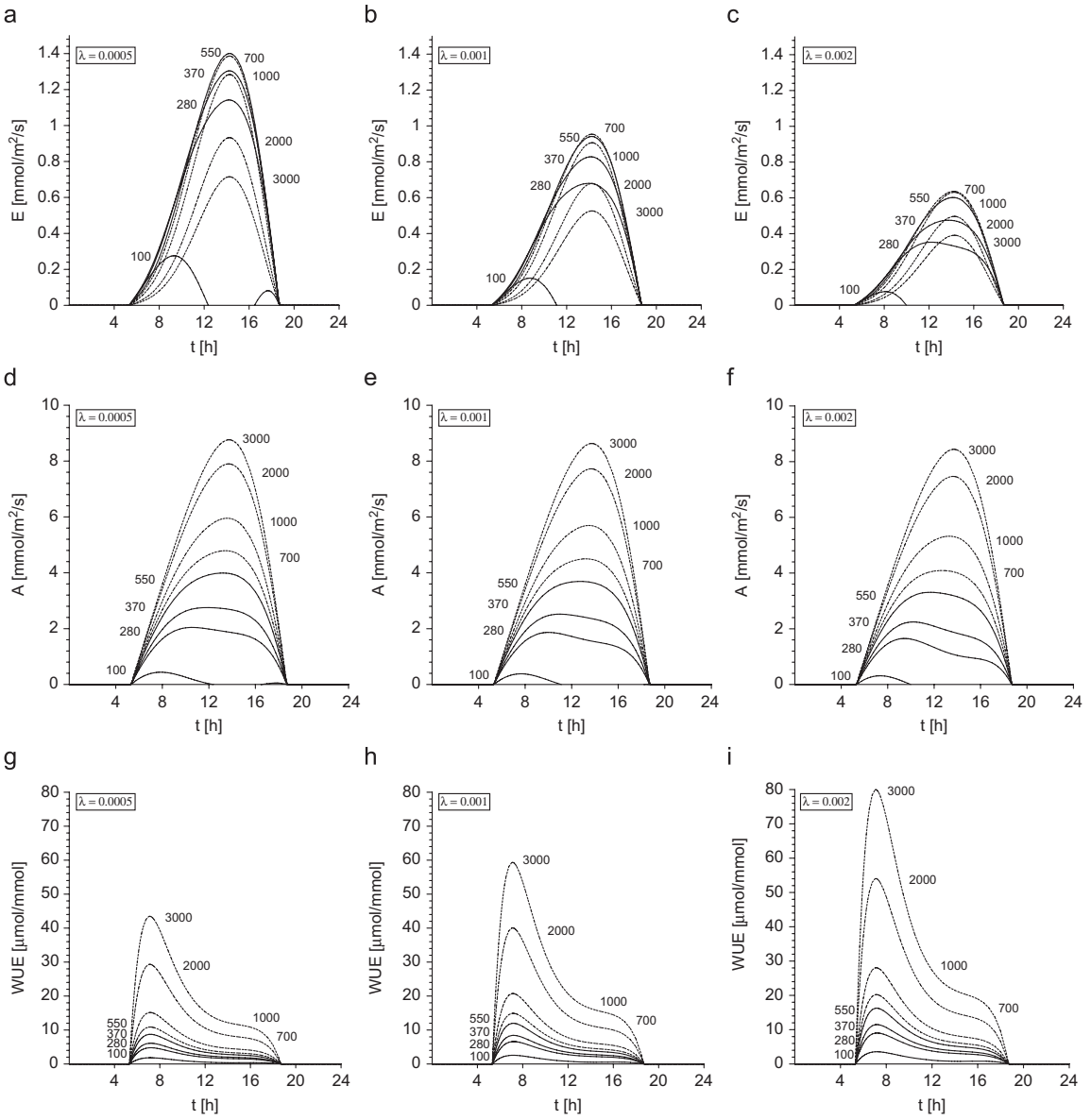

Fig. 8. Transpiration rate $E(t)$ (a,b,c), assimilation rate $A(t)$ (d,e,f) and water use efficiency $WUE(t) = A(t)/E(t)$ (g,h,i) as a function of t (diurnal variations) for various values of the cost of water λ. $E(t)$, $A(t)$ and $WUE(t)$ are calculated according to (21) and (35) from the diurnal variations of $Q(t)$, $T(t)$ and $w_a(t)$ shown in Fig. 5. The atmospheric CO_2 concentration C_a is held constant along each curve. Numbers close to the maxima of the curves give C_a in units of μmol/mol (700, 1000, 2000 and 3000 μmol/mol correspond to the broken curves). C_a is given in units of μmol/mol. $t = 0$ and 24 h denote midnight.

them. We use the parameters listed in Table 2 for *G. biloba* which were obtained in Sections 3.1.1 and 3.1.2. Additionally, we use the input functions depicted in Fig. 5 reflecting realistic diurnal variations of insolation $Q(t)$, temperature $T(t)$ and atmospheric water vapour concentration $w_{rel}(t)$ for a warm weather period during July 1991 in Berlin (Senatsverwaltung für Stadtentwicklung Berlin, 1993).

Figs. 4 and 8 show how the diurnal variations of conductance $g(t)$, assimilation rate $A(t)$, transpiration rate $E(t)$ and water use efficiency $WUE(t) = A(t)/E(t)$ depend on the cost of water λ and on the atmospheric CO_2 concentration C_a. Figs. 4(d)–(i) and 8 consist of families of curves which are generated by assigning the following C_a-values: $C_a = 100$ and $280\,\mu mol/mol$ (preindustrial CO_2-level), $C_a = 370\,\mu mol/mol$ (today's value), $C_a = 550\,\mu mol/mol$ (around year 2050), $C_a = 700\,\mu mol/mol$ (around year 2100), $C_a = 1000\,\mu mol/mol$ (Eocene, see Pagani et al., 2005), $C_a = 2000\,\mu mol/mol$ (Eocene, see Pagani et al., 2005), $C_a = 3000\,\mu mol/mol$ (Lower Devonian, see Berner and Kothvala, 2001) (for the predictions for the years 2050 and 2100 see Prentice et al., 2001). The following features of these curves are noteworthy:

- $g(t)$ and $E(t)$ decrease with increasing λ, $A(t)$, however, is nearly unaffected. Clearly, this asymmetry entails that $WUE(t) = A(t)/E(t)$ *in*creases along with λ, as is to be expected from the interpretation of λ as the cost of water. Mathematically, the different sensitivities of $A(t)$ and $E(t)$ with respect to λ can be understood from expressions (D.1) and (D.2), the series expansions of both quantities with respect to λ: for small values of λ the expansion of $A(t)$ is dominated by a constant term, while the expansion of $E(t)$ is dominated by a term proportional to $1/\sqrt{\lambda}$. Hence, variations in λ affect $A(t)$ only weakly, $E(t)$, however, strongly.
- The value of λ affects the maximum values, but does not alter significantly the shape of the curves $g(t)$, $g(C_a)$, $E(t)$, $A(t)$ and $WUE(t)$.
- The curves g, E and A in Fig. 9 indicate more clearly a feature already included in Figs. 4 and 8: Although both E and A are calculated via expressions (34) and (35) from the optimum stomatal conductance g, only E inherits the maximum of g with respect to C_a. Depending on the values of λ and t, it is located within the range $C_a \approx 100 \ldots 800\,\mu mol/mol$. (Since E is—with respect to the variable C_a—simply a multiple of g (see Eq. (21)), the maxima of both functions are necessarily located at the same value of C_a.) $A(C_a)$, however, increases monotonically with C_a.
- The midday depressions of $g(t)$, $E(t)$, $A(t)$ and $WUE(t)$ become more distinct with decreasing C_a. With $A(t)$ and $WUE(t)$ they are much less pronounced than with $g(t)$ and $E(t)$.
- In the FACE-experiments (Long et al., 2004; Ainsworth and Long, 2005) it has been found that the stomatal conductance g of C_3-plants decreases by about 20% while their assimilation rate A increases by 30%...50% if the atmospheric CO_2 is raised from the recent value of $C_a = 370$ to $C_a = 550\,\mu mol/mol$ (to be expected to occur around the year 2050). The predictions from the model are in accordance with both observations: Calculating the model responses for this C_a-increase from the input values of Table 2 we find for the relative changes of stomatal conductance and assimilation $\Delta g/g = -11\%$ and $\Delta A/A = 21\%$, respectively.

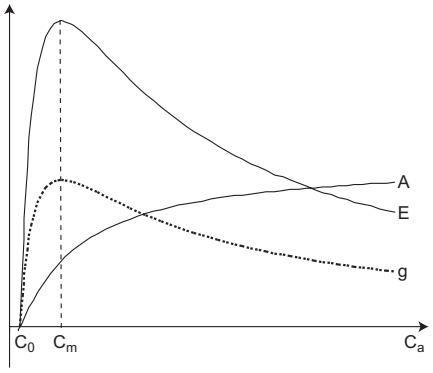

Fig. 9. Principal behaviour of optimum conductance g, assimilation rate A and transpiration rate E as a function of atmospheric C_a according to expressions (34), (21) and (35). A increases steadily with increasing C_a, although g and E show distinctive maxima at $C_a = C_m$ and decrease beyond their maxima. All three functions become zero at $C_a = C_0$.

Due to the structure of expression (36), the functions $g(C_a)$ and $v(C_a)$ share many properties in the range $C_a > 0$ (for details, consult Appendix E).

3.3. Sensitivity studies: identification of critical parameters

If the model is applied to reconstruct fossil C_a, errors can arise especially from the following sources: (i) from the high natural variance of stomatal data, (ii) from limited amount of knowledge about climatic parameters which existed when the fossil plants grew, (iii) from missing data concerning other leaf anatomical traits and (iv) from the necessity to use extant physiological data. Thus, it is necessary to explore to what extent uncertainties in the photosynthetic, environmental and anatomical parameters influence the $v(C_a)$-curves obtained from Eq. (37): if reliable results are desired, the most sensitive parameters should be known with great accuracy, for the less sensitive parameters rough estimates of their values may be sufficient (sensitivity means that small deviations in a parameter value cause large deviations in the stomatal density v). This can be achieved by performing sensitivity studies, in which the model parameters are varied systematically.

A set of curves was calculated for *G. biloba* by assigning various values to one of the input parameters (denoted by ξ) while keeping the other parameters constant. The constant values of the parameters are listed in Table 2. Comparison of the $v(C_a;\xi)$-curves allows to identify the most sensitive parameters.

3.3.1. Sensitivity of $v(C_a)$ against fluctuations of the photosynthetic parameters

Fig. 10 shows that the stomatal density v is most sensitive against variations of the parameter q (defined in (24)). An increase in q shifts the C_a that is signalled by a certain v to significantly higher values. Variations in K (defined in (25)) produce a much smaller change of v, and the effects of varying R_d and Γ are—compared with q—almost negligible. q has therefore to be considered as a very critical parameter.

3.3.2. Sensitivity of $v(C_a)$ against fluctuations of the environmental parameters

Of the environmental parameters, the wind speed u_{wind} has the least impact on v (see Fig. 11). The curves $v(C_a;u_{wind})$ are virtually indistinguishable for a very wide range of wind speeds. Only if u_{wind} approaches zero $v(C_a;u_{wind})$ increases somewhat. Variations in (relative) atmospheric humidity w_{rel}, cost of water λ or temperature T cause, however, effects which should not be neglected: the maxima of both $v(C_a;w_{rel})$ and $v(C_a;\lambda)$ increase and become sharper if humidity increases resp. if water becomes

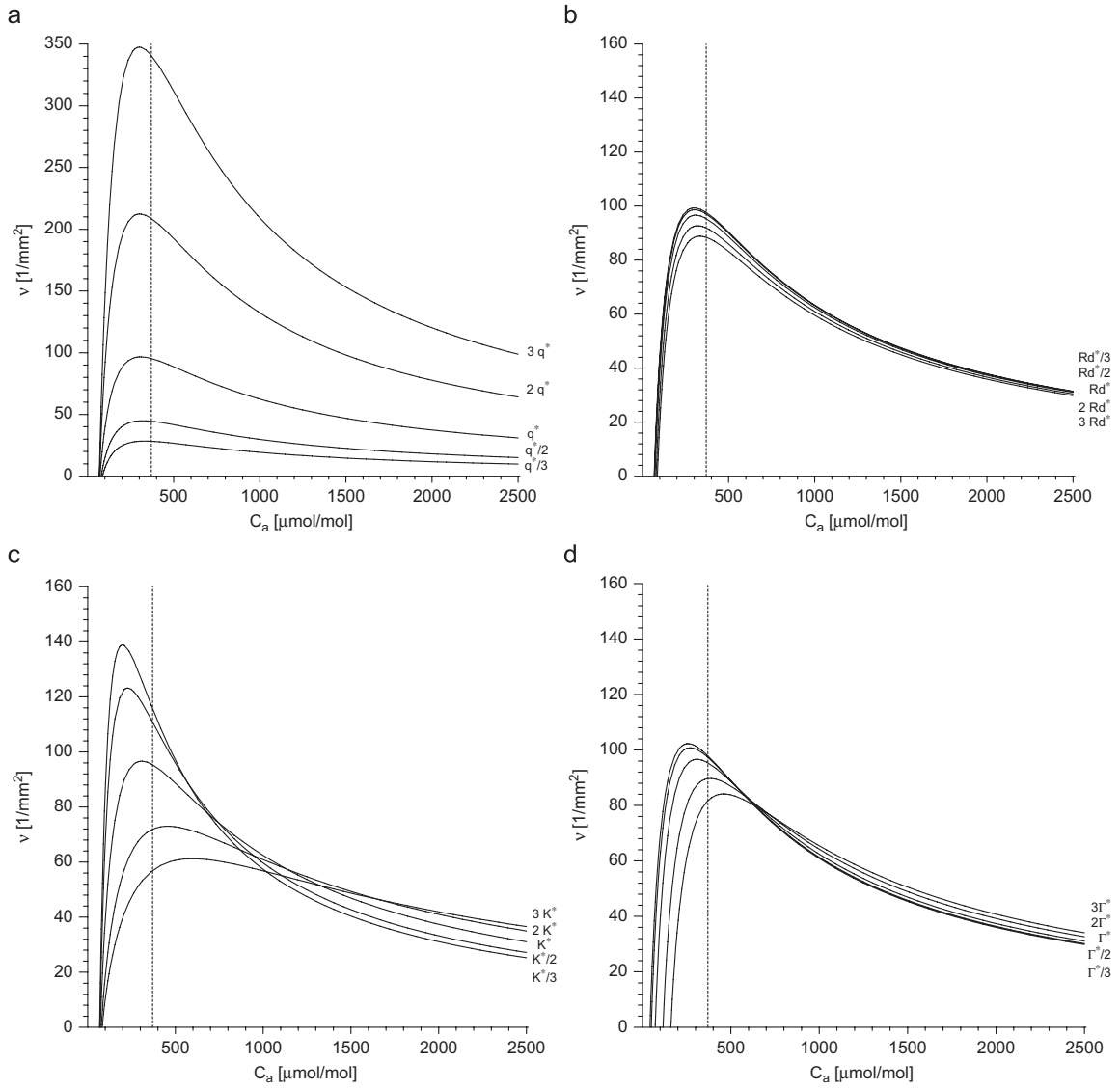

Fig. 10. Dependence of $\nu(C_a;\xi)$-curves on the photosynthetic parameters $\xi = q, R_d, K$ and Γ. Parameters are as in Table 2 and related to the adult *Ginkgo biloba* tree investigated in Overdieck and Strassemeyer (2005) in Berlin. Each family of $\nu(C_a;\xi)$-curves is generated by substituting $\xi = \xi^*/3, \xi^*/2, \xi^*, 2\,\xi^*, 3\,\xi^*$ into Eq. (37) where ξ^* is the parameter value given in Table 2. The present atmospheric CO_2 concentration $C_a \approx 370\,\mu\text{mol/mol}$ is indicated by vertical broken lines: (a) $\nu(C_a;q)$, (b) $\nu(C_a;R_d)$, (c) $\nu(C_a;K)$ and (d) $\nu(C_a;\Gamma)$.

cheaper. If the temperature T increases, the maxima of $\nu(C_a;T)$ also increase, they become, however, less pronounced and shift to higher C_a-values (Fig. 11).

Fig. 13 shows the behaviour of the $\nu(C_a)$-curves for a much wider range of combinations of temperature T and relative humidity w_{rel} than those presented in Figs. 11(a) and (c). The range of C_a is confined to the interval $C_a = 0 \ldots 600\,\mu\text{mol/mol}$, including the quaternary CO_2 minimum ($C_a \approx 180\,\mu\text{mol/mol}$, Beerling et al., 1995), the present atmospheric CO_2 ($C_a \approx 370\,\mu\text{mol/mol}$) and the atmospheric CO_2 to be expected to occur around the year 2050 ($C_a \approx 550\,\mu\text{mol/mol}$). Fig. 13 demonstrates that the position of the maximum of $\nu(C_a)$ is dependent on environmental parameters and that ν can attain much higher values than those which are usually observed under present conditions.

3.3.3. *Sensitivity of $\nu(C_a)$ against fluctuations of the anatomical parameters*

With decreasing maximum pore area a_{st}^{max}, the maximum of the $\nu(C_a)$-curve increases strongly to higher ν-values (see Fig. 12). Hence, the maximum pore area a_{st}^{max} has fundamental influence on the $\nu(C_a)$-relation. Under a pore area $a_{st}^{max} = 10\,\mu\text{m}^2$, for example, stomatal density $\nu = 105/\text{mm}^2$ implies an atmospheric CO_2

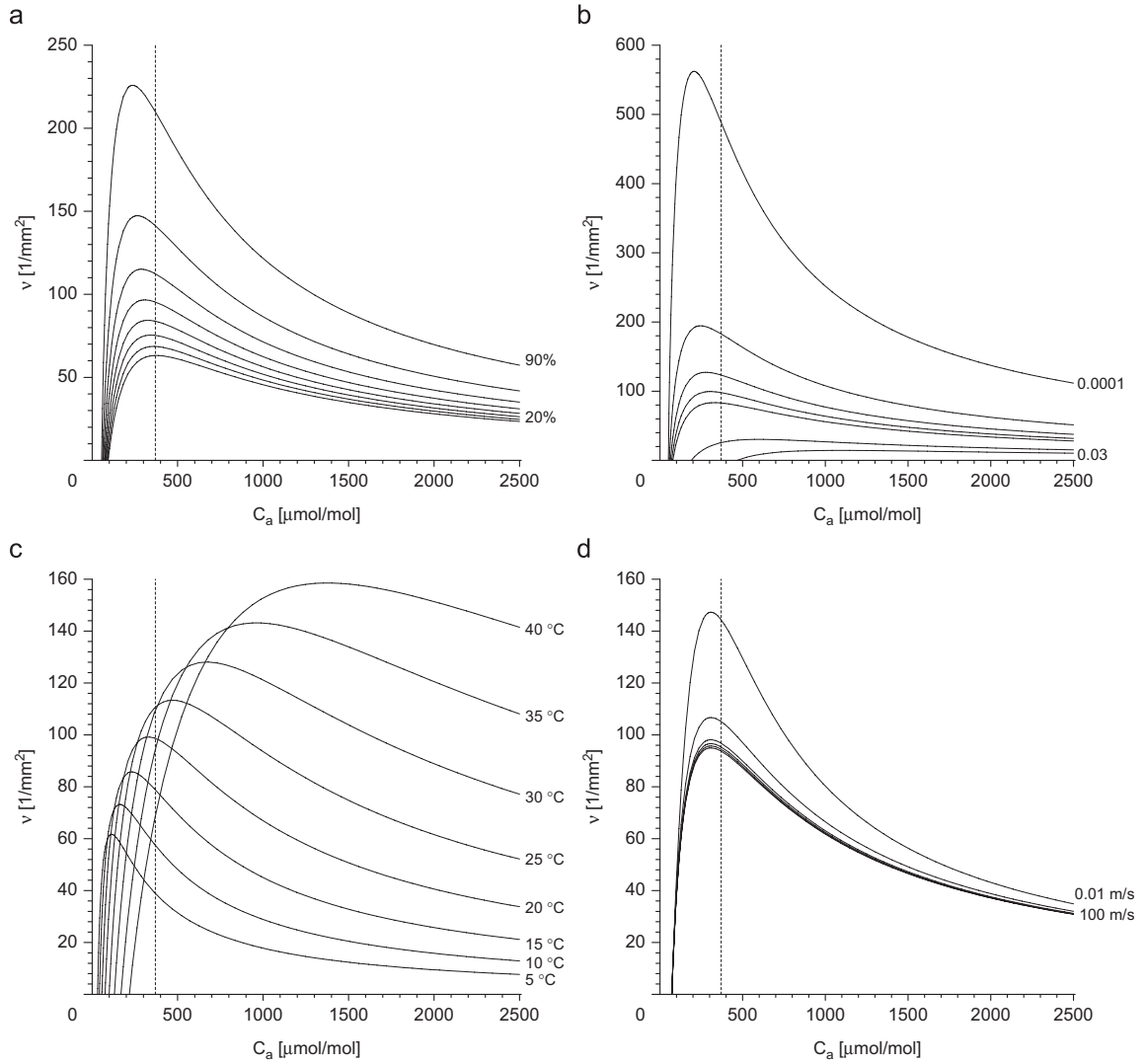

Fig. 11. Dependence of $\nu(C_a;\xi)$-curves on the environmental parameters atmospheric humidity, cost of water, temperature, and wind speed. Parameters used (except those which are varied) are as in Table 2 and related to the adult *Ginkgo biloba* tree investigated in Overdieck and Strassemeyer (2005) in Berlin. Values of varied quantities are indicated by the labels to the right of the curves. The present atmospheric CO_2 concentration $C_a \approx 370\,\mu$mol/mol is indicated by a vertical broken line. (a) The (relative) atmospheric humidity varies from 20% to 90% in steps of 10% ($\nu(C_a;w_{rel})$, w_{rel}: atmospheric humidity). (b) The cost of water varies. $\lambda = 0.0001$, 0.0005, 0.001, 0.0015, 0.002, 0.01 and 0.03 ($\nu(C_a;\lambda)$, λ: cost of water). (c) The temperature varies from 5 to 40 °C in steps of 5 °C ($\nu(C_a;T)$, T: temperature) and (d) The wind speed is varied. Values of u_{wind} are 0.01, 0.1, 1, 3, 10, 100 m/s (from upper- to lower-most curve) ($\nu(C_a;u_{wind})$, u_{wind}: wind speed).

concentration of $C_a = 370\,\mu$mol/mol. With pore areas $a_{st}^{max} = 8\,\mu m^2$, $a_{st}^{max} = 6\,\mu m^2$ or $a_{st}^{max} = 4\,\mu m^2$ the same stomatal density implies, however, $C_a = 720$, 1160 and $C_a = 1970\,\mu$mol/mol, respectively. A comparable effect results if the stomatal depth d_{st} is increased. In attempts to reconstruct palaeoatmospheric CO_2 from fossil stomatal density it is thus necessary to include information about maximum stomatal pore size and stomatal depth. In the case of *G. biloba*, there are indications that stomatal dimensions tend to increase from late Miocene to Pliocene (Denk and Velitzelos, 2002).

Inspection of Fig. 12 reveals that the other anatomical parameters describing the assimilating tissue (i.e. d_{as}, t_{as}, n_{as}) do not strongly influence the $\nu(C_a)$-curve. Still less important is the leaf length l (see Fig. 12).

3.4. Model parametrisation with Quercus petraea

In order to check the model behaviour for a different species, it is also applied to *Q. petraea*. This species was also repeatedly used for reconstructing C_a values of the past (Kürschner, 1996; Kürschner et al., 1998). The input parameters related to this species (see Table 2) lead to $\nu(C_a)$-curves which exhibit the same patterns as those obtained for *G. biloba*. (i) $\nu(C_a)$-curves show for

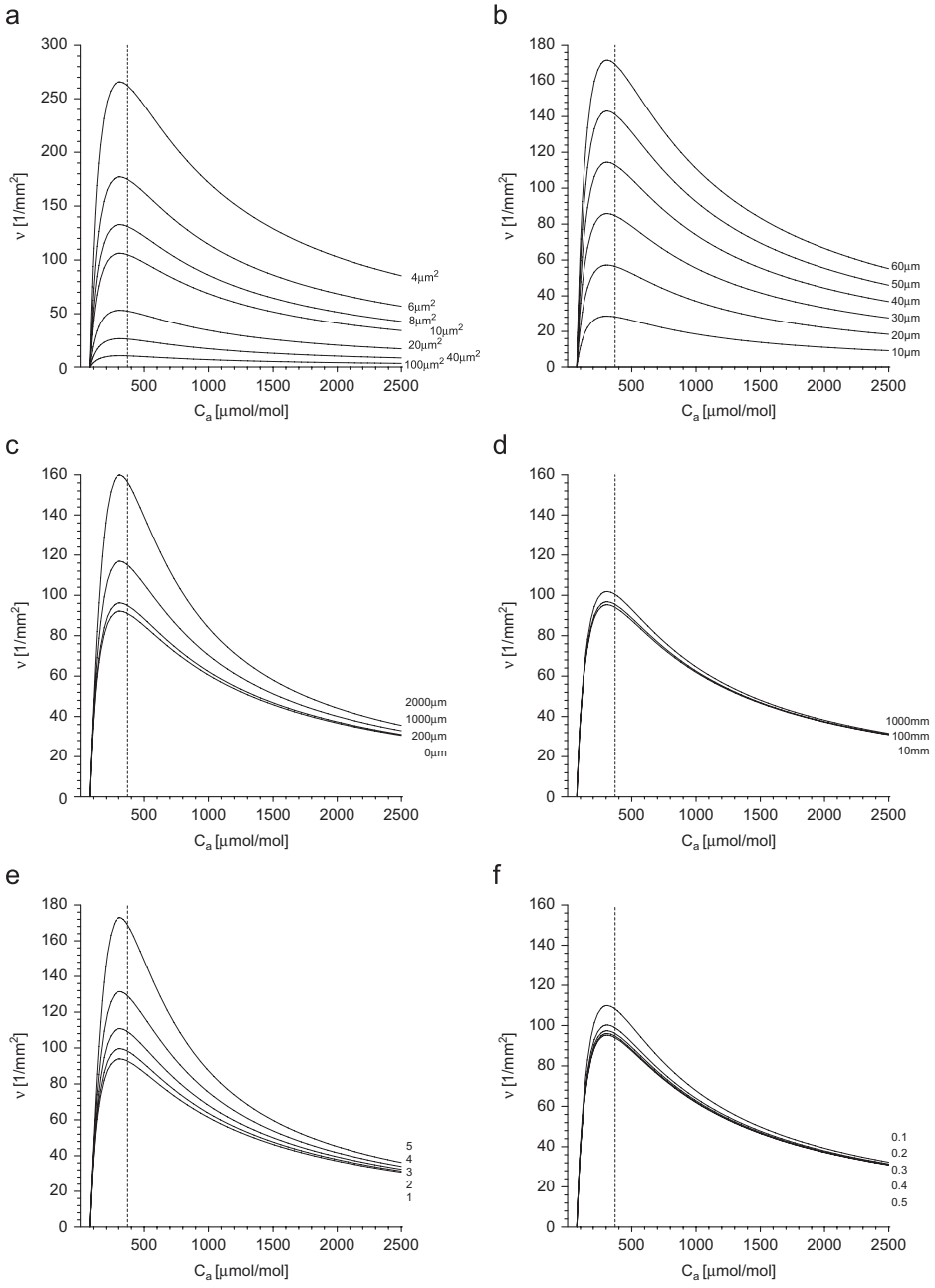

Fig. 12. Dependence of $\nu(C_a)$-curves on the anatomical parameters. Parameters used (except those which are varied) are as in Table 2 and related to the adult *Ginkgo biloba* tree investigated in Overdieck and Strassemeyer (2005) in Berlin. Values of varied quantities are indicated by the labels to the right of the curves. The present atmospheric CO_2 concentration $C_a \approx 370\,\mu$mol/mol is indicated by a vertical broken line: (a) $\nu(C_a; a_{st})$, a_{st}: stomatal area; (b) $\nu(C_a; d_{st})$, d_{st}: depth of stomatal pore; (c) $\nu(C_a; d_{as})$, d_{as}: thickness of assimilating tissue; (d) $\nu(C_a; l)$, l: length of a leaf; (e) $\nu(C_a; t_{as})$, t_{as}: tortuosity of assimilating tissue and (f) $\nu(C_a; n_{as})$, n_{as}: porosity of assimilating tissue.

both species the same responses with respect to shifts of the positions of the maxima when photosynthetic, environmental or leaf morphological parameters are varied. (ii) Sensitivity studies lead to the same hierarchy of critical parameters. Hence, we restrict the representation of the results obtained with *Q. petraea* to Fig. 14 which shows $\nu(C_a)$-curves resulting from variation of both temperature T and relative humidity w_{rel} (as are described in Section 3.3.2).

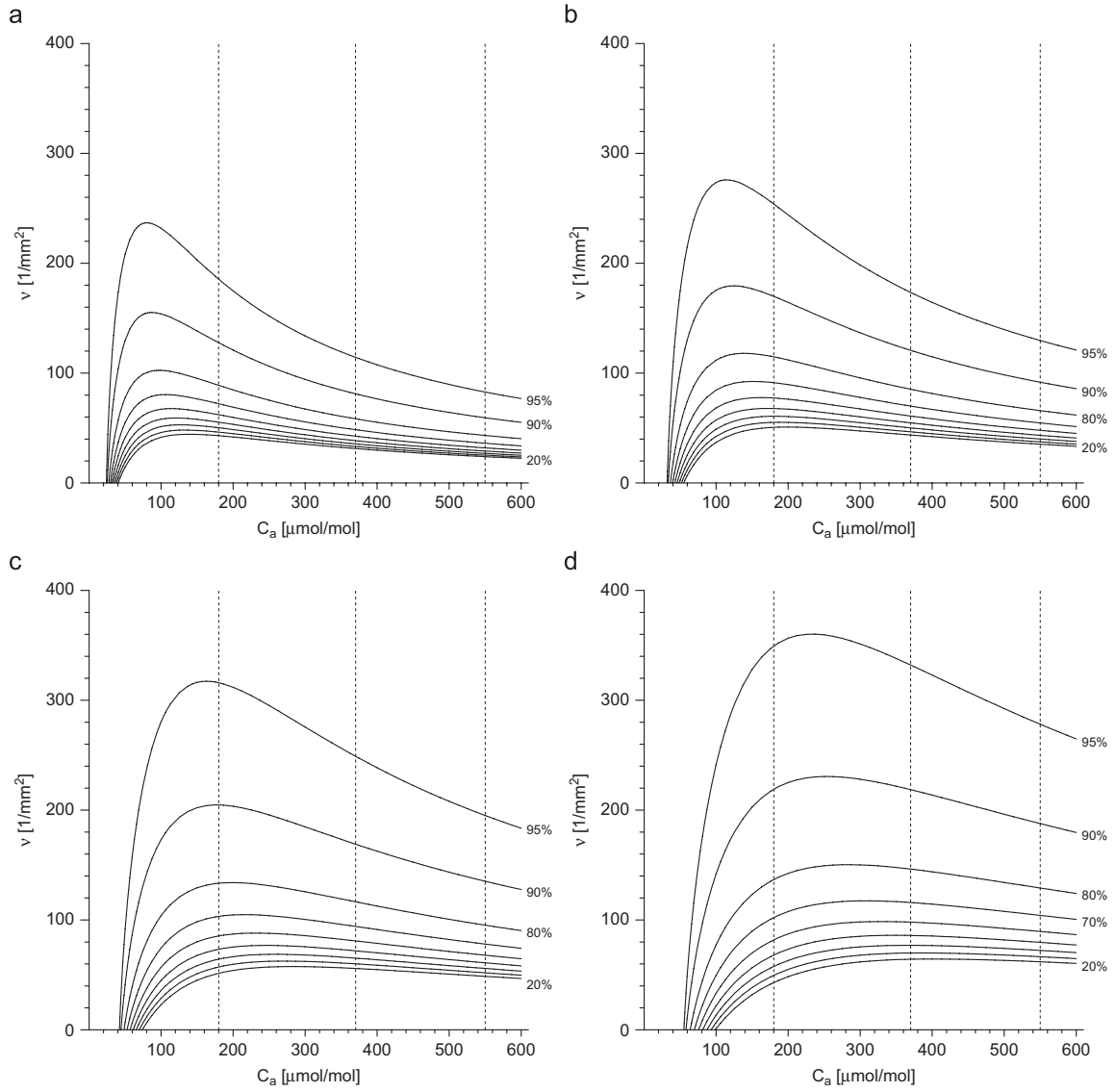

Fig. 13. Dependence of $\nu(C_a; w_{rel})$-curves on temperature. Parameters refer to *Ginkgo biloba* (see Table 2). The (relative) atmospheric humidity varies in steps of 10% between 20% to 90%. The atmospheric CO_2 concentrations of the quaternary minimum ($C_a \approx 180\,\mu$mol/mol), of the present ($C_a \approx 370\,\mu$mol/mol) and a prediction for the year 2050 ($C_a \approx 550\,\mu$mol/mol) are indicated by vertical broken lines: (a) $\nu(C_a; w_{rel})$, $T = 5\,^{\circ}$C; (b) $\nu(C_a; w_{rel})$, $T = 10\,^{\circ}$C; (c) $\nu(C_a; w_{rel})$, $T = 15\,^{\circ}$C and (d) $\nu(C_a; w_{rel})$, $T = 20\,^{\circ}$C.

4. Final considerations

The model presented in this contribution is based on an optimisation principle about the optimum use of the resource materials CO_2 and water and reflects the daily course of stomatal conductance which is usually due to stomatal aperture change. This approach was expanded in this paper by introducing structural data (e.g. stomatal density and pore area) which influence stomatal conductance on a fundamentally different time scale. This is possible because the optimisation principle holds also for structural parameters: if structural changes provide for an improvement under changing C_a and certain environmental conditions and if these changes cannot be realised by a phenotypic response, then these changes will occur during an evolutionary process which favours those genotypes which express the suitable adaptations. In fact, the differences in phenotypic $\nu(C_a)$ response can be large within a taxon for different genotypes, as demonstrated for different accessions of *Arabidopsis thaliana* (Woodward et al., 2002) and *Nothofagus cunninghamii* (Hovenden and Schimanski, 2000).

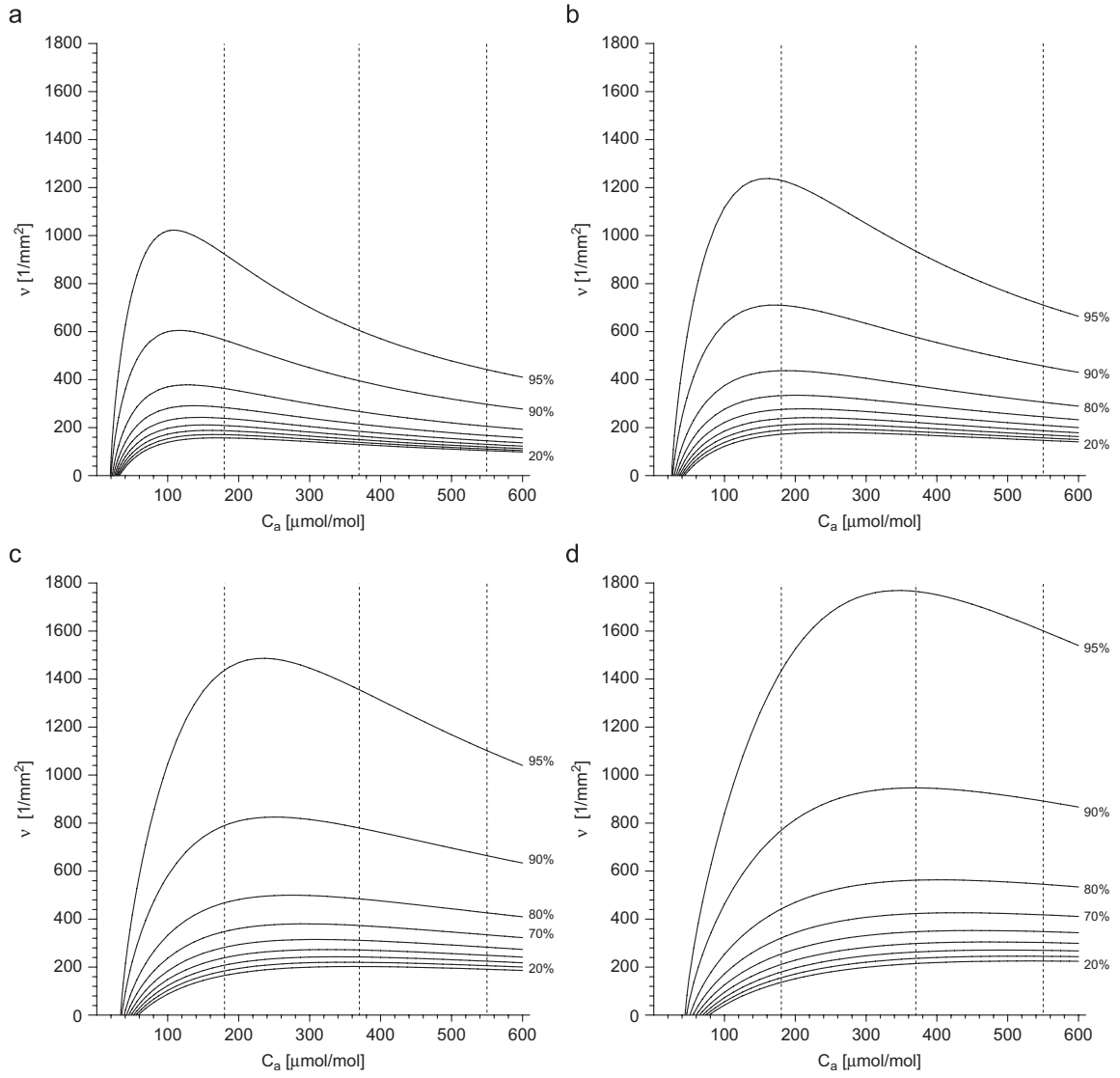

Fig. 14. Dependence of $\nu(C_a; w_{rel})$-curves on temperature. Parameters refer to *Quercus petraea* (see Table 2). The (relative) atmospheric humidity varies in steps of 10% between 20% to 90%. The atmospheric CO_2 concentrations of the quaternary minimum ($C_a \approx 180\,\mu$mol/mol), of the present ($C_a \approx 370\,\mu$mol/mol) and a prediction for the year 2050 ($C_a \approx 550\,\mu$mol/mol) are indicated by vertical broken lines: (a) $\nu(C_a; w_{rel})$, $T = 5\,^{\circ}$C; (b) $\nu(C_a; w_{rel})$, $T = 10\,^{\circ}$C; (c) $\nu(C_a; w_{rel})$, $T = 15\,^{\circ}$C and (d) $\nu(C_a; w_{rel})$, $T = 20\,^{\circ}$C.

The sensitivity analysis revealed both critical and non-critical parameters: critical parameters with respect to the $\nu(C_a)$ response are the photosynthetic parameters q (and, of secondary importance, K), (relative) atmospheric humidity w_{rel}, the cost of water λ and the temperature T, pore area a_{st} and depth d_{st} of the stomatal pore. The dominance of the environmental parameters which indicate the availability of water reflects the tight coupling between assimilation and transpiration. There are numerous indications for a tight coupling between water availability, water conduction and gas exchange (Katul et al., 2003). The various aspects of humidity (air humidity, soil water potential and soil type, precipitation) have therefore significant influence upon evolutionary $\nu(C_a)$-responses.

Plant response to increasing C_a is also affected by nutrient supply and metabolism, especially nitrogen (Reich et al., 2006). The general observation made in experiments under elevated C_a is that—on the leaf level—net assimilation increases while stomatal conductance and nitrogen content of leaves decrease (Ainsworth and Long, 2005; Ainsworth and Rogers, 2007). Furthermore, a decrease in V_{max} and J_{max} can be often observed (Ainsworth and Long, 2005; Ainsworth and Rogers, 2007). Apparently, trees show a low degree of photosynthesis acclimation, with a V_{max} decrease

of about 6% ... 10% and a J_{max} decrease close to zero (Medlyn et al., 1999; Ainsworth and Rogers, 2007). There is evidence that this down-regulation of the photosynthesis apparatus is enhanced under low N availability (Stitt and Krapp, 1999). This means that the C_a response will be affected also by environmental conditions involved in nutrient supply. In fact, plants grown under low N tend to show a greater decrease of V_{max} and J_{max} (Ainsworth and Long, 2005). It is therefore to be expected that the long-term effect of C_a on plants is also influenced by N availability. For reconstruction of C_a with stomatal data, it would be therefore desirable to incorporate this effect into the model although it is difficult to estimate N availability in the case of fossil environments. Another possibility would be to perform a sensitivity analysis which includes down-regulation of photosynthesis parameters under low N on the basis of the data set that is available so far.

The $v(C_a)$-response obtained from expression (37) is strongly influenced by other environmental parameters such as temperature or atmospheric humidity. Hence, inferring palaeoatmospheric C_a from fossil stomatal density v without taking possible modulations from the environment into account may be misleading. Reconstruction of palaeoatmospheric CO_2 by using the $v(C_a)$-response should therefore be accompanied by palaeoclimatic studies revealing parameters such as humidity and mean temperature during the growth period of the sites which are under consideration. The obtained values of palaeoclimatic parameters are then entered directly into the model. Palaeoclimatic studies may only provide parameter values which are highly uncertain. If such a parameter is critical with respect to the sensitivity of the model it is possible to insert the endpoints of its most probable range of values into the model. The model produces then a corresponding "envelope" of $v(C_a)$-curves.

Acknowledgements

Parts of the work were carried out within a visit to the National Museum for Natural History, Stockholm, Sweden, funded by the HIGHLAT programme (W.K. and A.R.-N.), which is gratefully acknowledged. We thank an anonymous reviewer for helpful comments and James Nebelsick, Tübingen, for critically reading the English manuscript.

Appendix A. Approximations

A.1. The porous medium approximation

The porous medium approximation is widely used to describe processes which take place in porous media (Aris, 1975) and in plant leaf tissue (see Parkhurst and Mott, 1990 and the review Parkhurst, 1994 and literature cited therein). Its central idea is the replacement of the discontinuous arrangement of cells and voids inside the real plant by a fictitious tissue whose continuous material properties are partly attributable to the cells and partly to the voids of the real plant. This is achieved by an averaging process which reduces the complex geometrical details of the cell and void architecture to just two quantities, the porosity n and the tortuosity τ, defined by

$$n := \frac{V_p}{V} \quad \text{and} \quad \tau := \frac{l_e}{l} \tag{A.1}$$

V_p and V are pore volume resp. total volume of a volume element. l_e denotes the length of the actual path which a molecule has to follow in order to move from one given point to another and l denotes the (geometrically) shortest distance between these same points. The effective conductance S is defined in terms of n, τ and the free air coefficient of diffusion D as

$$S := D\,\frac{n}{\tau^2} \tag{A.2}$$

Notice, that $D = D_{CO_2}$ or D_{H_2O}, depending on whether diffusion of CO_2 or H_2O molecules is considered.

A.2. Constancy of effective conductance

Plant leaves consist of several tissue layers (see stomatal and assimilation layers in Fig. 1). Due to the anatomical structure of leaves, porosity n and tortuosity τ change more or less abruptly between adjacent layers, but vary only slightly within the individual layers. The effective conductance S (defined in (A.2)) should behave similarly, i.e. $S = \text{const.}$ *within* a given layer.

A.3. Stationary conditions

We focus on stationary situations, i.e. we assume that the term $\partial c/\partial t$ on the right-hand side of Eq. (2) is much smaller than and can be neglected against the term $\mathrm{div}(S\,\mathrm{grad}\,c)$. This is true if molecules diffusing from a region of high towards a region of low concentration do not experience an appreciable change in the "concentration pattern" around them during their journey.

Water vapour molecules, for example, need roughly a time $t \approx l^2/(4\,D^{air}_{H_2O}) = 0.01\,\mathrm{s}$ to cover the distance $l \approx 1\,\mathrm{mm}$ from the interior of a leaf to the free atmosphere. Under normal weather conditions one can assume that atmospheric humidity needs a longer time to change appreciably (within the plant it is constant anyway). Since carbon dioxide molecules are heavier than water molecules, they move slightly slower in air than water vapour molecules, they need for the same distance $t \approx l^2/(4\,D^{air}_{CO_2}) = 0.017\,\mathrm{s}$. Atmospheric CO_2-content is practically constant during this time-span, and also the CO_2-concentration at the assimilating sites.

Appendix B. Temperature dependencies

B.1. Assimilation parameters

Bernacchi et al. (2003) give the following temperature dependencies:

$$\begin{aligned}
J_{max} &= J_{max,25\,^\circ\mathrm{C}} \times \mathrm{e}^{(17.57-(5236.760760/T))} \times \mu\mathrm{mol/m^2/s}\\
K &= k_{25\,^\circ\mathrm{C}} \times K_c(1 + p_o/K_o)\\
K_c &= \mathrm{e}^{(38.05-(9553.420009/T))} \times \mu\mathrm{mol/mol}\\
K_o &= \mathrm{e}^{(20.30-(4375.593855/T))} \times \mathrm{mmol/mol}\\
p_o &= 210\,\mathrm{mmol/mol}\\
R_d &= R_{d,25\,^\circ\mathrm{C}} \times \mathrm{e}^{(18.72-(5579.543675/T))} \times \mu\mathrm{mol/m^2/s}\\
V_{max} &= V_{max,25\,^\circ\mathrm{C}} \times \mathrm{e}^{(26.35-(7857.546634/T))} \times \mu\mathrm{mol/m^2/s}\\
\Gamma &= \gamma_{25\,^\circ\mathrm{C}} \times \mathrm{e}^{(19.02-(4549.992181/T))} \times \mu\mathrm{mol/mol}\\
\Theta_{PSII} &= 0.76 + 0.018\,T - 3.7 \times 10^{-4} T^2\\
\Phi_{PSII,max} &= 0.352 + 0.022\,T - 3.4 \times 10^{-4} T^2
\end{aligned} \tag{B.1}$$

T is measured in Kelvin. The factors $V_{max,25\,^\circ\mathrm{C}}$, $R_{d,25\,^\circ\mathrm{C}}$, $J_{max,25\,^\circ\mathrm{C}}$, $k_{25\,^\circ\mathrm{C}}$ and $\gamma_{25\,^\circ\mathrm{C}}$ which are part of the expressions V_{max}, R_d, J_{max}, K and Γ are required. (The introduction of $k_{25\,^\circ\mathrm{C}}$ and $\gamma_{25\,^\circ\mathrm{C}}$ represents a slight extension of the formulas of Bernacchi et al. (2003). The exact version of their formulas is recovered by setting $k_{25\,^\circ\mathrm{C}} = 1$ and $\gamma_{25\,^\circ\mathrm{C}} = 1$.)

B.2. Coefficients of diffusion

Nobel (1999) gives the following approximations for the temperature dependence of the coefficients of diffusion. They are (at least) valid in the range $T = 273.15 \ldots 313.15\,\mathrm{K}$ (resp. $0 \ldots 40\,^{\circ}\mathrm{C}$).

$$D_{CO_2} = \left(\frac{T}{273.15}\right)^{1.8} \times 1.33 \times 10^{-5}\ \frac{\mathrm{m}^2}{\mathrm{s}} \tag{B.2}$$

$$D_{H_2O} = \left(\frac{T}{273.15}\right)^{1.8} \times 2.13 \times 10^{-5}\ \frac{\mathrm{m}^2}{\mathrm{s}} \tag{B.3}$$

B.3. Saturation value of water vapour

The Clausius–Clapeyron equation provides an approximate (but for our purposes sufficiently correct) expression for $w_{sat}(T)$ (see Reif, 1974; Nobel, 1999)

$$w_{sat} := \frac{u}{T}\exp\left(-\frac{v}{T}\right) \tag{B.4}$$

with $u = 2.035 \times 10^{10}\,\mathrm{mol/m^3}$ and $v = 5306$ (T in K).

Appendix C. Relation between λ and hydraulic properties of soil and plant water conduits

In order to express λ in terms of quantities characterising the hydraulic properties of: (i) the soil on which the tree grows and (ii) the tree's water transport system between roots and leaves we proceed as follows.

Since photosynthesis consumes—compared to transpiration—only a small fraction of the water flux $j^{sl}_{H_2O}$ between soil and leaves we may conclude

$$-j^{sl}_{H_2O} = E = g(\lambda)a(w_{sat} - w_a) \tag{C.1}$$

where the right-hand side repeats Eq. (21) and $g(\lambda)$ represents expression (34). (The minus sign appears because we count fluxes going out of the leaves as negative.)

On the other hand (Katul et al., 2003), $j^{sl}_{H_2O}$ is related to the water potentials in soil (Ψ_s) and leaves (Ψ_l) and to the hydraulic resistances of the conduits between soil and roots (r_{sr}) and roots and leaves (r_{rl}) by

$$j^{sl}_{H_2O} = \frac{\Psi_s - \Psi_l}{r_{sr} + r_{rl}} \tag{C.2}$$

In unsaturated soils, r_{sr} and Ψ_s can be estimated from root and soil parameters (Clapp and Hornberger, 1978):

$$r_{sr}(\theta) = \frac{\pi L_d}{K(\theta)\sqrt{R_{AI}}} \tag{C.3}$$

$$K(\theta) = K_{sat}\left(\frac{\theta}{\theta_{sat}}\right)^{2b+3} \tag{C.4}$$

$$\Psi_s(\theta) = \Psi_{sat}\left(\frac{\theta}{\theta_{sat}}\right)^{-b} \tag{C.5}$$

L_d and R_{AI} denote the root-zone depth and the root area index, θ the soil moisture content and $b > 0$ is an empirical parameter depending on soil texture. θ_{sat} denotes the value of θ if the soil is saturated with water and K_{sat} and Ψ_{sat} are the values of the soil conductance $K(\theta)$ and of the soil water potential $\Psi_s(\theta)$ at $\theta = \theta_{sat}$.

Elimination of $j^{sl}_{H_2O}$ from (C.1) and (C.2) leads to

$$g(\lambda) = \frac{\Psi_l - \Psi_s(\theta)}{a(w_{sat} - w_a)(r_{sr}(\theta) + r_{rl})} \tag{C.6}$$

Results of Tyree and Sperry (1988) suggest that the water potential within the leaves approaches the critical value Ψ_l^{crit} at which cavitation commences when transpiration is at its diurnal maximum. Maximum transpiration implies maximum conductance $g_{max}(\lambda)$ between leaves and atmosphere. Hence, at maximum transpiration expression (C.6) becomes

$$g_{max}(\lambda) = \frac{\Psi_l^{crit} - \Psi_s(\theta)}{a(\widehat{w}_{sat} - \widehat{w}_a)(r_{sr}(\theta) + r_{rl})} \tag{C.7}$$

A hat above a quantity means that this quantity should be evaluated at the temperature and/or atmospheric humidity corresponding to g_{max} (see Figs. 5 and 4).

Equating (C.7) and (34) results in a quadratic equation for λ. One of its solutions represents an unphysical artefact. The meaningful solution reads as

$$\lambda = \frac{1}{2a(\widehat{w}_{sat} - \widehat{w}_a)}\left(\widehat{C}_a + \widehat{K} - \frac{Z}{N}\right) \tag{C.8}$$

where

$$Z := (\widehat{C}_a + \widehat{K})\left[\frac{(\widehat{C}_a + \widehat{K})(\Psi_l^{crit} - \Psi_s(\theta))}{a(\widehat{w}_{sat} - \widehat{w}_a)(r_{sr}(\theta) + r_{rl})} - (\widehat{q} - \widehat{R}_d)\right] + 2\,\widehat{q}(\widehat{K} + \widehat{\Gamma})$$

$$N := \sqrt{\left[\frac{(\widehat{C}_a + \widehat{K})(\Psi_l^{crit} - \Psi_s(\theta))}{a(\widehat{w}_{sat} - \widehat{w}_a)(r_{sr}(\theta) + r_{rl})} - (\widehat{q} - \widehat{R}_d)\right]^2 + 4\,\widehat{q}(\widehat{K} + \widehat{\Gamma})\frac{(\Psi_l^{crit} - \Psi_s(\theta))}{a(\widehat{w}_{sat} - \widehat{w}_a)(r_{sr}(\theta) + r_{rl})}}$$

and $r_{sr}(\theta)$ and $\Psi_s(\theta)$ are as given in (C.3) and (C.5).

Fig. 15 shows the result of applying expression (C.8) to a *Ginkgo biloba* growing on clay loam and on sand (see also Table 5). The shape of both $\lambda(\theta)$-curves corroborates the interpretation of the Lagrangian multiplier λ as indicating the "cost of water": (i) an increase in soil moisture content entails a decrease in λ, (ii) the variation of λ with θ is confined to the θ-interval between the soil moisture contents related to the permanent wilting point (θ_{PWP}) and the field capacity (θ_{FC}). $\lambda(\theta)$ is practically constant within the intervals $0 < \theta < \theta_{PWP}$ and $\theta_{FC} < \theta < \theta_{sat}$ (θ_{sat} represents soil saturation).

Appendix D. Expansion of assimilation rate *A* and transpiration rate *E* for small values of λ

Expanding expression (35) for A in a series with respect to $\lambda \ll 1$ we find the following structure:

$$A = a_0 + a_1\sqrt{\lambda} + a_3\sqrt{\lambda}^3 + a_5\sqrt{\lambda}^5 + \cdots \tag{D.1}$$

where the a_k are functions of the parameters in expression (35) (apart from λ).

Eq. (21) expresses the optimum transpiration rate E as a multiple of g (see expression (34)) according to $E = ag(w_{sat} - w_a)$. Expansion in a series with respect to $\lambda \ll 1$ results in

$$E = e_{-1}\frac{1}{\sqrt{\lambda}} + e_0 + e_1\sqrt{\lambda} + e_3\sqrt{\lambda}^3 + e_5\sqrt{\lambda}^5 + \cdots \tag{D.2}$$

The e_k are functions of the parameters in expression (34), they do not depend on λ.

Appendix E. Relationship between *g* and *v*

The function $g(C_a)$ (see expression (34) and Fig. 9) is characterised by the following features (in what follows, a prime $'$ denotes differentiation with respect to C_a): (i) a zero at $C_0 > 0$ (i.e. $g(C_0) = 0$), (ii) a maximum (i.e. $g'(C_m) = 0$) at $C_m > C_0$, (iii) an asymptotic value $\lim_{C_a \to \infty} g(C_a) = 0$, (iv) a positive derivative (i.e. $g'(C_a) > 0$) within the interval $C_0 < C_a < C_m$, (v) a negative derivative

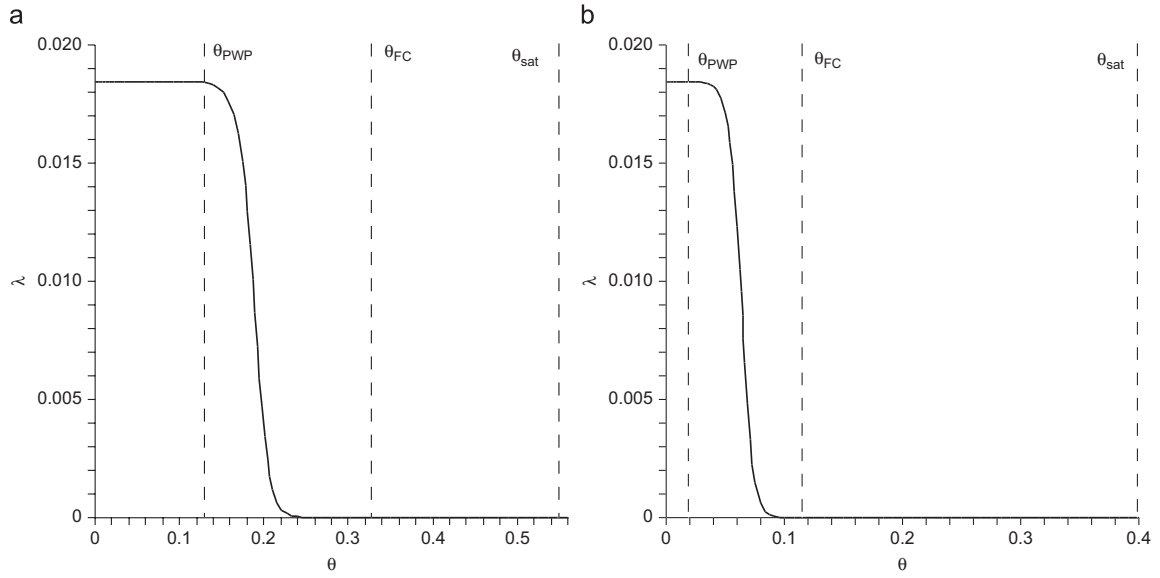

Fig. 15. Dependence of the Lagrangian multiplier λ ("cost of water") on the soil moisture content θ according to expression (C.8). Parameters used are as in Table 5. *Left*: $\lambda(\theta)$-curve of *Ginkgo biloba* growing on clay loam. *Right*: $\lambda(\theta)$-curve of *Ginkgo biloba* growing on sand. Vertical broken lines indicate soil moisture contents related to the permanent wilting point (θ_{PWP}), field capacity (θ_{FC}) and soil saturation (θ_{sat}): (a) clay loam and (b) sand.

Table 5
Hydraulic and ecophysiological parameters used in Fig. 15 (*Ginkgo biloba* growing on clay loam and on sand)

Symbol	Unit	Value for clay loam	Value for sand	Source/Remarks
Soil				
K_{sat}	m/s	3.39×10^{-6}	19.4×10^{-6}	Katul et al. (2003)
Ψ_{sat}	Pa	−1147	−637	Katul et al. (2003)
b	–	4.95	2.56	Katul et al. (2003)
θ_{sat}	–	0.55	0.40	Katul et al. (2003)
Root				
L_d	m	0.3	1.0	Katul et al. (2003)
R_{Al}	m^2/m^2	5.46	14.19	Katul et al. (2003)
Plant				
L_{Al}	m^2/m^2	3.8	1.8	Katul et al. (2003)
ψ_l^{crit}	MPa	−1.8	−1.8	Estimate
r_{rl}	Pa m^2 s/mol	1538	934	Katul et al. (2003)
w_a	mmol/mol	637	637	See Table 2
T	°C	19.07	19.07	See Table 2

(i.e. $g'(C_a)<0$) within the interval $C_a>C_m$. (Values of $g(C_a)$ for $C_a<C_0$ are not meaningful for us.)

We show now that the function

$$v(C_a)=\frac{1}{a_{st}}\frac{\left[d_{st}^{geom}+\sqrt{\frac{a_{st}}{\pi}}\right]g(C_a)}{\left\{D_{CO_2}-\left[d_{bl}+d_{as}\frac{\tau_{as}^2}{n_{as}}\right]g(C_a)\right\}} \tag{E.1}$$

$v(C_a)$ (as given in (36)) inherits the properties (i) through (v) from $g(C_a)$. Differentiating (E.1) with respect to C_a we find

$$v'(C_a)=\frac{1}{a_{st}}\frac{D_{CO_2}\left[d_{st}^{geom}+\sqrt{\frac{a_{st}}{\pi}}\right]}{\left\{D_{CO_2}-\left[d_{bl}+d_{as}\frac{\tau_{as}^2}{n_{as}}\right]g(C_a)\right\}^2}g'(C_a) \tag{E.2}$$

Provided that the braces in the denominators of (E.1) and (E.2) are strictly positive (which will be shown below), it is obvious that (E.1) implies $v(C_0)=0$ and $\lim_{C_a\to\infty}v(C_a)=0$. Since D_{CO_2} and the anatomical quantities are positive we may conclude from (E.2) $v'(C_m)=0$, $v'(C_a)>0$ for $C_0<C_a<C_m$, and $v'(C_a)<0$ for $C_a>C_m$.

In order to show that the expression $\{D_{CO_2}-[d_{bl}+d_{as}(\tau_{as}^2/n_{as})]g(C_a)\}$ is strictly positive for $C_a>C_0$ we start from expression $n_{st}=a_{st}\,v$ (see (13)) for the porosity of the stomatal layer. $a_{st}\,v=1$ is—irrespective of the value of C_a—certainly an upper limit for the stomatal density even if this upper limit is not realistic: it implies that the leaf surface is completely covered with stomatal openings. From (19) we conclude that the conductance corresponding to $a_{st}\,v=1$ reads as

$$g_{ul}=\frac{D_{CO_2}}{d_{bl}+d_{as}\frac{\tau_{as}^2}{n_{as}}+d_{st}} \tag{E.3}$$

Then we find for the denominators of (E.1) and (E.2)

$$\begin{aligned}\left\{D_{CO_2}-\left[d_{bl}+d_{as}\frac{\tau_{as}^2}{n_{as}}\right]g(C_a)\right\}&>D_{CO_2}-\left[d_{bl}+d_{as}\frac{\tau_{as}^2}{n_{as}}\right]g_{ul}\\&=D_{CO_2}-\frac{\left[d_{bl}+d_{as}\frac{\tau_{as}^2}{n_{as}}\right]D_{CO_2}}{d_{bl}+d_{as}\frac{\tau_{as}^2}{n_{as}}+d_{st}}\\&=\frac{D_{CO_2}\,d_{st}}{d_{bl}+d_{as}\frac{\tau_{as}^2}{n_{as}}+d_{st}}\geqslant 0\end{aligned} \tag{E.4}$$

where the first step uses the finding that g_{ul} represents an upper limit of $g(C_a)$ (i.e. $g_{ul}>g(C_a)$). The second step exploits (E.3). Additionally, we rely on all anatomical quantities being positive.

This completes the proof that $v(C_a)$ shares the properties (i) through (v) (and thus its shape) with $g(C_a)$.

References

Aalto, T., Juurola, E., 2002. A three-dimensional model of CO_2 transport in air-spaces and mesophyll cells of a silver birch leaf. Plant Cell Environ. 25, 1399–1409.

Ainsworth, E.A., Long, S.P., 2005. What have we learned from fifteen years of free air carbon dioxide enrichment (FACE)? A meta-analytic review of the responses of photosynthesis canopy properties and plant production to rising CO_2. New Phytol. 165, 351–372.

Ainsworth, E.A., Rogers, A., 2007. The response of photosynthesis and stomatal conductance to rising [CO_2]: mechanisms and environmental interactions. Plant Cell Environ. 30, 258–270.

Arfken, G., 1970. Mathematical Methods for Physicists. Academic Press, New York.

Aris, R., 1975. The Mathematical Theory of Diffusion and Reaction in Permeable Catalysts. The Theory of the Steady State. Oxford University Press, London.

Beerling, D.J., 2002. Low atmospheric CO_2 levels during the Permo-Carboniferous glaciation inferred from fossil lycopsids. PNAS 99, 12567–12571.

Beerling, D.J., Kelly, C.K., 1997. Stomatal density responses of temperate woodland plants over the past seven decades of CO_2 increase: a comparison of Salisbury (1927) with contemporary data. Am. J. Bot. 84, 1572–1583.

Beerling, D.J., Royer, D.L., 2002. Reading a CO_2 signal from fossil stomata. New Phytol. 153, 387–397.

Beerling, D.J., Birks, H.H., Woodwarf, F.I., 1995. Rapid late-glacial atmospheric CO_2, changes reconstructed from the stomatal density record of fossil leaves. J. Quat. Sci. 10, 379–384.

Beerling, D.J., McElwain, J.C., Osborne, C.P., 1998. Stomatal responses of the 'living fossil' *Ginkgo biloba* L. to changes in atmospheric CO_2 concentrations. J. Exp. Bot. 49, 1603–1607.

Bernacchi, C.J., Pimentel, C., Long, S.P., 2003. *In vivo* temperature response functions of parameters required to model RuBP-limited photosynthesis. Plant Cell Environ. 26, 1419–1430.

Berner, R.A., Kothvala, Z., 2001. GEOCARBIII: a revised model of atmospheric CO_2 over Phanerozoic time. Am. J. Sci. 301, 182–204.

Berninger, F., Mäkelä, A., Hari, P., 1996. Optimal control of gas exchange during drought: empirical evidence. Ann. Bot. 77, 469–476.

Buckley, T.N., Miller, J.M., Farquhar, G.D., 2002. The mathematics of linked optimisation for water and nitrogen use in a canopy. Silva Fenn. 36, 639–669.

Clapp, R., Hornberger, G., 1978. Empirical equations for some soil hydraulic properties. Water Resour. Res. 14, 601–604.

Copeland, E.B., 1902. The mechanism of stomata. Ann. Bot. 16, 327–364.

Cowan, I.R., 1977. Stomatal behaviour and environment. Adv. Bot. Res. 4, 117–228.

Cowan, I.R., Farquhar, G.D., 1977. Stomatal function in relation to leaf metabolism and environment. Symp. Soc. Exp. Biol. 31, 471–505.

Denk, T., Velitzelos, D., 2002. First evidence of epidermal structures of Ginkgo from the Mediterranean Tertiary. Rev. Palaeobot. Palynol. 120, 1–15.

Farquhar, G.D., von Caemmerer, S., Berry, J.A., 1980. A biochemical model of photosynthetic CO_2 assimilation in leaves of C_3 species. Planta 149, 78–90.

Farquhar, G.D., von Caemmerer, S., Berry, J.A., 2001. Models of photosynthesis. Plant Physiol. 125, 42–45.

Farquhar, G.D., Buckley, T.N., Miller, J.M., 2002. Optimal stomatal control in relation to leaf area and nitrogen content. Silva Fenn. 36, 625–637.

Garcia-Amorena, I., Wagner, F., van Hoof, T.B., Gomez Manzaneque, F.G., 2006. Stomatal responses in deciduous oaks from southern Europe to the anthropogenic atmospheric CO_2 increase; refining the stomatal-based CO_2 proxy. Rev. Palaeobot. Palynol. 141, 303–312.

Hari, P., Mäkelä, A., Korpilahti, E., Holmberg, M., 1986. Optimal control of gas exchange. Tree Physiol. 2, 169–175.

Hovenden, M.J., Schimanski, L.J., 2000. Genotypic differences in growth and stomatal morphology of Southern Beech, *Nothofagus cunninghamii*, exposed to depleted CO_2 concentrations. Aust. J. Plant Physiol. 27, 281–287.

Katul, G.G., Ellsworth, D.S., Lai, C.-T., 2000. Modelling assimilation and intercellular CO_2 from measured conductance: a synthesis of approaches. Plant Cell Environ. 23, 1313–1328.

Katul, G.G., Leuning, R., Oren, R., 2003. Relationship between plant hydraulic and biochemical properties derived from a steady-state coupled water and carbon transport model. Plant Cell Environ. 26, 339–350.

Kouwenberg, L.L., McElwain, J.C., Kürschner, W., Wagner, F., Beerling, D.J., Mayle, F.E., Visscher, H., 2003. Stomatal frequency adjustment of four conifer species to historical changes in atmospheric CO_2. Am. J. Bot. 90, 610–619.

Kürschner, W.M., 1996. Leaf stomata as biosensors of palaeoatmospheric CO_2 levels. Laboratory of Palaeobotany and Palynology. Utrecht University, Utrecht.

Kürschner, W.M., Kvacek, Z. Dilcher, D.L., 2008. The impact of Miocene atmospheric carbondioxide fluctuations on climate and the evolution of terrestrial ecosystems. PNAS 105, 449–453.

Kürschner, W.M., van der Burgh, J., Visscher, H., Dilcher, D.L., 1996. Oak leaves as biosensors of late Neogene and early Pleistocene palaeoatmospheric CO_2 concentrations. Mar. Micropalaeontol. 27, 299–312.

Kürschner, W.M., Stulen, I., Wagner, F., CKuiper, P.J., 1998. Comparison of palaeobotanical observations with experimental data on the leaf anatomy of Durmast oak [*Quercus petraea* (Fagaceae)] in response to environmental change. Ann. Bot. 81, 657–664.

Lake, J.A., Quick, W.P., Beerling, D.J., Woodward, F.I., 2001. Plant development—signals from mature to new leaves. Nature 411, 154.

Lake, J.A., Woodward, F.I., PQuick, W., 2002. Long-distance CO_2 signalling in plants. J. Exp. Bot. 53, 183–193.

Lawson, T., Craigon, J., Black, C.R., Colls, J.J., Landon, G., Weyers, J.D.B., 2002. Impact of elevated CO_2 and O_3 on gas exchange parameters and epidermal characteristics in potato (*Solanum tuberosum* L.). J. Exp. Bot. 53, 737–746.

Long, S.P., Ainsworth, E.A., Rogers, A., Ort, D.R., 2004. Rising atmospheric carbon dioxide: plants FACE the future. Annu. Rev. Plant Biol. 55, 591–628.

Mäkelä, A., Berninger, F., Hari, P., 1996. Optimal control of gas exchange during drought: theoretical analysis. Ann. Bot. 77, 461–467.

McElwain, J.C., Mayle, F.E., Beerling, D.J., 2002. Stomatal evidence for a decline in atmospheric CO_2 concentrations during the Younger Dryas stadial: a comparison with Antarctic ice core records. Quat. Sci. 17, 21–29.

Medlyn, B.E., Badeck, F.W., De Pury, D.G.G., Barton, C.V.M., Broadmeadow, M., Ceulemans, R., De Angelis, P., Forstreuter, M., Jach, M.E., Kellomäki, S., Laitat, E., Marek, M., Philippot, S., Rey, A., Strassemeyer, J., Laitinen, K., Liozon, R., Portier, B., Roberntz, P., Wang, K., Jarvis, PG., 1999. Effects of elevated [CO_2] on photosynthesis in European forest species: a meta-analysis of model parameters. Plant Cell Environ. 22, 1475–1495.

Medlyn, B.E., Barton, C.V.M., Broadmedow, M.S.J., Ceulemans, R., De Angelis, P., Forstreuter, M., Freeman, M., Jackson, S.B., Kellomäki, S., Laitat, E., Rey, A., Roberntz, P., Sigurdsson, B.D., Strassemeyer, J., Wang, K., Curtis, P.S., Jarvis, P.G., 2001. Stomatal conductance of forest species after long-term exposure to elevated CO_2 concentration: a synthesis. New Phytol. 149, 247–264.

Napp-Zinn, K., 1966. Anatomie des Blattes. I: Blattanatomie der Gymnospermen. Borntraeger, Berlin.

Nobel, P.S., 1999. Physicochemical and Environmental Plant Physiology, second ed. Academic Press, New York.

Overdieck, D., Strassemeyer, J., 2005. Gas exchange of *Ginkgo biloba* leaves at different CO_2 concentration levels. Flora 200, 159–167.

Pagani, M., Zachos, J.C., Freeman, K.H., Tipple, B., Bohaty, S., 2005. Marked decline in atmospheric carbon dioxide concentrations during the paleogene. Science 309, 600–603.

Parkhurst, D.F., 1994. Diffusion of CO_2 and other gases inside leaves. Phytology 126, 449–479.

Parkhurst, D.F., Mott, K.A., 1990. Intercellular diffusion limits to CO_2 uptake in leaves. Plant Physiol. 94, 1024–1032.

Penuelas, J., Matamala, R., 1990. Changes in N and S leaf content, stomatal density and specific leaf area in 14 plant species during the last three centuries. J. Exp. Bot. 41, 1119–1124.

Poole, I., Kürschner, W.M., 1999. Stomatal Density and Index: The Practice. The Geological Society, London.

Prentice, I., Farquhar, G., Fasham, M., Goulden, M., Heinmann, M., et al., 2001. The carbon cycle and atmospheric carbon dioxide. In: Houghton, J.T., Ding, Y., Griggs, D.J., Noguer, M., van der Linden, P.J., et al. (Eds.), Climate Change 2001: The Scientific Basis. Contributions of Working Group I to the Third Assessment Report of the Intergovernmental Panel on Climate Change. Cambridge University Press, Cambridge, UK, pp. 183–238.

Reich, P.B., Hungate, B.A., Luo, Y., 2006. Carbon–nitrogen interactions in terrestrial ecosystems in response to rising atmospheric carbon dioxide. Annu. Rev. Ecol. Evol. Systematics 37, 611–636.

Reid, C.D., Maherali, H., Johnson, H.B., Smith, S.D., Wullschleger, S.D., Jackson, R.B, 2003. On the relationship between stomatal characters and atmospheric CO_2. Geophys. Res. Lett. 30, Article no. 1983.

Reif, F., 1974. Fundamentals of Statistical and Thermal Physics. McGraw-Hill, New York.

Royer, D.L., 2001. Stomatal density and stomatal index as indicators of palaeoatmospheric CO_2 concentration. Rev. Palaeobot. Palynol. 114, 1–28.

Royer, D.L., Wing, S.L., Beerling, D.J., Jolley, D.W., Koch, P.L., Hickey, L.J., Berner, R.A., 2001. Paleobotanical evidence for near present-day levels of atmospheric CO_2 during part of the Tertiary. Science 292, 2310–2313.

Senatsverwaltung für Stadtentwicklung Berlin, 1993. Digitaler Umweltatlas Berlin (Ausgabe 1993), 04.04 Temperatur- und Feuchteverhältnisse in mäßig austauscharmen Strahlungsnächten, ⟨http://www.stadtentwicklung.berlin.de/umwelt/umweltatlas/din_404.htm⟩.

Stitt, M., Krapp, A., 1999. The interaction between elevated carbon dioxide and nitrogen nutrition: the physiological and molecular background. Plant Cell Environ. 22, 581–621.

Sun, B., Dilcher, D.L., Beerling, D.J., Zhang, C., Yan, D., Kowalski, E., 2003. Variation in *Ginkgo biloba* L. leaf characters across a climatic gradient in China. PNAS 100, 7141–7146.

Teng, N., Wang, J., Chen, T., Wu, X., Wang, Y., Lin, J., 2006. Elevated CO_2 induces physiological, biochemical and structural changes in leaves of *Arabidopsis thaliana*. New Phytol. 172, 92–103.

Tricker, P.J., Trewin, H., Kull, O., Clarkson, G.J.J., Eensalu, E., Tallis, M.J., Colella, A., Doncaster, C.P., Sabatti, M., Taylor, G., 2005. Stomatal conductance and not

stomatal density determines the long-term reduction in leaf transpiration of poplar in elevated CO_2. Oecologia 143, 652–660.
Tyree, M.T., Sperry, J.S., 1988. Do woody plants operate near the point of catastrophic xylem dysfunction caused by dynamic water stress? Plant Physiol. 88, 574–580.
van de Water, P.K., Leavitt, S.W., Betancourt, J.L., 1994. Trends in stomatal density and $^{13}C/^{12}C$ ratios of *Pinus flexilis* during last glacial–interglacial cycle. Science 264, 239–242.
Woodward, F.I., 1987. Stomatal numbers are sensitive to increases in CO_2 concentration from pre-industrial levels. Nature 327, 617–618.
Woodward, F.I., Bazzazz, F.A., 1988. The responses of stomatal density to CO_2 partial pressure. J. Exp. Bot. 39, 1771–1781.
Woodward, F.I., Lake, J.A., PQuick, W., 2002. Stomatal development and CO_2: ecological consequences. New Phytol. 153, 477–484.
Wynn, J.G., 2003. Towards a physically based model of CO_2-induced stomatal frequency response. New Phytol. 157, 394–398.

3.2 Grein, M., Utescher, T., Wilde, V., Roth-Nebelsick, A.: **Reconstruction of the middle Eocene climate of Messel using palaeobotanical data. - Neues Jahrbuch für Geologie und Paläontologie, Abhandlungen. (accepted for publication)**

Reconstruction of the middle Eocene climate of Messel using palaeobotanical data

Michaela Grein, Torsten Utescher, Volker Wilde & Anita Roth-Nebelsick

ABSTRACT

The middle Eocene Messel Pit represents the filling of a maar lake which has provided numerous well-preserved plant fossils including leaves, palynomorphs, fruits and seeds. Although a number of studies have been carried out with respect to the climatic conditions during the deposition of the Messel maar sediments, these resulted in estimates mainly based on general floral characteristics and not in quantitative data. Here, we apply the Coexistence Approach to the Messel plant taphocoenosis in order to obtain a quantitative reconstruction of the middle Eocene climate including mean annual temperature, mean temperature of the warmest and coldest month, mean annual precipitation, mean precipitation of the wettest, driest and warmest month as well as the mean relative air humidity. Since the correct identification of a nearest living relative species or genus is frequently problematic for Eocene species, climate calculations are based on family level. Thus, the present study serves as a case study for the application of the Coexistence Approach on family level to a plant taphocoenosis of Eocene age. In order to obtain supplementary data for climate, mean annual temperature was also calculated by Leaf Margin Analysis.

For Messel, our results indicate a mean annual temperature of approximately 22°C (up to ~24°C) with a mean temperature of the coldest month clearly above 10°C. Mean annual precipitation rates amounted to about 2540 mm and mean relative air humidity reached 77%. In spite of some uncertainties caused by the comparison on family level and potential changes in the climatic limitations of the respective families, both CA and LMA confirm a warm and humid, frost-free climate for the middle Eocene of Messel.

ABBREVIATIONS

CA	Coexistence Approach
LMA	Leaf Margin Analysis
MAP	mean annual precipitation in mm
MAT	mean annual temperature in °C
MRH	mean relative air humidity in %
NLR	Nearest Living Relative
P_{dry}	mean precipitation of the driest month in mm
P_{warm}	mean precipitation of the warmest month in mm
P_{wet}	mean precipitation of the wettest month in mm
T_{cold}	mean temperature of the coldest month in °C
T_{warm}	mean temperature of the warmest month in °C

INTRODUCTION

Global climate change represents one of the largest challenges for mankind in the 21st century. The reconstruction and understanding of past climates is vital for estimating consequences of future climate change. The Eocene represents a crucial geological period in which "greenhouse" conditions prevailed (for example ZACHOS et al. 1994; GREENWOOD & WING 1995; WILF et al. 1998; GINGERICH 2006; JAHREN 2007; HOLLIS et al. 2009). Following the Early Eocene Climatic Optimum (EECO), global cooling occurred towards the Oligocene, as is indicated by deep sea temperatures derived from isotope records (ZACHOS et al. 2001; DUPONT-NIVET et al. 2007). The decline in global temperatures was accompanied by a number of faunal and floral changes (for example FRANCIS & POOLE 2002; various contributions in PROTHERO et al. 2003). The cooling phase included various oscillations (TRIPATI et al. 2005; VILLA et al. 2008). There is evidence for sea ice already appearing in the middle Eocene during cold intervals (STICKLEY et al. 2009). Eocene climate change would thus have been not continuous but dynamic.

The majority of information about Eocene climate development is derived from marine data. Terrestrial data are more sparse, but important to understand the entire Eocene climate system and its transformations. In this contribution, the middle Eocene climate at a Central European spot, the Messel Pit close to Darmstadt (Hesse, Germany) is reconstructed. This well-dated site is characterized by numerous fossils showing an excellent preservation.

The typical laminated oilshale of the Middle Messel Formation (FELDER & HARMS 2004) was commercially mined for more than a hundred years until the early 1970ies. During mining and later scientific excavations, plenty of well-preserved plant remains were collected serving as a base for a number of systematic studies on leaves (e.g. ENGELHARDT 1922; STURM 1971, 1978; WILDE 1989), palynomorphs (e.g. THIELE-PFEIFFER 1988; LENZ et al. 2007), fruits/seeds (e.g. COLLINSON 1982, 1988), flowers (e.g. SCHAARSCHMIDT 1986) and occasional wood (WILDE & SÜß 2001).

In this study, climate reconstruction for Messel during the middle Eocene was performed by using plant fossils. Several approaches have been developed for palaeoclimate reconstructions of terrestrial environments based on plant remains. Leaf physiognomic data represent one essential data source for palaeoclimate estimates and calculations. Leaf Margin Analysis (LMA) deals with the distinct correlation of leaf margin characters in woody dicot leaves and mean annual temperatures (BAILEY & SINNOTT 1915, 1916; WOLFE 1979; SPICER & PARRISH 1986; PARRISH & SPICER 1988; WING & GREENWOOD 1993; WILF 1997; JACOBS 2002; GREENWOOD et al. 2004; TRAISER et al. 2005; ROYER & WILF 2006; YANG et al. 2007). The Climate-Leaf Analysis Multivariate Program (CLAMP) (WOLFE 1993, 1995; WOLFE & SPICER 1999), is based on the geographic distribution of a large set of woody dicot leaf physiognomic character states (currently 31, YANG et al. 2007). The European Leaf Physiognomic Approach (ELPA) is a multivariate leaf physiognomic approach based on a European calibration dataset (TRAISER 2004; TRAISER et al. 2005; TRAISER & MOSBRUGGER 2006). The semi-quantitative IPR (Integrative Plant Record) is based on a taxonomic/physiognomic grouping of all available organ assemblages of a site to evaluate the essential ecological features of the palaeovegetation and emphasizes the climate information provided by zonal taxa growing under mesic soil conditions (KOVAR-EDER & KVAČEK 2007; KOVAR-EDER et al. 2008).

Other common methods for palaeoclimate reconstruction use the climatic tolerances of nearest living relatives (NLR). Overlapping Distribution Analysis (ODA) is based on plant geographic and altitudinal distribution data (YANG et al. 2007), and the Coexistence Approach (CA) on a calibration dataset containing climatic requirements of over 800 Cenozoic plant taxa that have modern relatives (MOSBRUGGER & UTESCHER 1997). Although the CA has been applied successfully to Asian and European plant taphocoenoses from the Cenozoic (MOSBRUGGER & UTESCHER 1997; BRUCH 1998; PROSS et al. 1998; UTESCHER et al. 2000; IVANOV et al. 2002; KVAČEK et al. 2002; LIANG et al. 2003; UHL et al. 2003; ROTH-NEBELSICK et al. 2004; MOSBRUGGER et al. 2005; UTESCHER et al. 2009), most of these studies are restricted to the Miocene and Pliocene. MOSBRUGGER & UTESCHER (1997) expected the CA to produce the best results for Oligocene and younger plant taphocoenoses as the identification of a close living relative becomes more difficult with increasing age of the fossil. Therefore, a lower resolution with larger intervals for the individual climate parameters is expected for plant assemblages older than the Oligocene. In terms of extant taxa, Eocene plant remains can frequently only be reliably identified to the family level and, moreover, their climatic requirements may have changed with time. Application of both, the CA and LMA, to a late Eocene assemblage of plant remains resulted in significantly higher MAT values for the LMA compared to the CA (ROTH-NEBELSICK et al. 2004).

In the present study, the CA is applied to the diverse plant taphocoenosis of the middle Eocene Middle Messel Formation. Additionally, LMA is carried out on the Messel leaves to compare their MAT values to the MAT calculations as derived from CA. Previous studies concerning the middle Eocene climate of Messel resulted in only general statements (e.g. SCHAARSCHMIDT 1988; WILDE 1989, 2005; WILDE & MICKLICH 2007). Here, we present for the first time a quantitative reconstruction of various climate parameters for the Messel plant taphoecoenosis.

MATERIALS & METHODS

The middle Eocene Messel Formation represents the sedimentary infilling of a maar lake near Darmstadt (Hesse, Germany; 49°N, 8°E) which formed as a consequence of phreatomagmatic activity. As a famous site for excellently preserved fossils, Messel has been awarded UNESCO World Heritage status. The lapilli tuff sequence underlying the lacustrine deposits of the Messel Maar sediments has been dated to 47.8 Ma B.P. ± 0.2 myr (MERTZ & RENNE 2005). Sedimentation at Messel lasted to about 1 myr, with an age around 47 Ma for the top of the sediments. The Messel Formation therefore spans a limited time interval of the middle Eocene which is close to both the atmospheric carbon dioxide peak indicated by the data of PEARSON & PALMER (2000) as well as the thermal and mammalian species-diversity maximum of the early middle Eocene (BLONDEL 2001).

The coexistence approach (CA)

In the present paper, the coexistence approach (CA) of MOSBRUGGER & UTESCHER (1997) was applied in order to obtain a quantitative reconstruction of the middle Eocene climate for Messel. In this procedure climatic requirements of all ‘‘Nearest Living Relatives’’ (NLR) known for a fossil plant taphocoenosis are used to reconstruct the conditions under which the fossil plants existed assuming that their climatic requirements are similar. The CA relies on

the identification of the nearest living relatives of a fossil species. A meaningful identification of NLRs should be based on physiognomic characters and phylogenetic evidence (MOSBRUGGER & UTESCHER 1997). For Eocene species, the convincing identification of a nearest living relative species may be quite difficult (WILDE 1989), and there is a considerable amount of extinct genera in Northern Hemisphere Paleogene plant taphocoenoses as previously noted for some well studied examples including the early Eocene London Clay (fruits/seeds: COLLINSON 1983), the middle Eocene Clarno Nut Beds in western North America (fruits/seeds: MANCHESTER 1994; wood: WHEELER & MANCHESTER 2002), or the Claiborne Formation in south-eastern North America (leaves, fruits/seeds: DILCHER 2000). Therefore, comparisons and interpretations for Messel were mostly based on family level (e.g. WILDE 1989, 2004). Although the CA is commonly recommended to be ideally performed on the species level, in the case of a middle Eocene plant taphocoenosis like the one from Messel, identification on family level seems to be much more reliable than on genus or species level. Therefore, climate calculations in this study are based on the identification of taxa at the family level.

Plant families used in the CA (n = 55) *represented only by pollen/spores according to Wilde (2004)		
Aceraceae	Hamamelidaceae	Pinaceae*
Anacardiaceae	Hydrocharitaceae	Platanaceae (*Platanus* sp.)
Apocynaceae	Icacinaceae	Restionaceae*
Aquifoliaceae*	Juglandaceae	Rutaceae
Araceae	Lauraceae	Sapotaceae*
Araliaceae	Loranthaceae	Schizaeaceae
Arecaceae	Lythraceae(*)	Simaroubaceae
Berberidaceae	Magnoliaceae	Smilacaceae
Betulaceae*	Mastixiaceae	Staphyleaceae
Bombacaceae*	Menispermaceae	Sterculiaceae(*)
Buxaceae	Moraceae	Symplocaceae
Caprifoliaceae	Myricaceae	Theaceae
Chloranthaceae*	Myrtaceae	Thymelaeaceae*
Cornaceae	Nymphaeaceae	Tiliaceae
Cupressaceae	Nyssaceae	Ulmaceae
Cyrillaceae*	Olacaceae*	Vitaceae
Euphorbiaceae	Oleaceae*	Zingiberaceae
Fagaceae*	Osmundaceae	
Gleicheniaceae	Pandanaceae	

Tab. 1. List of all plant families compiled by Wilde (2004) and their use in the CA

insecure plant families (n = 45), excluded from the analysis		
Annonaceae	Iridaceae	Rubiaceae
Aristolochiaceae	Malpighiaceae	Santalaceae
Bignoniaceae	Melastomaceae	Styracaceae
Casuarinaceae	Monimiaceae	Cercidiphyllaceae
Cecropiaceae	Musaceae	Cyatheaceae
Celastraceae	Myristicaceae	Cyclanthaceae
Combretaceae	Myrsinaceae	Illiciaceae/Malvaceae
Convolvulaceae	Nelumbonaceae	Lecythidaceae
Coriariaceae	Piperaceae	Nyctaginaceae
Cunoniaceae	Pittosporaceae	Parkeriaceae
Cycadophyts	Poaceae	Sapindaceae
Ebenaceae	Podocarpaceae	Sargentodoxaceae
Eleagnaceae	Potamogetonaceae	Sparganiaceae
Flacourtiaceae	Proteaceae	Typhaceae
Ginkgophyts	Rhamnaceae	Verbenaceae

Cosmopolitans families, no data available (n = 8), excluded from the analysis		
Blechnaceae	Leguminosae	Salicaceae
Cyperaceae	Polypodiaceae	Selaginellaceae
Ericaceae	Rosaceae	

monotypic families (n = 3), excluded from the analysis		
Cephalotaxaceae	Eucommiaceae	Sciadopityaceae

Tab. 1. (continued)

In order to determine the most probable climate conditions for a plant taphocoenosis all known NLRs are used. For each NLR the interval (maximum and minimum) of a certain climate parameter is defined by comparing the taxon distribution to climate data. After defining the intervals of all NLRs known for a fossil taphocoenosis, the overlap for a certain climate parameter is determined. Finally, an interval is derived in which all these taxa could potentially coexist. Climatic tolerances were extracted from the PALAEOFLORA database (UTESCHER & MOSBRUGGER 2010) and imported as ASCII file into ClimStat (V1.02), a FORTRAN program used to determine the coexistence interval for climate parameters.

Here, eight climate parameters were calculated: 1) mean annual temperature (MAT), 2) mean temperature of the warmest month (T_{warm}), 3) mean temperature of the coldest month (T_{cold}), 4) mean annual precipitation (MAP), 5) mean precipitation of the wettest month (P_{wet}),

6) mean precipitation of the driest month (P_{dry}), 7) mean precipitation of the warmest month (P_{warm}), 8) mean relative air humidity (MRH).

The analysis is based on the most recent summary of the plant taphocoenosis from the middle Eocene oilshale of Messel (WILDE 2004) which lists 111 families of pteridophytes, lycophytes, gymnosperms and angiosperms. After excluding insecure taxa, cosmopolitans with no available climate data and monotypic families, the CA was applied to the remaining 55 families which included the macrofossil (leaves, fruits, seeds, flowers, cones, wood) and the microfossil (pollen, spores) record (Tab. 1). Since the results of separate analyses of the macro- and microfossils turned out to be rather similar, both were combined into an integrated analysis which is presented here.

Leaf margin analysis (LMA)

The monograph of WILDE (1989) provides a modern overview of the Messel leaf assemblage containing systematic descriptions of 60 dicotyledonous angiosperm leaf types. 53 of them were regarded as woody and were used for LMA. Aquatic plants, plants with insecure leaf margin type and herbs were excluded. Concerning Leguminosae, just three of five morphospecies were included into LMA because their parent plants could not be reliably assigned to be either woody or herbaceous types. As both of these types occur within the Leguminosae half of the morphospecies was excluded. In the present study, the simple LMA (considering only leaf margin type) is used because multiple characteristic approaches such as CLAMP may not necessarily be more reliable than the simple LMA (WILF 1997; WIEMANN et al. 1998). Leaf margins were determined according to descriptions and images of WILDE (1989) and STURM (1971). In order to cover all approaches to LMA, two procedures were used. In the first procedure, a taxon receives the score of "1" if its leaves are completely "entire", that is, without teeth, serrations, crenations and undulations. If a morphotaxon had both "entire" and "not entire" leaves, it received a score of "0.5". In the second procedure, a taxon received a score of "0" (toothed), if it showed only vascularized extension with an incision less than one quarter the distance from leaf margin to midrib. Following the recommendation of WILF (1997) all other extensions as well as lobes were not scored as teeth. Also in this approach, species showing both entire and non-entire margins received a score of "0.5".

The proportion of leaves with entire margin (or "non-toothed" margin respectively) was used in linear equations to calculate the MAT. These linear equations are the results of LMAs carried out and tested on extant floras of different geographical regions. Here, three equations were used (Tab. 2). Their standard deviation (sampling error) of MAT was calculated after WILF (1997).

Transfer function for MAT	**flora**	**authors**
1.141 + 0.306 x %entire	East Asia	WING & GREENWOOD 1993
2.240 + 0.286 x %entire	N-, M- and S-America	WILF 1997
0.512 + 0.314 x %entire	Europe	TRAISER et al. 2005

Tab. 2. Transfer functions of mean annual temperature used for LMA after different authors

RESULTS

Results of palaeoclimate calculations are listed in table 3 including the coexistence intervals and the families from which these intervals were derived.

Temperature

Temperature calculations obtained from CA (Figs. 1–3) suggest a MAT from 16.8 to 23.9°C and a T_{cold} from 10.6 to 19.4°C. In both cases the interval limits are constrained by Bombacaceae (lower limit) and Nyssaceae (upper limit). The calculation for T_{warm} indicates an interval of 24.7 to 27.9°C limited by Icacinaceae (lower limit) and Nyssaceae (upper limit). MAT calculations obtained from LMA indicate temperatures from 21.7 ± 1.8°C to 23.1 ± 1.9°C (average value: 22.4°C).

Precipitation

Precipitation calculations (Figs. 4–7) indicate values for MAP between 803 and 2540 mm with Cyrillaceae (lower limit) and Platanaceae/Restionaceae (upper limit) constraining the coexistence interval. Mastixiaceae set the lower limit of P_{wet} at 175 mm whereas the upper limit is defined by Cyrillaceae to about 329 mm. For P_{dry}, the CA indicates values between 9 and 56 mm with limits constrained by Araceae (lower limit) and Restionaceae (upper limit). Calculations for P_{warm} indicate an interval of about 139 to 154 mm limited by Chloranthaceae (lower limit) and Betulaceae (upper limit).

Mean relative humidity

MRH calculation (Fig. 8) indicates values between 73 and 77%. Interval boundaries are constrained by Myrtaceae (lower limit) and Juglandaceae/Restionaceae (upper limit). Nine families had to be excluded from analysis because of missing data: Berberidaceae, Cupressaceae, Gleicheniaceae, Magnoliaceae, Pinaceae, Schizaeaceae, Staphyleaceae, Ulmaceae and Vitaceae.

Climate calculations (n = 55)		**lower limit / upper limit defined by**
MAT	16.8 – 23.9 °C	Bombacaceae / Nyssaceae
T_{cold}	10.6 – 19.4 °C	Bombacaceae / Nyssaceae
T_{warm}	24.7 – 27.9 °C	Icacinaceae / Nyssaceae
MAP	803 – 2540 mm	Cyrillaceae / Platanaceae, Restionaceae
P_{wet}	175 – 329 mm	Mastixiaceae / Cyrillaceae
P_{dry}	9 – 56 mm	Araceae / Restionaceae
P_{warm}	139 – 154 mm	Chloranthaceae / Betulaceae
MRH*	73 – 77 %	Myrtaceae / Juglandaceae, Restionaceae

Tab. 3. Results of palaeoclimate calculations with the Coexistence Approach and list of families defining the palaeoclimate coexistence intervals (lower and upper limit); *n=46

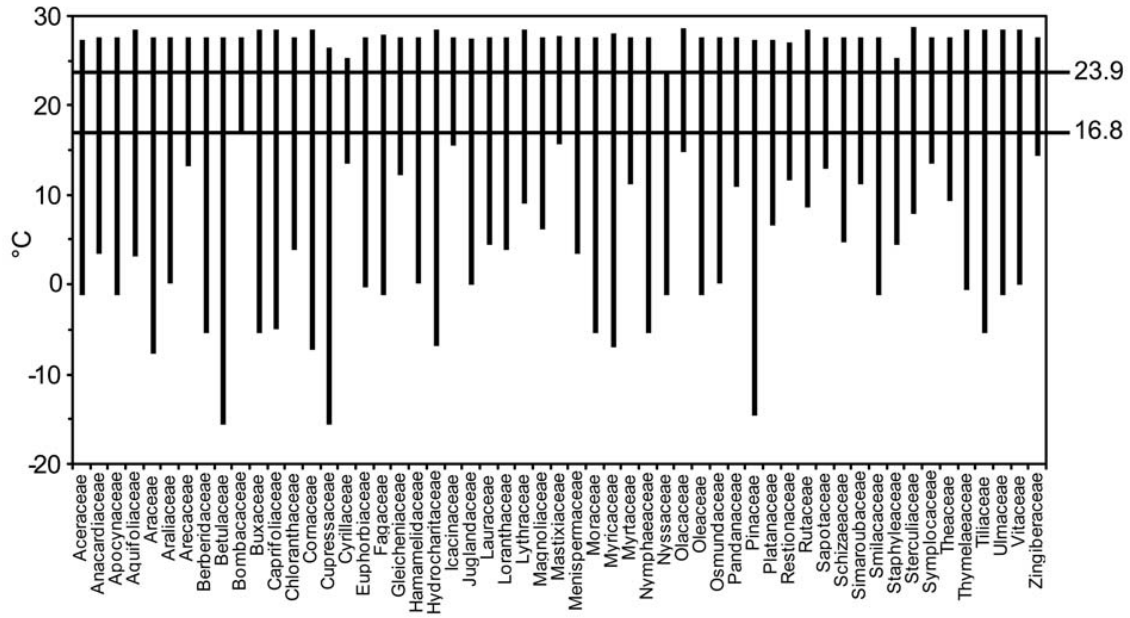

Fig. 1. Mean annual temperature in °C

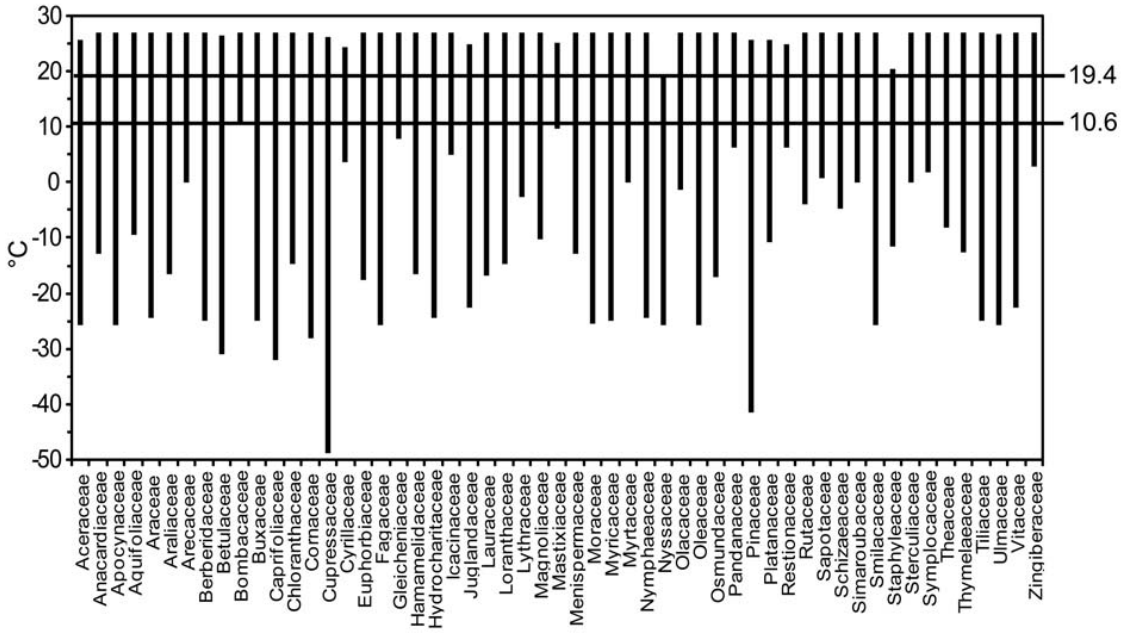

Fig. 2. Coldest month mean temperature in °C

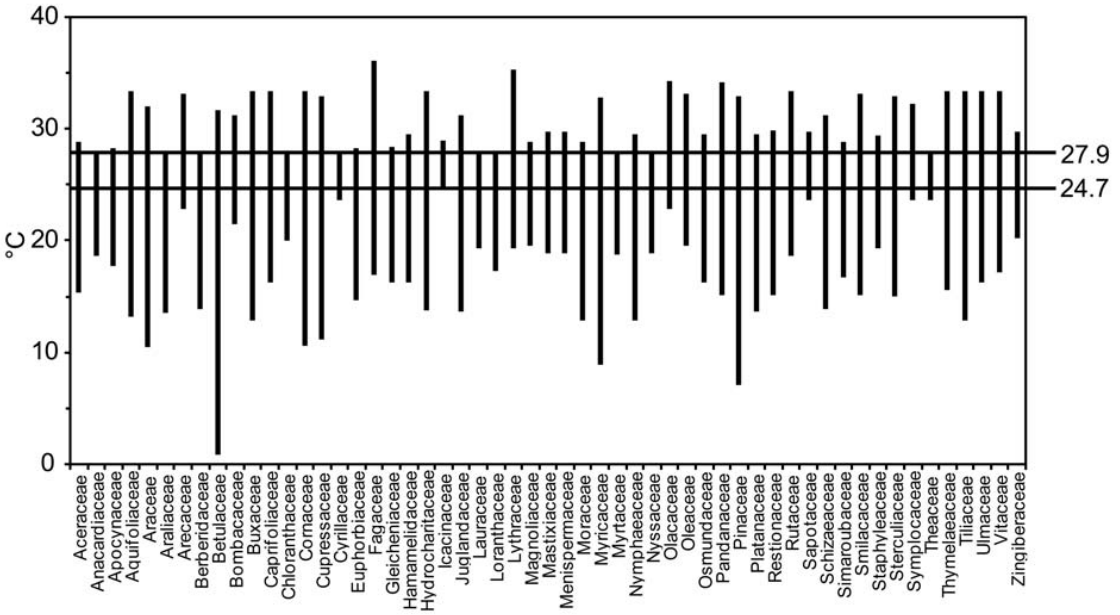

Fig. 3. Warmest month mean temperature in °C

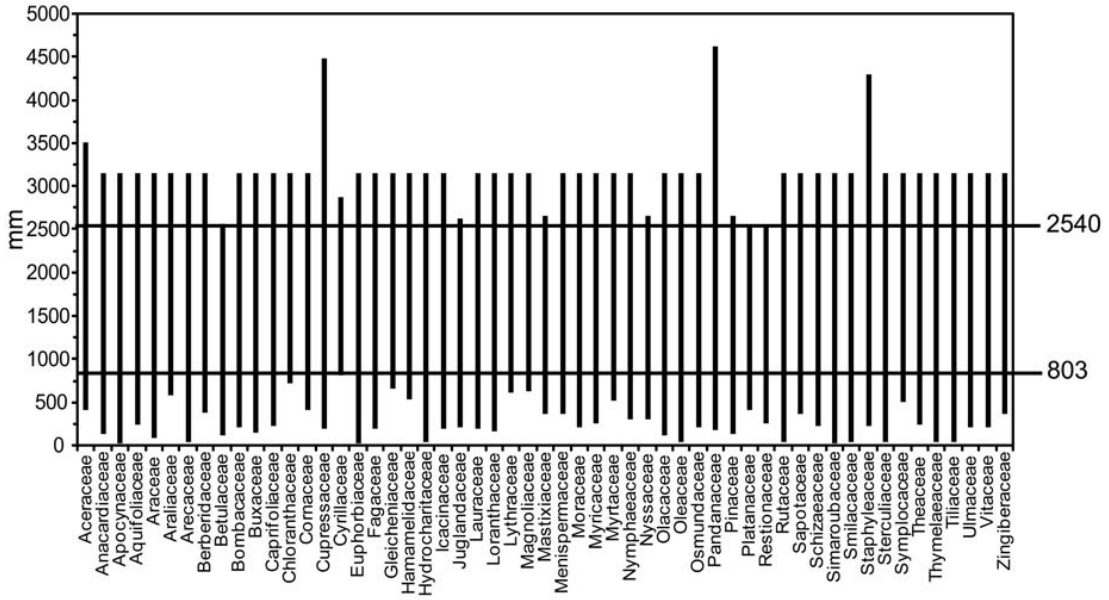

Fig. 4. Mean annual precipitation in mm

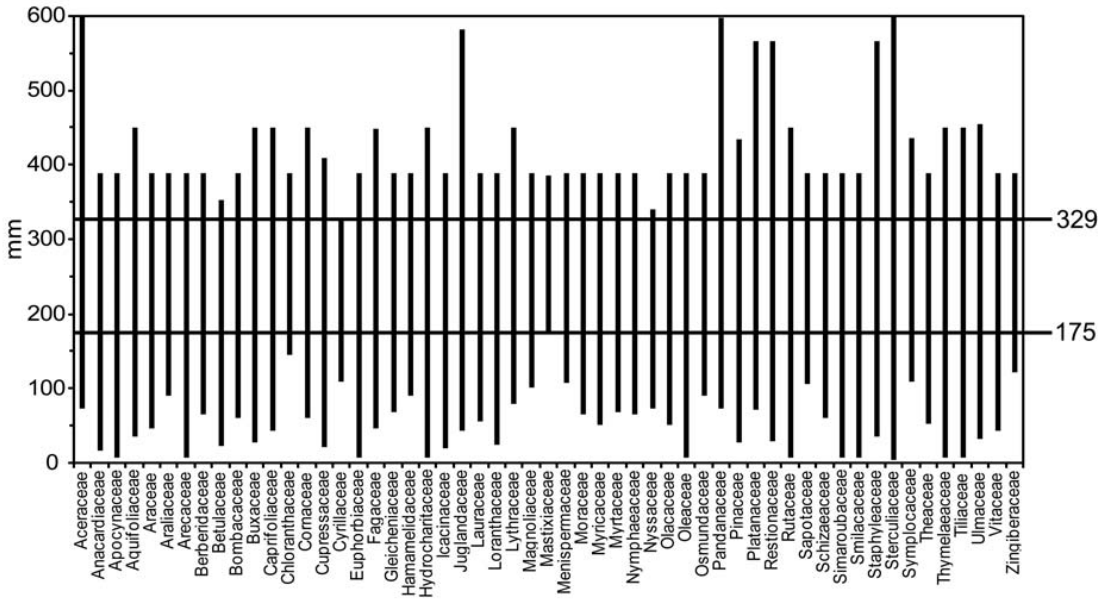

Fig. 5. Mean precipitation of the wettest month in mm

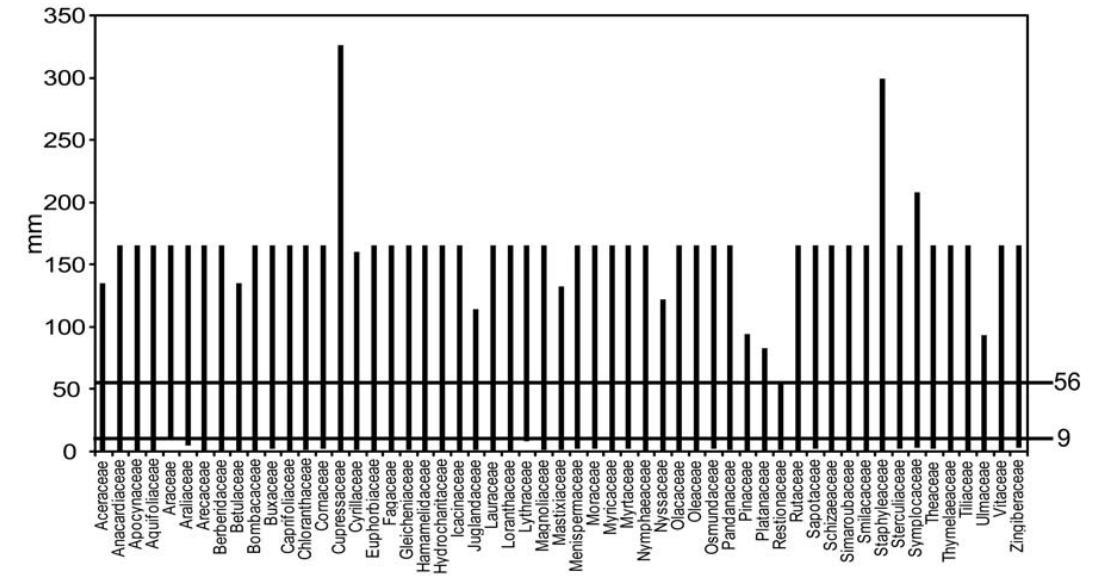

Fig. 6. Mean precipitation of the driest month in mm

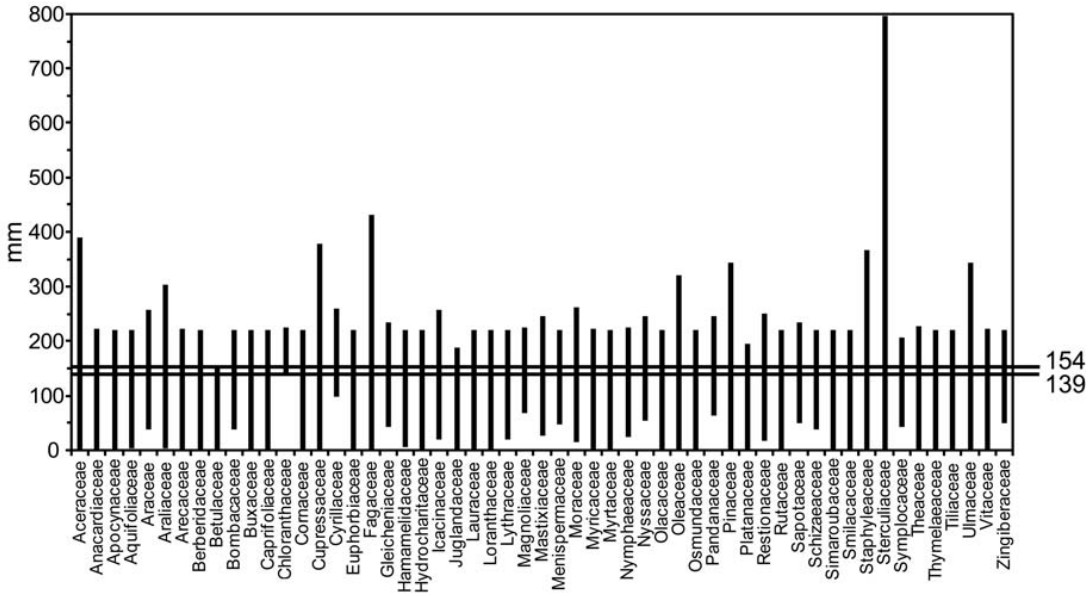

Fig. 7. Mean precipitation of the warmest month in mm

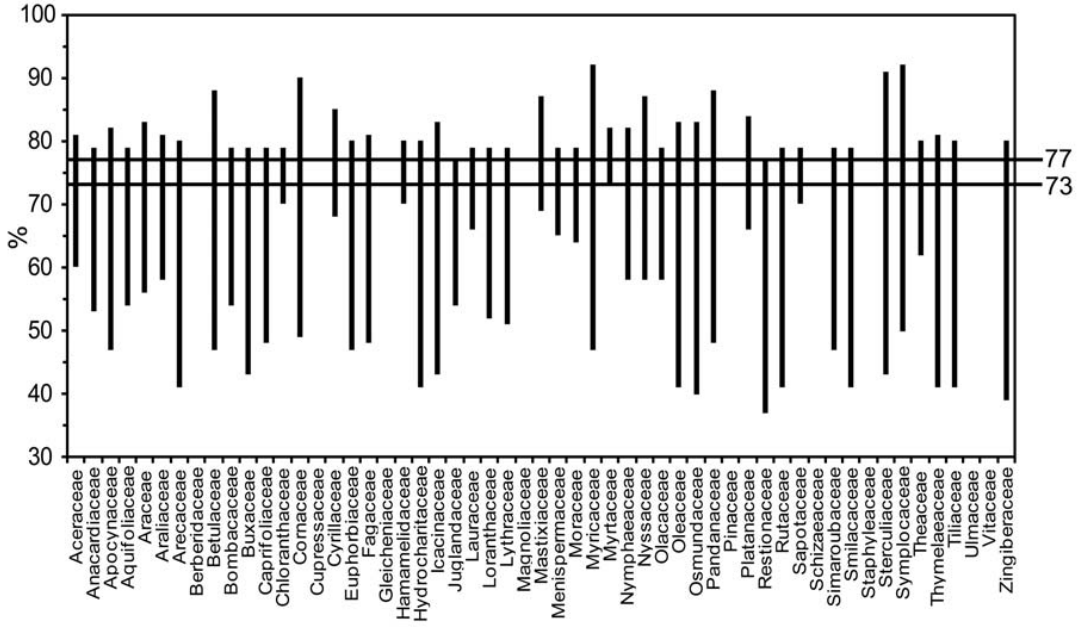

Fig. 8. Mean relative air humidity in %

DISCUSSION

Following WILDE & MICKLICH (2007) the palaeogeographic position of Messel during the middle Eocene was about 40° to 50° N (depending on reconstruction). Corresponding to MOSBRUGGER et al. (2005) the European tectonic plate moved relative to the magnetic reference frame ~3.8° to the north (Ocean Drilling Stratigraphic Network plate reconstruction service) during the last 45 Ma whereas after WHITE et al. (2008) the European plate moved just ~2.6°. According to this, the geographic position of the Messel maar in the middle Eocene has been ~46.4° N. Therefore, seasons should be expected at least with respect to the annual changes in the zenith angle of the sun and the day length (WILDE 2005; WILDE & MICKLICH 2007). Previous estimates for the middle Eocene climate of Messel were mainly based on general statements focusing on a more or less stable warm and moist subtropical/tropical climate (SCHAARSCHMIDT 1988; WILDE 1989 and citations therein; WILDE 2005; WILDE & MICKLICH 2007). Based on qualitative data WILDE (1989) suggested a paratropical climate for the middle Eocene of Messel with a mean annual temperature of clearly above 20°C (probably from 25 to 30°C) and a mean temperature of the coldest month clearly above 10°C. Precipitation might have been relatively high, possibly with seasonal fluctuations. In total, he suggested a warm and humid, probably seasonal climate without extended dry seasons. These qualitative conclusions are in good agreement to the results of the present quantitative study.

The term "paratropic" is used for climates with a mean annual temperature from 20 to 25°C and mean temperature of the coldest month between 13 and 24°C (WOLFE 1977). In contrast to a fully tropical climate, frost is not completely excluded. Precipitation might have been seasonal without extended periods of drought. Due to the fact that the present analysis was limited to the family level, the CA interval became inevitably broad, particularly for MAT and MAP. Although the lower limit of the coexistence interval for MAT obtained from CA for the Messel site is therefore below 20°C, results provided by LMA corroborate a MAT for Messel to clearly above 20°C, probably around 22°C. The summers were rather hot with temperatures of the warmest month between 24.7°C and 27.9°C. The temperature of the coldest month very likely exceeded 10°C implying a frost-free climate. The latter is also confirmed by the regular presence of crocodiles in the fossil record of Messel indicating mean temperatures of the coldest month between 10°C and 15°C (BERG 1964).

MAP amounts up to 2540 mm which is comparable to moist subtropical and tropical regions. High precipitation is also indicated by relatively high MRH. According to the data, some precipitation occurred even in the driest month and extended periods of drought in Messel are therefore rather unlikely. Nevertheless, the data indicate seasonal fluctuations with respect to differences in mean precipitation rates of warmest, driest and wettest month. According to the data, some degree of seasonality was therefore realized in Messel during the middle Eocene with respect to precipitation.

Climate data are sparse for the terrestrial middle Eocene of the considered region. Climate reconstruction by applying the CA was previously performed by MOSBRUGGER et al. (2005) for the middle Eocene of the Geiseltal, a lagerstätte in Sachsen-Anhalt (Central Germany) which is in fact comprising a number of individual sites with a minimum age of 40 Ma and a maximum age of about 48 Ma. For the Geiseltal, the CA indicated an interval for MAT between 22.9 and 25°C, a CMT interval between 16.9 and 23°C, a WMT interval between 26.7 and 28.1°C and a MAP between 1003 and 2091 mm. The data for the Geiseltal indicate

therefore a somewhat warmer, but possibly a less humid climate than for Messel. Both datasets therefore indicate a warm and frost-free climate with a low but distinct degree of seasonality in temperature and with a difference between WMT and CMT of about 12 – 13°C. This is in accordance with various available data on the Eocene climate for the time of deposition for the Messel Formation. Despite the general cooling trend succeeding the middle Eocene (ZACHOS et al. 2001), the conditions were still warm with some first sea ice appearing at about 47 Ma in the Arctic region (STICKLEY et al. 2009).

In order to compare the middle Eocene climate of Messel as revealed from the results of LMA and CA to a modern climate classification, the most frequently used classification of KOEPPEN (1900; updated by GEIGER 1954; GEIGER 1961) has been applied. Various modified versions of KOEPPEN´s climate classification have been published, for example by GRIFFITH (1976) and TREWARTHA (1954). Recently, the KOEPPEN world map was updated again by KOTTEK et al. (2006) and PEEL et al. (2007), the latter providing a new digital KOEPPEN-GEIGER world map on climate classification based on precipitation and temperature station data from 1901 to 2000. The classification system comprises five main groups of climate, characterized by the letters A (tropical), B (arid), C (temperate), D (cold) and E (polar), which are subdivided by criteria of precipitation and air temperature. The second letter considers the precipitation which can be for example W (desert), S (steppe), f (without dry season), s (dry summer), w (dry winter) and m (monsoon). The third letter describes the air temperature expressed as h (hot), k (cold), a (hot summer), b (warm summer), c (cold summer) or d (very cold winter).

For Messel, an A (tropical) climate seems most likely if we accept the upper limit of 19.4°C for T_{cold}. The criterion for a tropical climate requires a T_{cold} above 18°C. As P_{dry} was likely below 60 mm, Messel may not fit into the Af climate (tropical rainforest). Nevertheless, the value for P_{dry} is very close to the threshold value demanded. Moreover, the coexistence interval of P_{dry} is limited by Restionaceae which are represented only by pollen (microfossils). If the Restionaceae were excluded, the interval would be limited at P_{dry}= 83 mm by Platanaceae, represented by leaves in the fossil record. As a result, the criterion for an Af climate ($P_{dry} \geq 60$mm) would be met. If the results of the integrated analysis are accepted, then Messel is better characterized by an Am climate (tropical monsoon).

If T_{cold} is assumed to range below 18°C, the Messel climate would also fit into the C (temperate) climate zone which also includes subtropical areas. The coexistence intervals, however, are very wide, particularly with respect to temperature data. All other evidence suggests a tropical temperature regime. Unfortunately, various important criteria for climate classification were not calculated by the CA, particularly the precipitation of the driest month in summer or in winter. Furthermore, we have no data for the precipitation rate of the coldest month.

Whereas the CA indicates that P_{dry} ranged between 9 and 56 mm, it is not clear if this was in summer or in winter. However, the calculated precipitation rates of both wettest and warmest month are very high and it seems, therefore, quite possible that the driest month may have occurred in the colder season and, accordingly, the wettest month may have occurred in the warmer season of the year. The third part of the classification is easier to determine: As T_{warm} is clearly above 22°C a hot summer (a) is indicated. Thus, according to the obtained data, a climate of Cfa/Cwa-type seems possible as well, however, with a clear tendency towards tropical climates. Compared to modern climates, the Messel climate obtained from

CA and LMA corresponds best to climates occurring at locations in North America (Florida, Mexico), South America (Brazil, Paraguay), East Africa (Mozambique, Malawi, Madagascar), South-East Asia (China, border area of China, Laos and Vietnam, small areas in northern Burma/Myanmar and India) and Australia (Queensland). Most of these regions are situated at or close to eastern coasts (between 15° to 30° latitude N and S) showing a humid subtropical climate zone (Fig. 9). No comparable climate was found in Europe. According to UTESCHER et al. (2009), the climatic equivalent for the Geiseltal would be represented by local climata in Cuba. This is largely in accordance with the results of this study, with the exception of precipitation indicating a more humid climate with a more pronounced rainy season for Messel.

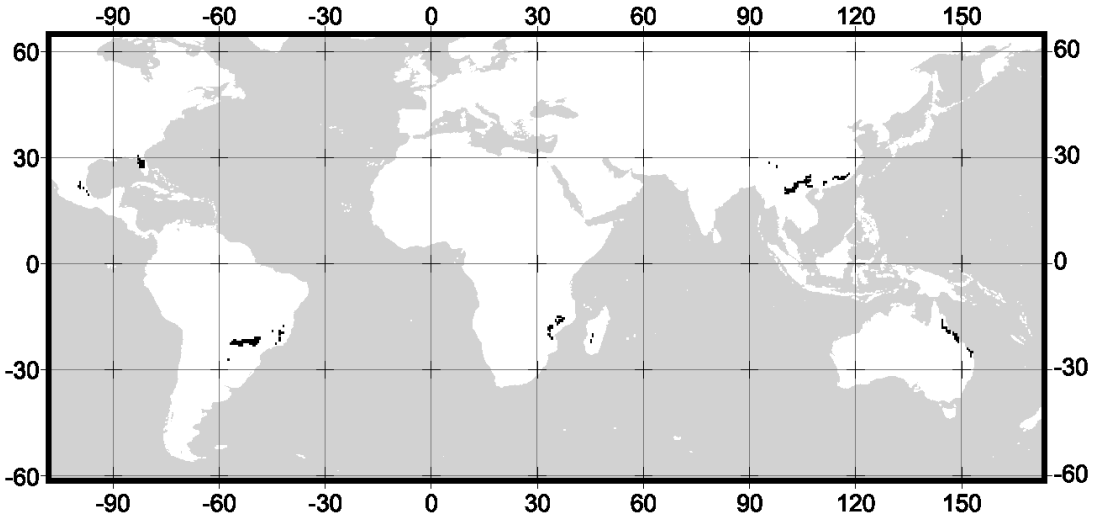

Fig. 9. Modern equivalents for the Messel climate (middle Eocene). Calculations are based on six climate parameters obtained from an integrated analysis of the Messel taphocoenosis (MAT, T_{warm}, T_{cold}, MAP, P_{dry} and P_{wet})

CONCLUSIONS

In the present study it was attempted for the first time to obtain quantitative data on temperature, precipitation, and humidity for the middle Eocene of Messel. Our results, obtained with the CA and LMA methods, indicate a mean annual temperature probably around 22°C with the mean temperature of the coldest month clearly ranging above 10°C. Mean annual precipitation rates reached values of 2540 mm and mean relative air humidity reached 77% at most. In spite of some uncertainties caused by the comparison on family level and potential changes in the climatic limitations of the respective families, previous suggestions of a comparatively warm and humid, frost-free climate for the middle Eocene of Messel are confirmed, especially by MAT, MAP and MRH.

ACKNOWLEDGEMENTS

We thank CHRISTOPHER TRAISER (University of Tübingen) for his help with Leaf Margin Analysis and JAMES NEBELSICK (University of Tübingen) for critically reading the English manuscript. Also the reviewers LILLA HABLY and GUY HARRINGTON are gratefully acknowledged.

This project was financially supported by the Landesgraduiertenförderung Baden-Württemberg.

REFERENCES

BAILEY, I. W. & SINNOTT, E. W. (1915): A botanical index of Cretaceous and Tertiary climates. - Science, **41**: 831-834.

- (1916): The climatic distribution of certain types of Angiosperm leaves. - American Journal of Botany, **3**: 24-39.

BERG, D. E. (1964): Krokodile als Klimazeugen. - Geologische Rundschau, **54**: 328-333.

BLONDEL, C. (2001): The Eocene-Oligocene ungulates from Western Europe and their environment. - Palaeogeography, Palaeoclimatology, Palaeoecology, **168**: 125-139.

BRUCH, A. A. (1998): Palynologische Untersuchungen im Oligozän Sloweniens - Paläo-Umwelt und Paläoklima im Ostalpenraum. - Tübinger Mikropaläontologische Mitteilungen, **18**: 1-193.

COLLINSON, M. E. (1982): A preliminary report on the Senckenberg-Museum collection of fruits and seeds from Messel bei Darmstadt. - Courier Forschungsinstitut Senckenberg, **56**: 49-57.

- (1983): Fossil plants of the London Clay. - Palaeontological Association Field Guides to Fossils, **1**: 1-121.

- (1988): The special significance of the Middle Eocene fruit and seed flora from Messel, West Germany. - Courier Forschungsinstitut Senckenberg, **107**: 187-197.

DILCHER, D. L. (2000): Geological history of the vegetation in southeast United States. - In: LIPSCOMB B. L., PIPOLY J. J., III, and SANDERS R. W. (eds.): Floristics in the new millenium: Proceedings of the Flora of the Southeast US Symposium. - Sida Botanical Miscellany, **18**: 1-21.

DUPONT-NIVET, G., KRIJGSMAN, W., LANGEREIS, C. G., ABELS, H. A., DAI, S. & FANG, X. (2007): Tibetan plateau aridification linked to global cooling at the Eocene-Oligocene transition. - Nature, **445**: 635-638.

ENGELHARDT, H. (1922): Die alttertiäre Flora von Messel bei Darmstadt. - Abhandlungen der Hessischen Geologischen Landesanstalt zu Darmstadt, **7**: 17-128.

FELDER, M. & HARMS, F.-J. (2004): Lithologie und genetische Interpretation der vulkano-sedimentären Ablagerungen aus der Grube Messel anhand der Forschungsbohrung Messel 2001 und weiterer Bohrungen. - Courier Forschungsinstitut Senckenberg, **252**: 151-203.

FRANCIS, J. E. & POOLE, I. (2002): Cretaceous and early Tertiary climates of Antarctica: Evidence from fossil wood. - Palaeogeography, Palaeoclimatology, Palaeoecology, **182**: 47-64.

GEIGER, R. (1954): Klassifikation der Klimate nach W. Köppen. - Landolt-Börnstein: Zahlenwerte und Funktionen aus Physik, Chemie, Astronomie, Geophysik und Technik, (alte Serie), Band **III** (Astronomie und Geophysik), 603-607; Berlin (Springer).

- (1961): Überarbeitete Neuausgabe von Geiger, R.: Koeppen-Geiger / Klima der Erde. (Wandkarte 1:16 Mill.). Gotha (Klett-Perthes).

GINGERICH, P. D. (2006): Environment and evolution through the Paleocene-Eocene thermal maximum. - Trends in Ecology and Evolution, **21**: 246-253.

GREENWOOD, D. R., WILF, P., WING, S. L. & CHRISTOPHEL, D. C. (2004): Paleotemperature estimation using leaf-margin analysis: Is Australia different? - Palaios, **19**: 129-142.

GREENWOOD, D. R. & WING, S. L. (1995): Eocene continental climates and latitudinal temperature gradients. - Geology, **23**: 1044-1048.

GRIFFITHS, J. F. (1976): Applied Climatology - An Introduction. 2nd Edition. - 150 pp.; London (Oxford University Press).

HOLLIS, C. J., HANDLEY, L., CROUCH, E. M., MORGANS, H. E. G., BAKER, J. A., CREECH, J., COLLINS, K. S., GIBBS, S. J., HUBER, M., SCHOUTEN, S., ZACHOS, J. C. & PANCOST, R. D. (2009): Tropical sea temperatures in the high-latitude South Pacific during the Eocene. - Geology, **37**: 99-102.

IVANOV, D., ASHRAF, A. R., MOSBRUGGER, V. & PALAMAREV, E. (2002): Palynological evidence for Miocene climate change in the Forecarpathian Basin (Central Paratethys, NW Bulgaria). - Palaeogeography, Palaeoclimatology, Palaeoecology, **178**: 19-37.

JACOBS, B. F. (2002): Estimation of low-latitude paleoclimates using fossil angiosperm leaves: examples from the Miocene Tugen Hills, Kenya. - Paleobiology, **28**: 399-421.

JAHREN, A. H. (2007): The arctic forest of the Middle Eocene. - Annual Review of Earth and Planetary Sciences, **35**: 509-540.

KOEPPEN, W. (1900): Versuch einer Klassifikation der Klimate, vorzugsweise nach ihren Beziehungen zur Pflanzenwelt. - Geographische Zeitschrift, **6**: 593-611, 657-679.

KOTTEK, M., GRIESER, J., BECK, C., RUDOLF, B. & RUBEL, F. (2006): World Map of the Koeppen-Geiger climate classification updated. - Meteorologische Zeitschrift, **15**: 259-263.

KOVAR-EDER, J., JECHOREK, H., KVAČEK, Z. & PARASHIV, V. (2008): The integrated plant record: An essential tool for reconstructing Neogene zonal vegetation in Europe. - Palaios, **23**: 97-111.

KOVAR-EDER, J. & KVAČEK, Z. (2007): The integrated plant record (IPR) to reconstruct Neogene vegetation: the IPR-vegetation analysis. - Acta Palaeobotanica, **47**: 391-418.

KVAČEK, Z., VELITZELOS, D. & VELITZELOS, E. (2002): Late Miocene Flora of Vegora, Macedonia, N. Greece. University of Athens. - 175 pp.; Athens (Korali Publications).

LENZ, O. K., WILDE, V., RIEGEL, W. & HEINRICHS, T. (2007): Distribution and paleoecologic significance of the freshwater dinoflagellate cyst *Messelodinium thielepfeifferae* gen. et sp. nov. from the Middle Eocene of Lake Messel, Germany. - Palynology, **31**: 119-134.

LIANG, M.-M., BRUCH, A. A., COLLINSON, M., MOSBRUGGER, V., LI, C.-S., SUN, Q.-G. & HILTON, J. (2003): Testing the climatic estimates from different palaeobotanical methods: an example from the Middle Miocene Shangwang Flora of China. - Palaeogeography, Palaeoclimatology, Palaeoecology, **198**: 279-301.

MANCHESTER, S. R. (1994): Fruits and seeds of the Middle Eocene Nut Beds flora, Clarno Formation, Oregon. - Palaeontographica Americana, **58**: 1-205.

MERTZ, D. F. & RENNE, P. R. (2005): A numerical age for the Messel fossil deposit (UNESCO World Heritage Site) derived from $^{40}Ar/^{39}Ar$ dating on a basaltic rock fragment. - Courier Forschungsinstitut Senckenberg, **255**: 67-75.

MOSBRUGGER, V. & UTESCHER, T. (1997): The coexistence approach - a method for quantitative reconstructions of Tertiary terrestrial paleoclimate data using plant fossils. - Palaeogeography, Palaeoclimatology, Palaeoecology, **134**: 61-86.

MOSBRUGGER, V., UTESCHER, T. & DILCHER, D. L. (2005): Cenozoic continental climatic evolution of Central Europe. - Proceedings of the National Academy of Sciences of the United States of America, **102**: 14964-14969.

PARRISH, J. T. & SPICER, R. A. (1988): Late Cretaceous terrestrial vegetation: a near-polar temperature curve. - Geology, **16**: 22-25.

PEARSON, P. N. & PALMER, M. R. (2000): Atmospheric carbon dioxide concentrations over the past 60 million years. - Nature, **406**: 695-699.

PEEL, M. C., FINLAYSON, B. L. & MCMAHON, T. A. (2007): Updated world map of the Köppen-Geiger climate classification. - Hydrology and Earth System Sciences, **11**: 1633-1644.

PROSS, J., BRUCH, A. A. & KVAČEK, Z. (1998): Paläoklima-Rekonstruktionen für den Mittleren Rupelton (Unter-Oligozän) des Mainzer Beckens auf der Basis mikro- und makrobotanischer Befunde. - Mainzer geowissenschaftliche Mitteilungen, **27**: 79-92.

PROTHERO, D. R., IVANY, L. C. & NESBITT, E. A. (2003): From greenhouse to icehouse: the marine Eocene-Oligocene transition. - 541 pp.; New York (Columbia University Press).

ROTH-NEBELSICK, A., UTESCHER, T., MOSBRUGGER, V., DIESTER-HAASS, L. & WALTHER, H. (2004): Changes in atmospheric CO_2 concentrations and climate from the Late Eocene to Early Miocene: palaeobotanical reconstruction based on fossil floras from Saxony, Germany. - Palaeogeography, Palaeoclimatology, Palaeoecology, **205**: 43-67.

ROYER, D. L. & WILF, P. (2006): Why do toothed leaves correlate with cold climates? Gas exchange at leaf margins provide new insights into a classic paleotemperature proxy. - International Journal of Plant Sciences, **167**: 11-18.

SCHAARSCHMIDT, F. (1986): Blüten von Pflanzen des Messeler Ölschiefers. - Courier Forschungsinstitut Senckenberg, **85**: 214-216.

- (1988): Der Wald, fossile Pflanzen als Zeugen eines warmen Klimas. - In: SCHAAL S. and ZIEGLER W.(eds.): Messel - Ein Schaufenster in die Geschichte der Erde und des Lebens, 27-52; Frankfurt am Main (Waldemar Kramer).

SPICER, R. A. & PARRISH, J. T. (1986): Paleobotanical evidence for cool North Polar climates in middle Cretaceous (Albian-Cenomanian) time. - Geology, **14**: 703-706.

STICKLEY, C. E., ST JOHN, K., KOÇ, N., JORDAN, R. W., PASSCHIER, S., PEARCE, R. B. & KEARNS, L. E. (2009): Evidence for middle Eocene Arctic sea ice from diatoms and ice-rafted debris. - Nature, **460**: 376-379.

STURM, M. (1971): Die eozäne Flora von Messel bei Darmstadt. I. Lauraceae. - Palaeontographica, B, **134**: 1-60.

- (1978): Maw contents of an Eocene horse (*Propalaeotherium*) out of the oil shale of Messel near Darmstadt. - Courier Forschungsinstitut Senckenberg, **30**: 120-122.

THIELE-PFEIFFER, H. (1988): Die Mikroflora aus dem mitteleozänen Ölschiefer von Messel bei Darmstadt. - Palaeontographica, B, **211**: 1-86.

TRAISER, C. (2004): Blattphysiognomie als Indikator für Umweltparameter: Eine Analyse rezenter und fossiler Floren (Leaf physiognomy as environmental indicator: An analysis of extant and fossil floras). - 113 pp., unpubl. Ph.D. Thesis, Geowissenschaftliche Fakultät, Universität Tübingen, IV.

TRAISER, C., KLOTZ, S., UHL, D. & MOSBRUGGER, V. (2005): Environmental signals from leaves - a physiognomic analysis of European vegetation. - New Phytologist, **166**: 465-484.

TRAISER, C. & MOSBRUGGER, V. (2006): European Leaf Physiognomic Approach ELPA; doi:10.1594/PANGAEA.552352; *Supplement to*: Traiser, C. (2004): Blattphysiognomie als Indikator für Umweltparameter: Eine Analyse rezenter und fossiler Floren (Leaf physiognomy as environmental indicator: An analysis of extant and fossil floras). - 113 pp.; Ph.D. Thesis, Geowissenschaftliche Fakultät der Eberhard-Karls Universität Tübingen, urn:nbn:de:bsz:21-opus-14947.

TREWARTHA, G. T. (1954): An introduction to climate. 3rd Edition. - 402 pp.; New York - London (McGraw-Hill).

TRIPATI, A., BACKMAN, J., ELDERFIELD, H. & FERRETTI, P. (2005): Eocene bipolar glaciation associated with global carbon cycle changes. - Nature, **436**: 341-346.

UHL, D., MOSBRUGGER, V., BRUCH, A. A. & UTESCHER, T. (2003): Reconstructing palaeotemperatures using leaf floras - case studies for a comparison of leaf margin analysis and the coexistence approach. - Review of Palaeobotany and Palynology, **126**: 49-64.

UTESCHER, T., IVANOV, D., HARZHAUSER, M., BOZUKOV, V., ASHRAF, A. R., ROLF, C., URBAT, M. & MOSBRUGGER, V. (2009): Cyclic climate and vegetation change in the late Miocene of Western Bulgaria. - Palaeogeography, Palaeoclimatology, Palaeoecology, **272**: 99-114.

UTESCHER, T. & MOSBRUGGER, V. (2010): Palaeoflora - Data base for palaeoclimate reconstructions using the Coexistence Approach; www.palaeoflora.de.

UTESCHER, T., MOSBRUGGER, V. & ASHRAF, A. R. (2000): Terrestrial climate evolution in Northwest Germany over the last 25 million years. - Palaios, **15**: 430-449.

VILLA, G., FIORONI, C., PEA, L., BOHATY, S. & PERSICO, D. (2008): Middle Eocene - late Oligocene climate variability: Calcareous nannofossil response at Kerguelen Plateau, Site 748. - Marine Micropaleontology, **69**: 173-192.

WHEELER, E. A. & MANCHESTER, S. R. (2002): Woods of the Eocene Nut Beds flora, Clarno Formation, Oregon, USA. - IAWA Journal, **Supplement 3**: 1-188.

WHITE, C. H., BOSENCE, D. W. J., ROSEN, B. R. & WALLACE, C. C. (2008): Response of *Acropora* to warm climates; lessons from the geological past. - In: Proceedings of the 11th International Coral Reef Symposium, Ft. Lauderdale, Florida, Session number **1**: 7-12.

WIEMANN, M. C., MANCHESTER, S. R., DILCHER, D. L., HINOJOSA, L. F. & WHEELER, E. A. (1998): Estimation of temperature and precipitation from morphological characters of dicotyledonous leaves. - American Journal of Botany, **85**: 1796-1802.

WILDE, V. (1989): Untersuchungen zur Systematik der Blattreste aus dem Mitteleozän der Grube Messel bei Darmstadt (Hessen, Bundesrepublik Deutschland). - Courier Forschungsinstitut Senckenberg, **115**: 1-213.

- (2004): Aktuelle Übersicht zur Flora aus dem mitteleozänen "Ölschiefer" der Grube Messel bei Darmstadt (Hessen, Deutschland). - Courier Forschungsinstitut Senckenberg, **252**: 109-114.
- (2005): The green Eocene. The diverse flora of a paratropical climate. - Vernissage UNESCO World Heritage Series, **21**: 14-19.

WILDE, V. & MICKLICH, N. (2007): Lebensraum Messel-See. Der See und seine Uferzonen. - In: GRUBER G. and MICKLICH N. (eds.): Messel - Schätze der Urzeit (Begleitbuch zur Ausstellung "Messel on Tour"), 52-55; Hessisches Landesmuseum Darmstadt (Theiss).

WILDE, V. & SÜß, H. (2001): First wood with anatomically preserved details from the Middle Eocene oilshale of Messel (Hesse, Germany). - Acta Palaeobotanica, **41**: 133-139.

WILF, P. (1997): When are leaves good thermometers? A new case for Leaf Margin Analysis. - Paleobiology, **23**: 373-390.

WILF, P., WING, S. L., GREENWOOD, D. R. & GREENWOOD, C. L. (1998): Using fossil leaves as paleoprecipitation indicators: An Eocene example. - Geology, **26**: 203-206.

WING, S. L. & GREENWOOD, D. R. (1993): Fossils and fossil climate: the case for equable continental interiors in the Eocene. - Philosophical Transactions of the Royal Society of London B, **341**: 243-252.

WOLFE, J. A. (1977): Palaeogene floras from the Gulf of Alaska region. - US Geological Survey Professional Paper, **997**: 1-108.
- (1979): Temperature parameters of humid to mesic forests of eastern Asia and their relation to forests of other regions of the Northern Hemisphere and Australasia. - U.S. Geological Survey Professional Paper, **1106**: 1-37.
- (1993): A method of obtaining climatic parameters from leaf assemblages. - U.S. Geological Survey Bulletin, **2040**: 1-71.
- (1995): Paleoclimate estimates from tertiary leaf assemblages. - Annual Review of Earth and Planetary Sciences, **23**: 119-142.

WOLFE, J. A. & SPICER, R. A. (1999): Fossil leaf character states: multivariate analysis. - In: JONES T. P. and ROWE N. P. (eds.): Fossil plants and spores: modern techniques. Geological Society, 233-239; London (Geological Society Publ. House).

YANG, J., WANG, Y. F., SPICER, R. A., MOSBRUGGER, V., LI, C. S. & SUN, Q. G. (2007): Climatic reconstruction at the Miocene Shanwang basin, China, using leaf margin analysis, CLAMP, Coexistence approach, and overlapping distribution analysis. - American Journal of Botany, **94**: 599-608.

ZACHOS, J. C., PAGANI, M., SLOAN, L., THOMAS, E. & BILLUPS, K. (2001): Trends, rhythms, and aberrations in global climate 65 Ma to present. - Science, **292**: 686-693.

ZACHOS, J. C., STOTT, L. D. & LOHMANN, K. C. (1994): Evolution of early Cenozoic marine temperatures. - Paleoceanography, **9**: 353-387.

3.3 Grein, M., Roth-Nebelsick, A., Wilde, V.: Carbon isotope composition of middle Eocene leaves. (submitted)

Carbon isotope composition of middle Eocene leaves

Michaela Grein, Anita Roth-Nebelsick & Volker Wilde

ABSTRACT

The $^{13}C/^{12}C$ ratios ($\delta^{13}C$) of leaves from the middle Eocene of the Messel Pit (Middle Messel Formation) were measured to determine the ratios of leaf-internal to ambient carbon dioxide concentration (c_i/c_a) for the respective time. For extant plants this parameter provides information about their ecophysiological state. Fossil leaves belonging to three species were analyzed: *Laurophyllum lanigeroides* (Lauraceae), *Daphnogene crebrigranosa* (Lauraceae) and *Rhodomyrtophyllum sinuatum* (Myrtaceae). In order to determine the range of $\delta^{13}C$ across a single leaf (intra-leaf variability) samples from the basal, central and apical region were separately prepared and analyzed. The results are compared to $\delta^{13}C$ and c_i/c_a ratios in extant evergreen Lauraceae (*Laurus nobilis, Cinnamomum camphora, Persea americana*) and Myrtaceae (*Myrtus communis, Psidium littorale/cattleianum*). Furthermore, leaves of extant deciduous *Castanea sativa* (Fagaceae) were sampled for comparison.

The $\delta^{13}C$ of the fossil cuticles varies from –30 ‰ to -27 ‰ in the Lauraceae and from –29 ‰ to -26 ‰ in the Myrtaceae, which are typical ranges for extant C_3-plants. Results of intra-leaf analyses indicate that $\delta^{13}C$ varies slightly across the leaves but intra-leaf variability is statistically not significant. Mean Eocene c_i/c_a-ratios as calculated from the measured $\delta^{13}C$ values varied from 0.78 to 0.87. The c_i/c_a-ratios of extant Lauraceae are substantially lower (average 0.69) than for the fossil material. In Myrtaceae, c_i/c_a-ratios are almost the same for extant and fossil material (extant Myrtaceae average at about 0.8).

ZUSAMMENFASSUNG

Das $^{13}C/^{12}C$-Verhältnis ($\delta^{13}C$) von fossilen Blättern aus dem Mitteleozän der Grube Messel (Mittlere Messel Formation) wurde gemessen und daraus das Verhältnis von blattinternem zu atmosphärischem Kohlendioxid (c_i/c_a) für die betreffende Zeit bestimmt. Bei heutigen Pflanzen erlaubt diese Größe eine Einschätzung des ökophysiologischen Zustands. Es wurden die Blätter von drei fossilen Arten analysiert: *Laurophyllum lanigeroides* (Lauraceae), *Daphnogene crebrigranosa* (Lauraceae) und *Rhodomyrtophyllum sinuatum* (Myrtaceae). Um Schwankungen des $\delta^{13}C$ innerhalb eines Blattes (blattinterne Variabilität) bestimmen zu können, wurden getrennte Proben aus dem basalen, dem mittleren und dem apikalen Bereich genommen und analysiert. Die Ergebnisse wurden mit dem $\delta^{13}C$ und c_i/c_a rezenter immergrüner Lauraceae (*Laurus nobilis, Cinnamomum camphora, Persea americana*) und Myrtaceae (*Myrtus communis, Psidium littorale/cattleianum*) verglichen. Darüber hinaus wurden zum Vergleich Blätter der rezenten laubwerfenden Art *Castanea sativa* (Fagaceae) beprobt.

Das $\delta^{13}C$ der fossilen Kutikulen variiert von –30 ‰ bis -27 ‰ innerhalb der Lauraceae und von -29 ‰ bis -26 ‰ innerhalb der Myrtaceae, was im Bereich moderner C_3-Pflanzen liegt. Die Ergebnisse der blattinternen Analysen zeigen, dass der $\delta^{13}C$-Wert innerhalb eines Blattes variiert, diese blattinterne Variabilität statistisch jedoch nicht signifikant ist. Das c_i/c_a-Verhältnis für das Mitteleozän, das mit den gemessenen $\delta^{13}C$-Werten berechnet wurde,

schwankt zwischen durchschnittlich 0.78 und 0.87. Die c_i/c_a-Verhältnisse für rezente Lauraceae sind deutlich geringer (durchschnittlich 0.69) als die für die beiden fossilen Arten errechneten Werte. Bei den Myrtaceae unterscheiden sich die mitteleozänen und rezenten c_i/c_a-Verhältnisse kaum, rezente Myrtaceae liegen hier durchschnittlich bei etwa 0.8.

INTRODUCTION

Although "greenhouse conditions" prevailed (e.g. ZACHOS et al. 1994; GREENWOOD & WING 1995; WILF et al. 1998; GINGERICH 2006; JAHREN 2007; HOLLIS et al. 2009) the Eocene experienced faunal and floral changes (for example FRANCIS & POOLE 2002; various contributions in PROTHERO et al. 2003) due to a slight but almost continuous global cooling trend following the Early Eocene Climatic Optimum (ZACHOS et al. 2001; DUPONT-NIVET et al. 2007). Most information about Eocene climate dynamics is still derived from the marine realm (e.g. ZACHOS et al. 2001). In order to understand the entire Eocene climate system and its changes terrestrial data are equally important. Fossil leaves represent an easily accessible and plentiful terrestrial archive that allows an insight into the climate history of the Earth. Many studies dealing with the response of plants to changing climates and varying CO_2 concentrations include measurements of the carbon isotopic composition ($^{13}C/^{12}C$) of leaf tissues (e.g. LLOYD & FARQUHAR 1994; KÜRSCHNER 1996; LOCKHEART et al. 1998; HEATON 1999; NGUYEN TU et al. 2004; SCHWEIZER et al. 2007; AUCOUR et al. 2008). The carbon isotope discrimination of C_3-plants in favor of the light ^{12}C isotopes shifts the carbon isotope ratio towards more negative values between approximately -36‰ to -22‰. The carbon isotope discrimination, however, differs among species and among individuals in a population. Moreover, it is related to the c_i/c_a-ratio (ratio between intra-leaf and atmospheric CO_2) which is in turn influenced by a number of environmental parameters such as leaf temperature, humidity and irradiation (e.g. FARQUHAR et al. 1982; EVANS et al. 1986; FARQUHAR et al. 1989; LEAVITT & NEWBERRY 1992; EHLERINGER & CERLING 1995). Particularly, the c_i/c_a-ratio indicates the degree of stomatal conductance (= gas permeability of the epidermis). Since a high stomatal conductance usually requires adequate availability of water, the carbon isotope signal of leaves can be used as a source of information for the ecophysiological state of the respective plants and therefore to a certain degree for environmental conditions.

For the present study, we analyzed the carbon isotope composition of fossil leaf material from the middle Eocene Messel Formation.

MATERIAL & METHODS

Fossil and extant leaf material

For the present study, fossil leaf material from the early middle Eocene of the Messel Pit (Middle Messel Formation) near Darmstadt (Hesse, Germany), a UNESCO World Heritage Site, has been analyzed. In the Messel Pit the typical laminated oilshale-filling of an Eocene maar lake (FELDER & HARMS 2004) was commercially mined for more than hundred years. The oilshale became famous for numerous fossils showing an excellent preservation. The eruption giving rise to the maar lake at Messel has been dated at about 47.8 Ma (MERTZ & RENNE 2005).

$\delta^{13}C$ measurements were carried out for six leaves of *Laurophyllum lanigeroides* (Lauraceae), four leaves of *Daphnogene crebrigranosa* (Lauraceae) and seven leaves of *Rhodomyrtophyllum sinuatum* (Myrtaceae). For detailed descriptions and discussions of the species compare WILDE (1989). Furthermore, recent plant material from the same families was analyzed: *Laurus nobilis* (Lauraceae, five leaves), *Cinnamomum camphora* (Lauraceae, three leaves), *Persea americana* (Lauraceae, two leaves), *Myrtus communis* (Myrtaceae, five leaves) and *Psidium littorale/cattleianum* (Myrtaceae, three leaves). Additionally, we considered three leaves of a deciduous species, *Castanea sativa* (Fagaceae) for comparison. The recent plant material was collected in the Botanical Garden of Tübingen (Baden-Württemberg, Germany).

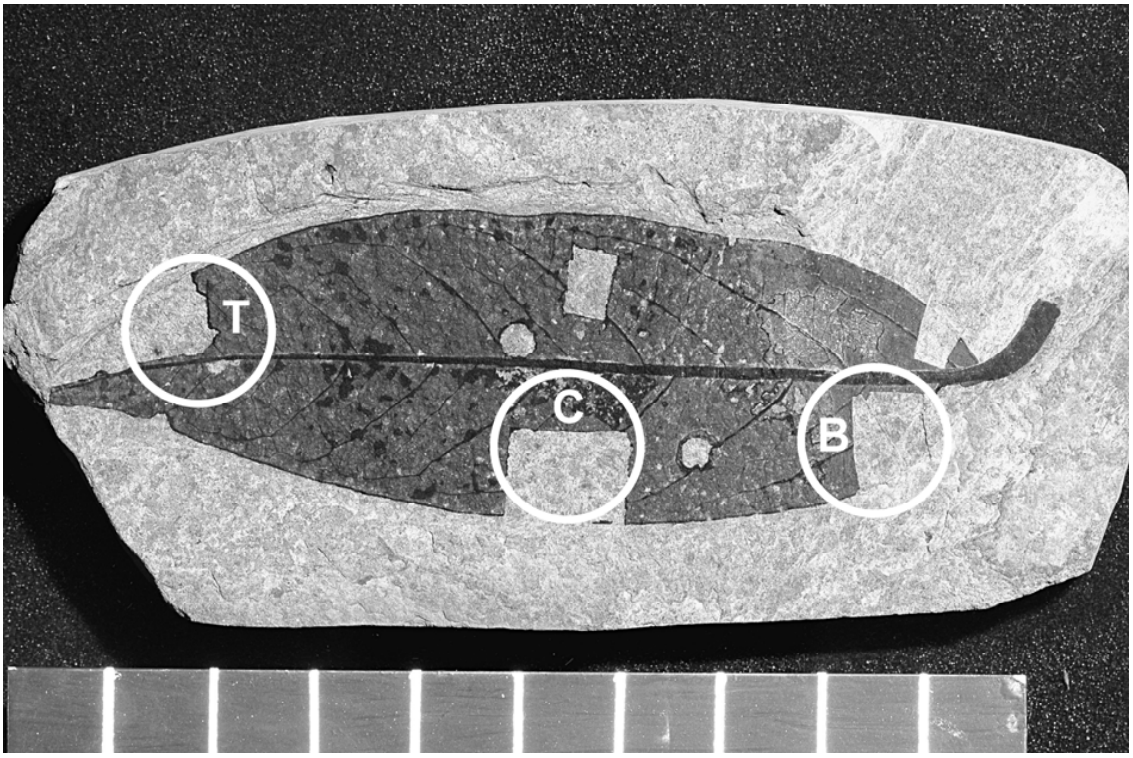

Fig. 1. Fossil leaf of *Laurophyllum lanigeroides* showing the sampling sites for isotope analysis. The locations tip (T), center (C) and base (B) are marked (photo: M. Mueller, SFN – Frankfurt/Main). – Scale: 1 cm.

Preparation of leaf material

Here, we used remnant tissues of completely to almost completely preserved fossil leaves. Whenever possible, three samples per specimen were analyzed in order to illustrate intra-leaf variability of $\delta^{13}C$ except for *Daphnogene crebrigranosa* where only one sample per leaf was available because the material was not sufficient for more. Samples from the basal, central and apical (or tip) region were cut out of the leaf blade and thoroughly rinsed with water

(Figure 1). In order to remove the adhering sediment all fossil material was treated with hydrofluoric acid (HF) again followed by rinsing with water. Afterwards the samples were put in SCHULZE´s Solution, a mixture of crystalline potassium chlorate ($KClO_3$) and nitric acid (HNO_3), until their colour turned from black to light brown or yellow. After maceration samples were neutralized in ammonia solution (NH_3+H_2O) followed by washing in water again. Extant plant material was just rinsed with water without any further chemical preparation. For isotope measurements, samples of extant and fossil material were finally dried at room-temperature for at least 7 days followed by drying in an oven for at least three days at about 30-60°C.

Carbon isotope composition and c_i/c_a-ratio

The C-isotopic composition ($\delta^{13}C$) was measured at the Department for Geochemistry, Institute for Geosciences, University of Tübingen, Germany, with a NC 2500 connected to a Thermo Quest Delta+XL mass spectrometer, Finnigan MAT. Samples were calibrated to $\delta^{13}C$ values of a standard, USGS 24 ($\delta^{13}C$= -16 ‰, relative to VPDB). The reproducibility is ±0.1 ‰.

The ratio of leaf-internal to atmospheric carbon dioxide concentration (c_i/c_a) was calculated according to the equation of FARQUHAR et al. (1989) which is suitable for C_3 plants. The carbon isotope discrimination (Δ) is calculated as

$$\Delta = \frac{\delta^{13}C_{atm} - \delta^{13}C_{plant}}{1 + \delta^{13}C_{plant}} \quad (1)$$

with

$$\Delta = a + (b - a) \times \frac{c_i}{c_a} \quad (2)$$

$\delta^{13}C_{atm}$ is the carbon isotope composition of the atmosphere, $\delta^{13}C_{plant}$ is the carbon isotope composition of the plant tissue, a is the fractionation caused by diffusion of CO_2 through stomata (a = 4.4 ‰) and b is the fractionation due to carboxylation by Rubisco (b = 27.0 ‰). Middle Eocene atmospheric $\delta^{13}C_{atm}$ was derived from the carbon isotope composition of marine carbonates which is approximately +0.8 ‰ at 47 Ma (five-point running mean curve) provided by ZACHOS et al. (2001). With the assumption that the composition of atmospheric CO_2 is regulated on a long-term basis by equilibrium with marine carbonates with about 7‰ more negative (MORA et al. 1996; BEERLING et al. 1998; BEERLING 2000; BEERLING & ROYER 2002) this results in $\delta^{13}C_{atm}$ = -6.2 ‰ for the middle Eocene atmosphere. Modern atmospheric carbon isotope composition is about $\delta^{13}C_{atm}$ = -8.2 ‰ (e.g. NGUYEN TU et al. 2004). These differences in Eocene and modern $\delta^{13}C_{atm}$ directly influence the calculated carbon isotope discrimination and, thus, $\delta^{13}C$-derived c_i/c_a-ratio (see also Tab. 1).

Statistical analysis was performed by using SPSS 16.01.

RESULTS

Measurements of $\delta^{13}C$ on the fossil leaf material indicate some differences in the carbon isotope composition of the middle Eocene Lauraceae and Myrtaceae from Messel. The $\delta^{13}C$ varied from about –30 ‰ to -27 ‰ in the two species of Lauraceae and from –29 ‰ to -26 ‰ in the single species of Myrtaceae tested (Fig. 2). Results of intra-leaf analyses (Fig. 3) indicate that $\delta^{13}C$ varies slightly across the leaves, however, application of one-way ANOVA (ANalysis Of VAriance) shows that the variation is statistically not significant. Mean c_i/c_a-ratios derived from $\delta^{13}C$ measurements of the fossils varied from 0.78 in *Rhodomyrtophyllum sinuatum* to 0.87 in *Daphnogene crebrigranosa* (Tab. 1); values for *Laurophyllum lanigeroides* are intermediate with c_i/c_a= 0.83. The mean c_i/c_a-ratios for extant Lauraceae are clearly lower (between 0.63 and 0.74) than the ratios for the fossil species (0.83 to 0.87). For fossil and extant Myrtaceae, c_i/c_a-ratios hardly differ with values ranging between 0.78 and 0.81. The average value for all of the analyzed fossil leaves from the middle Eocene of Messel is $\delta^{13}C$ = -28.4 ± 1.1 ‰ (n = 17) corresponding to an average c_i/c_a-ratio of 0.82 ± 0.05.

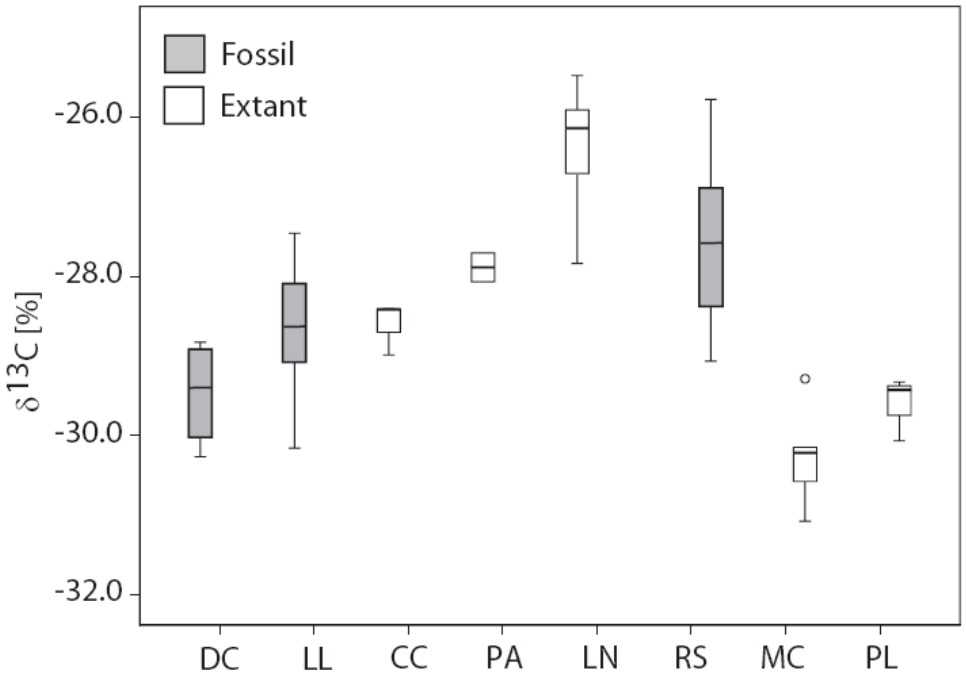

Fig. 2. Carbon isotope composition ($\delta^{13}C$ in ‰) of fossil and extant leaves. Lauraceae: DC: *Daphnogene crebrigranosa*. LL: *Laurophyllum lanigeroides*. CC: *Cinnamomum camphora*. PA: *Persea americana*. LN: *Laurus nobilis*. Myrtaceae: RS: *Rhodomyrtophyllum sinuatum.* MC: *Myrtus communis*. PL: *Psidium littorale.* With the exception of DC, the data represent the pooled results from all three leaf positions. The results are presented as box–whisker plots. The vertical lines connect the highest and lowest value, and the boxes span the 50% interquartile. The median is indicated by the horizontal line within the boxes.

DISCUSSION

$\delta^{13}C$ values of modern C_3 plants range typically from -36 to -22 ‰ (e.g. FARQUHAR et al. 1989; O'LEARY 1995; CERLING et al. 2004; KINGSTON & HARRISON 2007; and citations therein) with local and temporal (diurnal/seasonal) variations, depending on the species. During the past centuries, the $\delta^{13}C$ values of modern plants were influenced by changes in the carbon isotope composition of the atmospheric CO_2 due to human activity. The concentration of atmospheric CO_2, however, appears to have only minor influence on $\delta^{13}C$ (NGUYEN TU et al. 2004). The $\delta^{13}C$ values of the Messel leaves fit into the range typical for modern C_3-species. Our average value for $\delta^{13}C$ = -28.4 ± 1.1 ‰ (n = 17) is somewhat more negative than the values of SCHWEIZER et al. (2007), who analyzed the carbon isotopic composition of a larger number (n=63) of unspecified "terrestrial leaves" from the Messel Pit. The $\delta^{13}C$ values of their "terrestrial leaves" ranged between approximately -30 ‰ and -25 ‰ with an average of -26.8 ‰ ± 0.8 ‰. Following SCHWEIZER et al. (2007) this could have been caused by the fact that fossil leaves are particularly sensitive to contamination and diagenetic alteration because of their large surface area-to-volume ratio. However, the results of SCHWEIZER et al. (2007) indicate that the Messel oilshale is depleted in ^{13}C relative to "terrestrial leaves" and leaves of water lilies. The compositional differences between the fossil leaves and the oilshale matrix in their study therefore obviously confirms that isotopic exchange between the fossils and their matrix was not extensive enough to produce distinct isotopic alteration (SCHWEIZER et al. 2007). The fact that our $\delta^{13}C$ values for the fossil leaves are close to the oilshale values provided by SCHWEIZER et al. (2007) therefore appears to be accidental. The differences in the mean values for leaves in both studies may have been caused by the fact that our study is based on material from three distinct species whereas SCHWEIZER et al. (2007) used a larger random sample of unspecified "terrestrial leaves".

The c_i/c_a-ratio and, thus, carbon isotope discrimination for modern plants depends on stomatal conductance and the photosynthetic rate which are in turn influenced by several environmental factors such as light, water supply, nutrients, atmospheric CO_2 concentration and temperature (e.g. FARQUHAR et al. 1989; TIESZEN 1991; EHLERINGER & CERLING 1995; O'LEARY 1995). The c_i/c_a-ratio is frequently maintained at a constant (or almost constant) level typically around 0.7 (mainly between 0.6 to 0.8) (e.g. EHLERINGER & CERLING 1995; LARCHER 2003). Indeed, with c_i/c_a = 0.7 modern *Castanea sativa* provided values typical for C_3-plants. A high c_i/c_a-ratio indicates non-conservative water use, that is, no strict water saving strategies resulting in a trend for high stomatal conductance, and a high assimilation rate (e.g. LLOYD & FARQUHAR 1994; FRANKS & FARQUHAR 1999). EHLERINGER et al. (1987) studied 128 plant species (C_3, C_4 and CAM) from a subtropical monsoon forest in southern China. They showed that among C_3 species, $\delta^{13}C$ tended to become more negative with decreasing light availability from open to closed habitats. Among Myrtaceae $\delta^{13}C$ values ranged between about -30 to -27 ‰ (2 trees and 2 shrubs from open and intermediate habitats) and among Lauraceae $\delta^{13}C$ values ranged from approximately -35 to -29 ‰ (5 trees and 1 shrub from intermediate and closed habitats). EHLERINGER et al. (1986; 1987) also demonstrated that in some species the c_i/c_a-ratio changed because of decreasing intercellular CO_2 concentration with increasing light.

The c_i/c_a-ratio may thus vary within various terrestrial habitats. For example, differences exist between Australian evergreen trees, Mediterranean evergreen sclerophyllous shrubs, xerophytic trees, dry tropical trees and rain forest trees (e.g. BEYSCHLAG et al. 1987; LLOYD et

al. 1992; SHERIFF 1992; LLOYD & FARQUHAR 1994; ISHIDA et al. 1996). In several tropical rainforest species, the c_i/c_a-ratios estimated from carbon isotope discrimination are relatively high (LLOYD & FARQUHAR 1994; ISHIDA et al. 1996) indicating a relatively small stomatal limitation to assimilation rate and non-conservative water use. This indicates a tropical climate with high water availability for Messel showing a relatively high average c_i/c_a-ratio of 0.82 for the three studied species. Among the fossil species, the Lauraceae were obviously more lavish regarding to efficiency in water use than the Myrtaceae. Today, high c_i/c_a-ratios were also recorded for Canarian *Laurus azorica* (Lauraceae) varying from 0.67 to 0.95 (GONZALEZ-RODRIGUEZ et al. 2001) and two subtropical Lauraceae, *Cryptocarya chinensis* and *Lindera chunii*, varying between approximately 0.8 and 0.9 (DE LILLIS & SUN 1990).

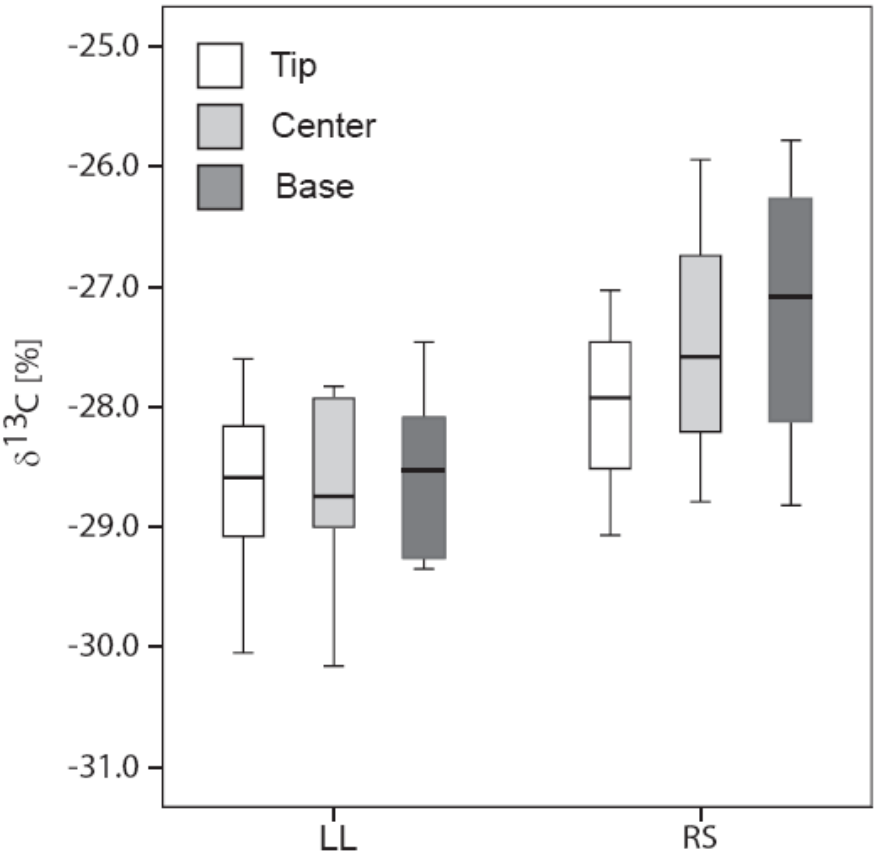

Fig. 3. Carbon isotope composition ($\delta^{13}C$ in ‰) of fossil leaf material of *Laurophyllum lanigeroides* (LL) and *Rhodomyrtophyllum sinuatum* (RS) from the three different positions on the leaf. The results are represented as box–whisker plots. The vertical lines connect the highest and lowest value, and the boxes span the 50% interquartile. The median is indicated by the horizontal line within the boxes.

CONCLUSIONS

$\delta^{13}C$ values of three species of fossil dicotyledonous angiosperm leaves from the early middle Eocene oilshale of Lake Messel fit in the range typical for modern C_3 plants. Intra-leaf analyses indicate slight $\delta^{13}C$ variations across individual leaves, which are, however, statistically not significant and much lower than the variability within the leaves of a distinct species.

The c_i/c_a-ratios as derived from $\delta^{13}C$ measurements are comparably high indicating a relatively small stomatal limitation to assimilation rate and non-conservative water use (e.g. ISHIDA et al. 1996; GONZALEZ-RODRIGUEZ et al. 2001). The $\delta^{13}C$ data therefore reflect the warm and humid climate that has previously been suggested for the early middle Eocene at Messel (SCHAARSCHMIDT 1988; WILDE 1989 and citations therein; WILDE 2005; WILDE & MICKLICH 2007; GREIN et al., accepted).

species (family)	**n**	**age**	**$\delta^{13}C$ ‰**	**Δ ‰**	**c_i/c_a**
Laurus nobilis (L)	5	extant	-26.4 ± 0.9	18.7 ± 1.0	0.63 ± 0.04
Cinnamomum camphora (L)	3	extant	-28.6 ± 0.3	21.0 ± 0.3	0.74 ± 0.02
Persea americana (L)	2	extant	-27.9 ± 0.3	20.3 ± 0.3	0.70 ± 0.01
Laurophyllum lanigeroides (L)	6	fossil	-28.7 ± 0.8	23.1 ± 0.8	0.83 ± 0.04
Daphnogene crebrigranosa (L)	4	fossil	-29.5 ± 0.7	24.0 ± 0.7	0.87 ± 0.03
Myrtus communis (M)	5	extant	-30.3 ± 0.7	22.8 ± 0.7	0.81 ± 0.03
Psidium littorale/cattleianum (M)	3	extant	-29.6 ± 0.4	22.1 ± 0.4	0.78 ± 0.02
Rhodomyrtophyllum sinuatum (M)	7	fossil	-27.6 ± 0.9	22.0 ± 1.0	0.78 ± 0.04
Castanea sativa (F)	3	extant	-28.1 ± 0.5	20.5 ± 0.6	0.71 ± 0.03
Messel (combined results)	17	fossil	-28.4 ± 1.1	22.9 ± 1.2	0.82 ± 0.05

Tab. 1. Carbon isotope composition ($\delta^{13}C$) and derived c_i/c_a-ratios for extant and fossil Lauraceae (L), Myrtaceae (M) and Fagaceae (F), number of leaves (n), calculated carbon isotope discrimination (Δ) and $\delta^{13}C$-derived c_i/c_a-ratio presented as average values with standard deviation.

ACKNOWLEDGEMENTS

We thank the staff of the Department of Messel Research, Senckenberg Forschungsinstitut und Naturmuseum, Frankfurt am Main, for excellent technical assistance and support. Furthermore, the technical support of Bernd Steinhilber, Institute for Geosciences, Tübingen, is gratefully acknowledged. We thank James Nebelsick, Institute for Geosciences, Tübingen, Germany, for critically reading the English manuscript.

This study was financially supported by the Federal State of Baden-Württemberg by a grant to M. G. within the program "Landesgraduiertenförderung".

REFERENCES

AUCOUR, A.-M., GOMEZ, B., SHEPPARD, S. M. F. & THÉVENARD, F. (2008): $\delta^{13}C$ and stomatal number variability in the Cretaceous conifer *Frenelopsis*. - Palaeogeography, Palaeoclimatology, Palaeoecology, **257**: 462-473.

BEERLING, D. J. (2000): Increased terrestrial carbon storage across the Palaeocene-Eocene boundary. - Palaeogeography, Palaeoclimatology, Palaeoecology, **161**: 395-405.

BEERLING, D. J., MCELWAIN, J. C. & OSBORNE, C. P. (1998): Stomatal responses of the 'living fossil' *Ginkgo biloba* L. to changes in atmospheric CO_2 concentrations. - Journal of Experimental Botany, **49**: 1603-1607.

BEERLING, D. J. & ROYER, D. L. (2002): Fossil plants as indicators of the Phanerozoic global carbon cycle. - Annual Review of Earth and Planetary Sciences, **30**: 527-556.

BEYSCHLAG, W., LANGE, O. L. & TENHUNEN, J. D. (1987): Diurnal patterns of leaf internal CO_2 partial pressure of the sclerophyll shrub *Arbutus unedo* growing in Portugal. - In: TENHUNEN J. D., CATARINO F. M., LANGE O. L. and OECHEL W. C. (eds.): Plant Response to Stress. Functional Analysis in Mediterranean Ecosystems, Berlin (Springer-Verlag).

CERLING, T. E., HART, J. A. & HART, T. B. (2004): Stable isotope ecology in the Ituri Forest. - Oecologia, **138**: 5-12.

DE LILLIS, M. & SUN, G. C. (1990): Stomatal response patterns and photosynthesis of dominant trees in a tropical monsoon forest. - Acta Oecologica, **11**: 545-555.

DUPONT-NIVET, G., KRIJGSMAN, W., LANGEREIS, C. G., ABELS, H. A., DAI, S. & FANG, X. (2007): Tibetan plateau aridification linked to global cooling at the Eocene-Oligocene transition. - Nature, **445**: 635-638.

EHLERINGER, J. R. & CERLING, T. E. (1995): Atmospheric CO_2 and the ratio of intercellular to ambient CO_2 concentrations in plants. - Tree Physiology, **15**: 105-111.

EHLERINGER, J. R., FIELD, C. B., LIN, Z. F. & KUO, C. Y. (1986): Leaf carbon isotope ratio and mineral composition in subtropical plants along an irradiance cline. - Oecologia, **70**: 520-526.

EHLERINGER, J. R., LIN, Z. F., FIELD, C. B., SUN, G. C. & KUO, C. Y. (1987): Leaf carbon isotope ratios of plants from a subtropical monsoon forest. - Oecologia, **72**: 109-114.

EVANS, J. R., SHARKEY, T. D., BERRY, J. A. & FARQUHAR, G. D. (1986): Carbon isotope discrimination measured concurrently with gas exchange to investigate CO_2 diffusion in leaves of higher plants. - Australian Journal of Plant Physiology, **13**: 281-292.

FARQUHAR, G. D., EHLERINGER, J. R. & HUBICK, K. T. (1989): Carbon isotope discrimination and photosynthesis. - Annual Review of Plant Physiology and Plant Molecular Biology, **40**: 503-537.

FARQUHAR, G. D., O´LEARY, M. H. & BERRY, J. A. (1982): On the relationship between carbon isotope discrimination and the intercellular carbon dioxide concentration in leaves. - Australian Journal of Plant Physiology, **9**: 121-137.

FELDER, M. & HARMS, F.-J. (2004): Lithologie und genetische Interpretation der vulkano-sedimentären Ablagerungen aus der Grube Messel anhand der Forschungsbohrung Messel 2001 und weiterer Bohrungen. - Courier Forschungsinstitut Senckenberg, **252**: 151-203.

FRANCIS, J. E. & POOLE, I. (2002): Cretaceous and early Tertiary climates of Antarctica: Evidence from fossil wood. - Palaeogeography, Palaeoclimatology, Palaeoecology, **182**: 47-64.

FRANKS, P. J. & FARQUHAR, G. D. (1999): A relationship between humidity response, growth form and photosynthetic operating point in C_3 plants. - Plant, Cell and Environment, **22**: 1337-1349.

GINGERICH, P. D. (2006): Environment and evolution through the Paleocene-Eocene thermal maximum. - Trends in Ecology and Evolution, **21**: 246-253.

GONZALEZ-RODRIGUEZ, A. M., MORALES, D. & JIMENEZ, M. S. (2001): Gas exchange characteristics of a Canarian laurel forest tree species (*Laurus azorica*) in relation to environmental conditions and leaf canopy position. - Tree Physiology, **21**: 1039-1045.

GREENWOOD, D. R. & WING, S. L. (1995): Eocene continental climates and latitudinal temperature gradients. - Geology, **23**: 1044-1048.

GREIN, M., UTESCHER, T., WILDE, V. & ROTH-NEBELSICK, A.: Reconstruction of the middle Eocene climate of Messel using palaeobotanical data. - Neues Jahrbuch für Geologie und Paläontologie, Abhandlungen, (accepted for publication).

HEATON, T. H. E. (1999): Spatial, Species, and Temporal Variations in the $^{13}C/^{12}C$ Ratios of C_3 Plants: Implications for Palaeodiet Studies. - Journal of Archaeological Science, **26**: 637-649.

HOLLIS, C. J., HANDLEY, L., CROUCH, E. M., MORGANS, H. E. G., BAKER, J. A., CREECH, J., COLLINS, K. S., GIBBS, S. J., HUBER, M., SCHOUTEN, S., ZACHOS, J. C. & PANCOST, R. D. (2009): Tropical sea temperatures in the high-latitude South Pacific during the Eocene. - Geology, **37**: 99-102.

ISHIDA, A., TOMA, T., MATSUMOTO, Y., YAP, S. K. & MARUYAMA, Y. (1996): Diurnal changes in leaf gas exchange characteristics in the uppermost canopy of a rain forest tree, *Dryobalanops aromatica* Gaertn. f. - Tree Physiology, **16**: 779-785.

JAHREN, A. H. (2007): The arctic forest of the Middle Eocene. - Annual Review of Earth and Planetary Sciences, **35**: 509-540.

KINGSTON, J. D. & HARRISON, T. (2007): Isotopic dietary reconstructions of Pliocene herbivores at Laetoli: Implications for early hominin paleoecology. - Palaeogeography, Palaeoclimatology, Palaeoecology, **243**: 272-306.

KÜRSCHNER, W. M. (1996): Leaf stomata as biosensors of palaeoatmospheric CO_2 levels. - PhD thesis, Laboratory of Palaeobotany and Palynology.

LARCHER, W. (2003): Physiological plant ecology: Ecophysiology and stress physiology of functional groups. 4th ed. - 513 pp.; Berlin (Springer).

LEAVITT, S. W. & NEWBERRY, T. (1992): Systematics of stable-carbon isotopic differences between gymnosperm and angiosperm trees. - Plant Physiology (Life Science Advances), **11**: 257-262.

LLOYD, J. & FARQUHAR, G. D. (1994): ^{13}C discrimination during CO_2 assimilation by the terrestrial biosphere. - Oecologia, **99**: 201-215.

LLOYD, J., SYVERTSEN, J. P., KRIEDEMANN, P. E. & FARQUHAR, G. D. (1992): Low conductances for CO_2 diffusion from stomata to the sites of carboxylation in leaves of woody species. - Plant, Cell and Environment, **15**: 873-899.

LOCKHEART, M. J., POOLE, I., VAN BERGEN, P. F. & EVERSHED, R. P. (1998): Leaf carbon isotope compositions and stomatal characters: important considerations for palaeoclimate reconstructions. - Organic Geochemistry, **29**: 1003-1008.

MERTZ, D. F. & RENNE, P. R. (2005): A numerical age for the Messel fossil deposit (UNESCO World Heritage Site) derived from $^{40}Ar/^{39}Ar$ dating on a basaltic rock fragment. - Courier Forschungsinstitut Senckenberg, **255**: 67-75.

MORA, C. I., DRIESE, S. G. & COLARUSSO, L. A. (1996): Middle to Late Paleozoic atmospheric CO_2 levels from soil carbonate and organic matter. - Science, **271**: 1105-1107.

NGUYEN TU, T. T., KÜRSCHNER, W. M., SCHOUTEN, S. & VAN BERGEN, P. F. (2004): Leaf carbon isotope compositon of fossil and extant oaks grown under differing atmospheric CO_2 levels. - Palaeogeography, Palaeoclimatology, Palaeoecology, **212**: 199-213.

O'LEARY, M. H. (1995): Environmental effects on carbon isotope fractionation in terrestrial plants,. - In: WADA E., YONEYAMA T., MINIGAWA M., ANDO T. and FRY B. D. (eds.): Stable Isotopes in the Biosphere, 78-91; Kyoto (Kyoto University Press).

PROTHERO, D. R., IVANY, L. C. & NESBITT, E. A. (2003): From greenhouse to icehouse: the marine Eocene-Oligocene transition. - 541 pp.; New York (Columbia University Press).

SCHAARSCHMIDT, F. (1988): Der Wald, fossile Pflanzen als Zeugen eines warmen Klimas. - In: SCHAAL S. and ZIEGLER W. (ed.)^(eds.): Messel - Ein Schaufenster in die Geschichte der Erde und des Lebens, 27-52; Frankfurt am Main (Waldemar Kramer).

SCHWEIZER, M. K., STEELE, A., TOPORSKI, J. K. W. & FOGEL, M. L. (2007): Stable isotopic evidence for fossil food webs in Eocene Lake Messel. - Paleobiology, **33**: 590-609.

SHERIFF, D. W. (1992): Roles of carbon gain and allocation in growth at different nitrogen nutrition in *Eucalyptus camaldulesis* and *Eucalyptus globulus* seedlings. - Australian Journal of Plant Physiology, **19**: 637-652.

TIESZEN, L. L. (1991): Natural variations in the carbon isotope values of plants: implications for archaeology, ecology, and paleoecology. - Journal of Archaeological Science, **18**: 227-248.

WILDE, V. (1989): Untersuchungen zur Systematik der Blattreste aus dem Mitteleozän der Grube Messel bei Darmstadt (Hessen, Bundesrepublik Deutschland). - Courier Forschungsinstitut Senckenberg, **115**: 1-213.

- (2005): The green Eocene. The diverse flora of a paratropical climate. - Vernissage UNESCO World Heritage Series, **21**: 14-19.

WILDE, V. & MICKLICH, N. (2007): Lebensraum Messel-See. Der See und seine Uferzonen. - In: GRUBER G. and MICKLICH N. (eds.): Messel - Schätze der Urzeit (Begleitbuch zur Ausstellung "Messel on Tour"), 52-55; Hessisches Landesmuseum Darmstadt (Theiss).

WILF, P., WING, S. L., GREENWOOD, D. R. & GREENWOOD, C. L. (1998): Using fossil leaves as paleoprecipitation indicators: An Eocene example. - Geology, **26**: 203-206.

ZACHOS, J. C., PAGANI, M., SLOAN, L., THOMAS, E. & BILLUPS, K. (2001): Trends, rhythms, and aberrations in global climate 65 Ma to present. - Science, **292**: 686-693.

ZACHOS, J. C., STOTT, L. D. & LOHMANN, K. C. (1994): Evolution of early Cenozoic marine temperatures. - Paleoceanography, **9**: 353-387.

3.4 Grein, M., Roth-Nebelsick, A., Konrad, W., Wilde, V., Utescher, T.: Reconstruction of atmospheric CO_2 during the middle Eocene by application of a gas exchange model to fossil plants. (submitted)

Reconstruction of atmospheric CO_2 during the middle Eocene by application of a gas exchange model to fossil plants

Michaela Grein, Anita Roth-Nebelsick, Wilfried Konrad, Volker Wilde & Torsten Utescher

ABSTRACT

Previous proxy data provide equivocal information on the level of atmospheric CO_2 during the middle Eocene. Contrary to geochemical models, Boron isotope based data indicate low CO_2 levels between 52 to 47 Ma. In this study, atmospheric CO_2 during the early middle Eocene (47 to 48 Ma) is reconstructed using fossil plants from the Messel Formation close to Darmstadt, Germany. CO_2 concentration is calculated using a mechanistic model of gas exchange which optimizes CO_2 uptake by photosynthesis against water vapour loss by transpiration, a strategy that is commonly realized in land plants. Input data for the model are stomatal data (density and pore length), paleoclimate data obtained by two different approaches and biochemical parameters of photosynthesis. Two species of leaves belonging to different families were studied: *Laurophyllum lanigeroides* (Lauraceae) and *Rhodomyrtophyllum sinuatum* (Myrtaceae). The resulting CO_2 ranges of the two taxa range from 563 to 1098 ppm with an overlapping interval from 703 to 836 ppm. Stomatal data therefore indicate a CO_2 concentration that was substantially higher than today. The reconstructed range of CO_2 concentration is close to data provided by geochemical modeling results. This agrees with models that require a CO_2 concentration of less than 750 ppm for the onset of ice sheet formation on Antarctica.

INTRODUCTION

The early Cenozoic was a period in earth-history during which greenhouse conditions prevailed (ZACHOS et al. 1994; WILF et al. 1998; GINGERICH 2006; JAHREN 2007). After the Early Eocene Climatic Optimum (EECO), global temperature declined until polar glaciation developed at the Eocene/Oligocene boundary (ZACHOS et al. 2001; DUPONT-NIVET et al. 2007). The level of atmospheric CO_2 (expressed as C_a throughout the rest of the text) represents one important – albeit not the only - factor which is credited for the development of global temperatures during the Palaeocene/Eocene (RAYMO 1991; BERNER & KOTHAVALA 2001; CROWLEY & BERNER 2001; ROYER 2006). For example, a crucial role in triggering glaciation is attributed to C_a (DECONTO & POLLARD 2003; TRIPATI et al. 2005; PEARSON et al. 2009; POLLARD & DECONTO 2009). The majority of the different available proxy data indicate a high level of C_a during the EECO, with a subsequent general decline in C_a during the rest of the Eocene (EKART et al. 1999; YAPP 2004; PAGANI et al. 2005; LOWENSTEIN & DEMICCO 2006; BOHATY et al. 2009). According to Boron isotope data, a strong decline of C_a occurred (PEARSON & PALMER 2000) in the middle Eocene, together with first indications on ice formation in the Arctic (STICKLEY et al. 2009). However, results of different approaches to the level of C_a disagree (RUDDIMAN 2010).

In this contribution, C_a of a well-defined time interval in the middle Eocene is determined by using stomatal data of fossil leaves. Stomata are micropores on the leaf surface that are

required to let CO_2, the substrate of photosynthesis, diffuse into the leaf towards the chloroplasts. Since water vapour escapes via the same pathway, common regulation strategies of stomatal conductance represent a mechanistic approach to reconstruct C_a by modelling gas exchange of fossil plants (KONRAD et al. 2008). The material was collected from the Messel Formation of the Messel pit, a UNESCO World Heritage site close to Darmstadt, Hessen, Germany. The Messel Formation is ideally suited for reconstructing C_a of the middle Eocene since it is well-dated, spans a limited time interval and provides a rich reservoir of excellently preserved fossil material. The lapilli tuff sequence which underlies the Messel maar sediments is dated at 47.8 Ma $\pm$ 0.2 Ma (MERTZ & RENNE 2005). The duration of the sedimentation amounted to about 1 myr, with an age of about 47 Ma for the top layer.

THE MODEL

Stomatal density ν affects stomatal conductance g, the permeability of the leaf for gases. A certain g is necessary since photosynthesis requires diffusional CO_2 influx into the leaf interior. The commonly observed inverse relationship between ν and C_a represents very probably the result of an adaptation of pore density according to the availability of carbon dioxide in the atmosphere. It therefore appears that C_a can principally be derived from stomatal density by considering the dependence of the assimilation rate A on g and the gradient between C_a and C_i (with C_i = leaf internal concentration of CO_2):

$$A = g\ (C_a - C_i) \qquad (1)$$

This simple approach is, however, not applicable due to the following reasons. Firstly, g is not only dependent on ν, but also on stomatal pore area a_{st} and pore depth d_{st} (PARLANGE & WAGGONER 1970). Secondly, a_{st} is not fixed but is dynamically controlled by the plant, reaching from complete closure to maximum aperture over one day (LARCHER 2003). Thirdly, C_i is coupled to A by a second relation describing photosynthesis:

$$A = q\,\frac{C_i - \Gamma}{C_i + K} - R_d \qquad (2)$$

with the biochemical parameters q = carboxylation limited by Rubisco or RuBP, K = parameter containing Michaelis-Menten constants of carboxylation and oxygenation, $\Gamma = CO_2$ compensation point and R_d = mitochondrial respiration rate (FARQUHAR et al. 1980, 2001; KONRAD et al. 2008).

The dynamic interrelationship between A, g and C_i thus prevents a straightforward derivation of C_a from stomatal parameters. A possibility of obtaining C_a from stomatal data, however, exists due to the strategy of optimized water use that is realized in land plants. Under most conditions, water availability is – at least seasonally – restricted and plants are therefore forced to control stomatal conductance and transpiration. A very low stomatal conductance that would result in a very low water loss, however, leads to a severely restricted rate of carbon gain by photosynthesis. Plants which are able to gain a maximum of carbon

with a minimum of water loss should be favoured by natural selection (GIVNISH 1986). In fact, plants commonly pursue an optimization strategy to achieve a maximum of carbon gain with a given amount of available water (COWAN 1977; BERNINGER et al. 1996). This can be expressed as

$$\int_{\Delta t} A(t)\,dt = \text{maximum} \tag{3a}$$

$$\int_{\Delta t} E(t)\,dt = W_0 \tag{3b}$$

with E = transpiration rate and W_0 = water supply that is available during the time span Δt. By applying the method of Lagrangian multipliers (ARFKEN 1970), an optimisation procedure can be performed that eventually leads to the desired $\nu(C_a)$ dependency. This optimisation principle was successfully applied in plant ecology, for example for *Pinus* species by BERNINGER et al. (1996), AALTO et al. (2002) and KATUL et al. (2010). By applying this principle, an optimum g and A can be expressed as a function of C_a and photosynthesis parameters. This requires – besides photosynthesis parameters and stomatal parameters – also climate parameters because photosynthesis and gas exchange are influenced by environmental conditions. Since g is dependent on stomatal density and stomatal pore size, the desired $\nu(C_a)$ relationship can then be derived. The underlying equations are provided in the Supplementary Information. A detailed derivation and discussion can be found in KONRAD et al. (2008). The model is currently running as a MAPLE Sheet which is available from the authors upon request.

MODEL INPUT PARAMETERS

Four kinds of parameters are necessary to run the model (Table 1). 1) Stomatal density and pore geometry dictate the maximum stomatal conductance that can be developed by a leaf. 2) Biochemical parameters of photosynthesis provide the behavior of the assimilation process. 3) Environmental data (temperature and humidity) affect diffusion, photosynthesis and transpiration and characterize the availability of water. 4) The $\delta^{13}C$ value of the fossil leaf material allows for assessing the ratio of C_i/C_a that was realized by the plant during its lifetime (FARQUHAR et al. 1989). Since C_i/C_a is calculated during model application, $\delta^{13}C$ of the fossil material represents a valuable additional parameter allowing for constraining λ and the biochemical parameters (KONRAD et al. 2008). The model input parameters are described and summarized in Table 1 to 3. For a detailed description about obtaining the necessary model input parameters comprising stomatal density and other leaf anatomical data, biochemical parameters, the carbon isotope signal and environmental parameters see Supplementary Information.

FOSSIL AND EXTANT LEAF MATERIAL

Two fossil species from two different plant families were considered: *Laurophyllum lanigeroides* (Lauraceae) and *Rhodomyrtophyllum sinuatum* (Myrtaceae). These species, whose taxonomic affinities are discussed in WILDE (1989) and GLINKA & WALTHER (2003), were selected because they present frequent elements of the Messel Pit taphocoenosis. In

total, 24 leaves of *Rhodomyrtophyllum sinuatum* and 28 leaves of *Laurophyllum lanigeroides* were collected and analyzed.

To validate the approach, the model was applied to two extant species from the same families, *Cinnamomum camphora* (Lauraceae) and *Psidium littorale* (Myrtaceae).

RESULTS AND DISCUSSION

In this study, stomatal data are used for the first time to reconstruct C_a levels for the middle Eocene. Usually, reconstructions of ancient C_a from stomatal data are based on empirical transfer functions produced by fitting a function through $\nu(C_a)$ data of extant and/or subfossil material which grew under known C_a (BEERLING & ROYER 2002; MCELWAIN et al. 2002; KÜRSCHNER et al. 2008). This approach limits the applicability of stomatal data for C_a reconstruction. Firstly, the production of a transfer function is only possible if the fossil material can be confidently assigned to extant taxa (for example ROYER et al. 2001; KÜRSCHNER et al. 2008). Secondly, the $\nu(C_a)$-response provided by transfer functions is nonlinear and its gradient decreases with increasing C_a rendering reliable calculation of C_a by the transfer function difficult, particularly under C_a higher than today (BEERLING & ROYER 2002; BEERLING et al. 2009). Thirdly, the use of transfer functions based on extant and subfossil material does not consider the effect of pore length change that appears to occur often with C_a and which represents a substantial parameter for gas exchange (KONRAD et al. 2008; FRANKS & BEERLING 2009). The use of a gas exchange model avoids these difficulties and appears therefore especially suitable for 1) stomatal-based reconstruction of high-level C_a and 2) for times in earth history providing only fossil material without sufficiently close extant relatives.

In the test run for the extant material, the gas exchange model provides a total range of C_a of about 267 to 526 ppm for both species, with an overlapping interval between 350 to 393 ppm (Figure 1). Direct CO_2 measurements on Mauna Loa, Hawaii, provided a C_a of about 382 ppm in 2006 (TANS 2010) which is in good agreement to the "reconstructed" extant C_a.

For the fossil material, the gas exchange model results in a total range of C_a of about 563 to 1098 ppm for both fossil taxa (Figure 2). The ranges for the single taxa are 563 to 836 ppm for *Rhodomyrtophyllum sinuatum* and 703 to 1098 ppm for *Laurophyllum lanigeroides*.

The C_a data previously obtained for the time interval of the Messel Formation by geochemical modelling and Boron isotopes range between values that are significantly below the extant level (DEMICCO et al. 2003), about one and a half times higher (PEARSON & PALMER 2000), about twice as high (ROTHMAN 2002) and up to two to three times higher (BERNER & KOTHAVALA 2001) (Figure 2). The maximum of the C_a range obtained by our study is close to the maximum value of BERNER & KOTHAVALA (2001) while the minimum is close to the upper limit of the range in PEARSON & PALMER (2000). Both taxa considered in our study show an overlapping interval roughly between 700 and 840 ppm. If this interval is accepted as C_a signal, the stomatal results of our study point to a moderately high C_a in the range of about 700 to 800 ppm. This is almost fitting to the overlapping interval of data provided by the geochemical modelling results of BERNER & KOTHAVALA (2001) (Figure 2), but somewhat above the results of ROTHMAN (2002) and the C_a based on foraminiferal $\delta^{11}B$ (PEARSON & PALMER 2000). The results of our study do not support a low-level C_a for 47 – 48 Ma as resulting from a recalculation of the $\delta^{11}B$ data set by DEMICCO et al. (2003).

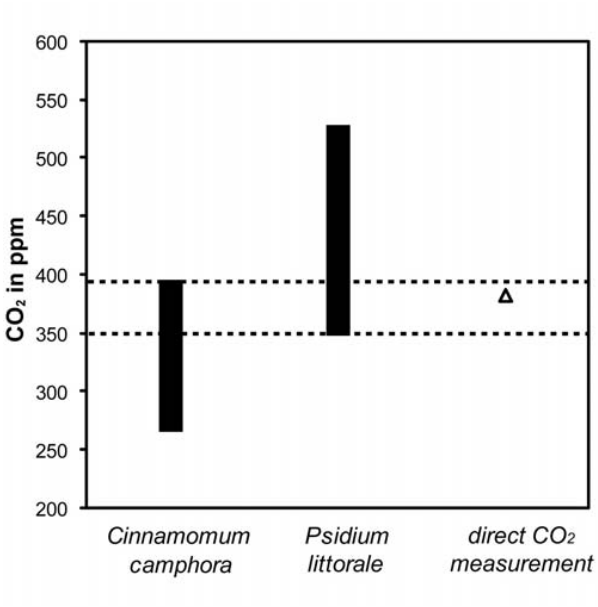

Figure 1. C_a ranges provided by the two extant taxa *Cinnamomum camphora* and *Psidium littorale* (black rectangles). The resulting overlapping interval is marked with black dotted lines. The figure also includes a data point representing direct CO_2 measurements at Mauna Loa/Hawaii in 2006 (triangle) provided by TANS (2010).

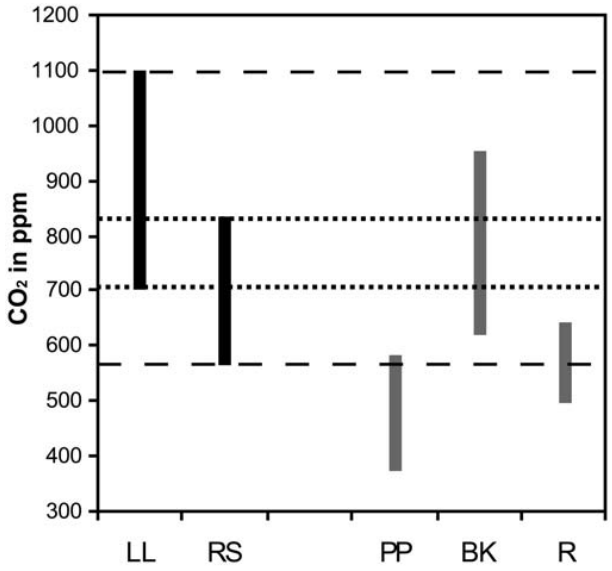

Figure 2. C_a ranges provided by the two fossil taxa *Rhodomyrtophyllum sinuatum* (RS) and *Laurophyllum lanigeroides* (LL). The data ranges obtained within this study are represented as black rectangles (dashed lines = total range of C_a). The resulting overlapping interval is marked with black dotted lines. The figure also includes already existing C_a data for the Messel time interval. These are represented as grey rectangles. PP: Data point provided by PEARSON & PALMER (2000). BK: Data for the time interval between 50 and 40 Ma B.P. derived from BERNER & KOTHAVALA (2001). R: Data for the time interval between ~ 50 and 40 Ma B.P. derived from ROTHMAN (2002).

Symbol	Description	unit
Environmental parameters		
RH	relative atmospheric humidity	%
T	temperature	°C
V_{wind}	wind velocity	m/s
Anatomical parameters		
d_{as}	depth of assimilation tissue	µm
d_{st}	depth of stomatal pore	µm
h_{st}	length of stomatal pore	µm
w_{st}	width of stomatal pore	µm
l_{leaf}	leaf length	mm
η_{as}	porosity of assimilation tissue	-
τ_{as}	tortuosity of assimilation tissue	-
ν	stomatal density	1/mm²
$\delta^{13}C$ derived parameters		
c_i/c_a	ratio of leaf-internal to ambient CO_2	-
λ	water availability "cost of water"	-
Photosynthetic parameters		
K	Michaelis-Menten constant	µmol/mol
Γ	CO_2 compensation point	µmol/mol
q	maximum RuBP-saturated rate of carboxylation	µmol/m²s
R_d	mitochondrial respiration rate in the light	µmol/m²s

Tab. 1. Model input parameters

Symbol	*L. lanigeroides*	*R. sinuatum*	*C. camphora*	*P. littorale*	Ref.
Environmental parameters*					
RH [%]	77	77	75.2	75.2	1
T [°C]	22	22	16.8	16.8	1
V_{wind} [m/s]	1	1	0.5	0.5	1, 2
Anatomical parameters					
d_{as} [µm]	90 ± 8	117 ± 55	88 ± 8	117 ± 55	1
d_{st} [µm]	21.8 ± 1.4	13.2 ± 1.3	16.3 ± 1.0	13.2 ± 1.3	1
h_{st} [µm]	7.1 ± 1.5	7.6 ± 2.0	6.6 ± 1.1	7.8 ± 1.4	1
w_{st} [µm]	3.6	3.8	3.3	3.9	1
l_{leaf} [mm]	67 ± 21	63 ± 14	92 ± 19	69 ± 12	1
η_{as} [-]	0.33	0.33	0.33	0.33	3
τ_{as} [-]	1.571	1.571	1.571	1.571	3
ν [1/mm²]	410	282	307	362	1
Photosynthetic parameters					
q [µmol/m²s]	*varied*	*varied*	40.3	52	4
R_d [µmol/m²s]	0.7	1.5	0.7	1.0	4

[1]this study
[2]rough estimate (moderate wind velocity under standard situations)
[3]KONRAD et al. (2008)
[4]typical values for extant Lauraceae and Myrtaceae estimated after different authors and citations therein: e.g. KIRSCHBAUM & FARQUHAR (1984), WULLSCHLEGER (1993), PATTISON et al. (1998), REICH et al. (1998), WOODALL et al. (1998), NIINEMETS et al. (2005), KOSUGI & MATSUO (2006), FUNK (2008), CAI et al. (2009)
*extant climate data were provided by "Schwäbisches Tagblatt, Uhlandstraße"

Tab. 2. Constant parameters used for CO_2 modelling

A C_a value at about 700 to 800 ppm fits well to climatic conditions generally suggested for the middle Eocene. Global climate was still warm during the deposition of the Messel Formation, and the oceans were largely ice-free (GREENWOOD et al. 2010). This is also reflected by warm and humid conditions for that area as derived from the paleovegetation (MOSBRUGGER et al. 2005). Bipolar glaciation started much later (PEKAR & CHRISTIE-BLICK 2008), probably promoted by declining C_a (DECONTO & POLLARD 2003; TRIPATI et al. 2005;

DECONTO et al. 2008). According to modelling results (DECONTO et al. 2008), threshold values below which Antarctic glaciation may have started amount to about 750 ppm C_a. This finding is corroborated by our results indicating C_a between 700 to 800 ppm and that are not in conflict with the lacking evidence of substantial ice during the middle Eocene (RUDDIMAN 2010).

Symbol	*Laurophyllum lanigeroides*	*Rhodomyrtophyllum sinuatum*	*Cinnamomum camphora*	*Psidium littorale*	Ref.
Maximum RuBP-saturated rate of carboxylation *q* (µmol/m²s)					
max	45	55			1, 2
best guess	40	50	*constant*	*constant*	1, 2
min	35	45			1, 2
c_i/c_a-ratio*					
max	0.85	0.80	0.76	0.80	1
measured	0.83	0.78	0.74	0.78	1
min	0.81	0.76	0.72	0.76	1

[1]this study
[2]derived from typical ranges for extant Lauraceae, Myrtaceae, tropical rain forest species and sclerophylleous shrubs after different authors and citations therein: WULLSCHLEGER (1993), NIINEMETS et al. (2005), KOSUGI & MATSUO (2006), FUNK (2008), PALLARDY (2008)
*The measured value represents the mean value of the isotope measurements; maximum and minimum values were constructed by ±0.02

Tab. 3. Ranges of varied parameters used for CO_2 modelling

ACKNOWLEDGEMENTS

Thanks are due to KARIN SCHMIDT, MARTIN MÜLLER, MARION GROPPO, UTA KIEL and MICHAEL ACKERMANN, Senckenberg Forschungsinstitut und Naturmuseum, Frankfurt am Main (Germany), for assistance in the lab and in the field. Furthermore, the technical support of BERND STEINHILBER (isotope measurements), Institute for Geosciences, Tübingen, MAREN BABBICK and RÜDIGER HAMPP (gas exchange measurements), Department of Physiological Ecology of Plants, Tübingen, is gratefully acknowledged. We thank JAMES NEBELSICK, Institute for Geosciences, Tübingen, Germany, for critically reading the English manuscript.

This study was supported by a grant to M. G. within the program "Landesgraduierten-förderung" of the Federal State of Baden-Württemberg.

REFERENCES

AALTO, T., HARI, P. & VESALA, T. (2002): Comparison of an optimal stomatal regulation model and a biochemical model in explaining CO_2 exchange in field conditions. - Silva Fennica, **36**: 615-623.

ARFKEN, G. (1970): Mathematical Methods for Physicists. 2nd. - 815 pp.; New York (Academic Press).

BEERLING, D. J., FOX, A. & ANDERSON, C. W. (2009): Quantitative uncertainty analyses of ancient atmospheric CO_2 estimates from fossil leaves. - American Journal of Science, **309**: 775-787.

BEERLING, D. J. & ROYER, D. L. (2002): Reading a CO_2 signal from fossil stomata. - New Phytologist, **153**: 387-397.

BERNER, R. A. & KOTHAVALA, Z. (2001): GEOCARB III: a revised model of atmospheric CO_2 over Phanerozoic time. - American Journal of Science, **301**: 182-204.

BERNINGER, F., MÄKELA, A. & HARI, P. (1996): Optimal Control of Gas Exchange during Drought: Empirical Evidence. - Annals of Botany, **77**: 469-476.

BOHATY, S. M., ZACHOS, J. C., FLORINDO, F. & DELANEY, M. L. (2009): Coupled greenhouse warming and deep-sea acidification in the middle Eocene. - Paleoceanography, **24**: PA2207, doi: 10.1029/2008PA001676.

CAI, Z.-Q., SCHNITZER, S. A. & BONGERS, F. (2009): Seasonal differences in leaf-level physiology give lianas a competitive advantage over trees in a tropical seasonal forest. - Oecologia, **161**: 25-33.

COWAN, I. R. (1977): Stomatal behaviour and environment. - Advances in Botanical Research, **4**: 117-227.

CROWLEY, T. J. & BERNER, R. A. (2001): Enhanced: CO_2 and Climate Change. - Science, **292**: 870-872.

DECONTO, R. M. & POLLARD, D. (2003): Rapid Cenozoic glaciation of Antarctica induced by declining atmospheric CO_2. - Nature, **421**: 245-249.

DECONTO, R. M., POLLARD, D., WILSON, P., PALIKE, H., LEAR, C. & PAGANI, M. (2008): Thresholds for Cenozoic bipolar glaciation. - Nature, **455**: 653-656.

DEMICCO, R. V., LOWENSTEIN, T. K. & HARDIE, L. A. (2003): Atmospheric pCO_2 since 60 Ma from records of seawater pH, calcium, and primary carbonate mineralogy. - Geology, **31**: 793-796.

DUPONT-NIVET, G., KRIJGSMAN, W., LANGEREIS, C. G., ABELS, H. A., DAI, S. & FANG, X. (2007): Tibetan plateau aridification linked to global cooling at the Eocene-Oligocene transition. - Nature, **445**: 635-638.

EKART, D. D., CERLING, T. E., MONTAÑEZ, I. P. & TABOR, N. J. (1999): A 400 million year carbon isotope record of pedogenic carbonate: Implications for paleoatmospheric carbon dioxide. - American Journal of Science, **299**: 805-827.

FARQUHAR, G. D., EHLERINGER, J. R. & HUBICK, K. T. (1989): Carbon isotope discrimination and photosynthesis. - Annual Review of Plant Physiology and Plant Molecular Biology, **40**: 503-537.

FARQUHAR, G. D., VON CAEMMERER, S. & BERRY, J. A. (1980): A biochemical model of photosynthetic CO_2 assimilation in leaves of C_3 species. - Planta, **149**: 78-90.

- (2001): Models of Photosynthesis. - Plant Physiology, **125**: 42-45.

FRANKS, P. J. & BEERLING, D. J. (2009): Maximum leaf conductance driven by CO_2 effects on stomatal size and density over geologic time. - Proceedings of the National Academy of Sciences of the United States of America, **106**: 10343-10347.

FUNK, J. L. (2008): Differences in plasticity between invasive and native plants from a low resource environment. - Journal of Ecology, **96**: 1162-1173.

GINGERICH, P. D. (2006): Environment and evolution through the Paleocene-Eocene thermal maximum. - Trends in Ecology and Evolution, **21**: 246-253.

GIVNISH, T. J. (1986): Optimal stomatal conductance, allocation of energy between leaves and roots, and the marginal cost of transpiration. - In: GIVNISH T. J. (ed.) On the economy of plant form and function, 171-213; Cambridge (Cambridge University Press).

GLINKA, U. & WALTHER, H. (2003): *Rhodomyrtophyllum reticulosum* (ROSSM.) KNOBLOCH & Z.KVACEK – ein bedeutendes eozänes Florenelement im Tertiär Mitteleuropas. - Feddes Repertorium, **114**: 30–55.

GREENWOOD, D. R., BASINGER, J. F. & SMITH, R. Y. (2010): How wet was the Arctic Eocene rain forest? Estimates of precipitation from Paleogene Arctic macrofloras. - Geology, **38**: 15-18.

JAHREN, A. H. (2007): The arctic forest of the Middle Eocene. - Annual Review of Earth and Planetary Sciences, **35**: 509-540.

KATUL, G. G., MANZONI, S., PALMROTH, S. & OREN, R. (2010): A stomatal optimization theory to describe the effects of atmospheric CO_2 on leaf photosynthesis and transpiration. - Annals of Botany, **105**: 431-442.

KIRSCHBAUM, M. U. F. & FARQUHAR, G. D. (1984): Temperature dependence of whole-leaf photosynthesis in *Eucalyptus pauciflora* Sieb. ex Spreng. - Australian Journal of Plant Physiology, **11**: 519-538.

KONRAD, W., ROTH-NEBELSICK, A. & GREIN, M. (2008): Modelling of stomatal density response to atmospheric CO_2. - Journal of Theoretical Biology, **253**: 638–658.

KOSUGI, Y. & MATSUO, N. (2006): Seasonal fluctuations and temperature dependence of leaf gas exchange parameters of co-occuring evergreen and deciduous trees in a temperate broad-leaved forest. - Tree Physiology, **26**: 1173-1184.

KÜRSCHNER, W. M., KVACEK, Z. & DILCHER, D. L. (2008): The impact of Miocene atmospheric carbon dioxide fluctuations on climate and the evolution of terrestrial ecosystems. - Proceedings of the National Academy of Sciences of the United States of America, **105**: 449-453.

LARCHER, W. (2003): Physiological plant ecology: Ecophysiology and stress physiology of functional groups. 4th ed. - 513 pp.; Berlin (Springer).

LOWENSTEIN, T. K. & DEMICCO, R. V. (2006): Elevated Eocene atmospheric CO_2 and its subsequent decline. - Science, **313**: 1928.

MCELWAIN, J. C., MAYLE, F. E. & BEERLING, D. J. (2002): Stomatal evidence for a decline in atmospheric CO_2 concentrations during the Younger Dryas stadial: a comparison with Antarctic ice core records. - Journal of Quaternary Science, **17**: 21-29.

MERTZ, D. F. & RENNE, P. R. (2005): A numerical age for the Messel fossil deposit (UNESCO World Heritage Site) derived from $^{40}Ar/^{39}Ar$ dating on a basaltic rock fragment. - Courier Forschungsinstitut Senckenberg, **255**: 67-75.

MOSBRUGGER, V., UTESCHER, T. & DILCHER, D. L. (2005): Cenozoic continental climatic evolution of Central Europe. - Proceedings of the National Academy of Sciences of the United States of America, **102**: 14964-14969.

NIINEMETS, Ü., CESCATTI, A., RODEGHIERO, M. & TOSENS, T. (2005): Leaf internal diffusion conductance limits photosynthesis more strongly in older leaves of Mediterranean evergreen broad-leaved species. - Plant, Cell and Environment, **28**: 1552-1566.

PAGANI, M., ZACHOS, J. C., FREEMAN, K. H., TIPPLE, B. & BOHATY, S. (2005): Marked Decline in Atmospheric Carbon Dioxide Concentrations During the Paleogene. - Science, **309**: 600-603.

PALLARDY, S. G. (2008): Physiology of woody plants. 3. - 464 pp.; San Diego, CA, USA (Academic Press).

PARLANGE, J.-Y. & WAGGONER, P. E. (1970): Stomatal dimensions and resistance to diffusion. - Plant Physiology, **46**: 337-342.

PATTISON, R. R., GOLDSTEIN, G. & ARES, A. (1998): Growth, biomass allocation and photosynthesis of invasive and native Hawaiian rainforest species. - Oecologia, **117**: 449-459.

PEARSON, P. N., FOSTER, G. L. & WADE, B. S. (2009): Atmospheric carbon dioxide through the Eocene-Oligocene climate transition. - Nature, **461**: 1110-1114.

PEARSON, P. N. & PALMER, M. R. (2000): Atmospheric carbon dioxide concentrations over the past 60 million years. - Nature, **406**: 695-699.

PEKAR, S. F. & CHRISTIE-BLICK, N. (2008): Resolving apparent conflicts between oceanographic and Antarctic climate records and evidence for a decrease in pCO_2 during the Oligocene through early Miocene (34-16 Ma). - Palaeogeography, Palaeoclimatology, Palaeoecology, **260**: 41-49.

POLLARD, D. & DECONTO, R. M. (2009): Modelling West Antarctic ice sheet growth and collapse through the past five million years. - Nature, **458**: 329-333.

RAYMO, M. E. (1991): Geochemical evidence supporting Chamberlin, T.C.`s theory of glaciation. - Geology, **19**: 344-347.

REICH, P. B., WALTERS, M. B., ELLSWORTH, D. S., VOSE, J. M., VOLIN, J. C., GRESHAM, C. & BOWMAN, W. D. (1998): Relationships of leaf dark respiration to leaf nitrogen, specific leaf area and leaf life-span: a test across biomes and functional groups. - Oecologia, **114**: 471-482.

ROTHMAN, D. H. (2002): Atmospheric carbon dioxide levels for the last 500 million years. - Proceedings of the National Academy of Sciences of the United States of America, **99**: 4167-4171.

ROYER, D. L. (2006): CO_2-forced climate thresholds during the Phanerozoic. - Geochimica et Cosmochimica Acta, **70**: 5665-5675.

ROYER, D. L., WING, S. L., BEERLING, D. J., JOLLEY, D. W., KOCH, P. L., HICKEY, L. J. & BERNER, R. A. (2001): Paleobotanical evidence for near present-day levels of atmospheric CO_2 during part of the Tertiary. - Science, **292**: 2310-2313.

RUDDIMAN, W. F. (2010): A Paleoclimatic Enigma? - Science, **328**: 838-839.

STICKLEY, C. E., ST JOHN, K., KOÇ, N., JORDAN, R. W., PASSCHIER, S., PEARCE, R. B. & KEARNS, L. E. (2009): Evidence for middle Eocene Arctic sea ice from diatoms and ice-rafted debris. - Nature, **460**: 376-379.

TANS, P. (2010): Mauna Loa CO_2 annual mean data. NOAA/ESRL (www.esrl.noaa.gov/gmd/ccgg/trends/); Access Date: 25th May 2010.

TRIPATI, A., BACKMAN, J., ELDERFIELD, H. & FERRETTI, P. (2005): Eocene bipolar glaciation associated with global carbon cycle changes. - Nature, **436**: 341-346.

WILDE, V. (1989): Untersuchungen zur Systematik der Blattreste aus dem Mitteleozän der Grube Messel bei Darmstadt (Hessen, Bundesrepublik Deutschland). - Courier Forschungsinstitut Senckenberg, **115**: 1-213.

WILF, P., WING, S. L., GREENWOOD, D. R. & GREENWOOD, C. L. (1998): Using fossil leaves as paleoprecipitation indicators: An Eocene example. - Geology, **26**: 203-206.

WOODALL, G. S., DODD, I. C. & STEWART, G. R. (1998): Contrasting leaf development within the genus *Syzygium*. - Journal of Experimental Botany, **49**: 79-87.

WULLSCHLEGER, S. D. (1993): Biochemical limitations to carbon assimilation in C_3 plants - a retrospectve analysis of the A/C_i curves from 109 species. - Journal of Experimental Botany, **44**: 907-920.

YAPP, C. J. (2004): $Fe(CO_3)OH$ in goethite from a mid-latitude North American Oxisol: estimate of atmospheric CO_2 concentration in the Early Eocene "climatic optimum". - Geochimica et Cosmochimica Acta, **68**: 935-947.

ZACHOS, J. C., PAGANI, M., SLOAN, L., THOMAS, E. & BILLUPS, K. (2001): Trends, rhythms, and aberrations in global climate 65 Ma to present. - Science, **292**: 686-693.

ZACHOS, J. C., STOTT, L. D. & LOHMANN, K. C. (1994): Evolution of early Cenozoic marine temperatures. - Paleoceanography, **9**: 353-387.

Supplementary Information

Grein et al.

Derivation of the $\nu(C_a)$-relationship by a mechanistic model

The model is thoroughly discussed in Konrad et al. (2008). The model is currently running as a MAPLE sheet which is available from the authors upon request.

Submodel diffusion

Leaves and atmosphere exchange CO_2 and H_2O by diffusion. Fick's Law connects transpiration rate E with stomatal conductance g and the H_2O concentrations within leaves (w_i) and atmosphere (w_a) and similarly for the assimilation rate A and the CO_2 concentrations C_i and C_a:

$$E = g\, a\, (w_i - w_a) \tag{1}$$

$$A = g\ (C_a - C_i) \tag{2}$$

where $a := D_{H_2O}/D_{CO_2}$, D_{H_2O} and D_{CO_2} are the diffusion constants of H_2O resp. CO_2 in air. Furthermore, estimated ranges for temperature are required since it affects gas exchange (for details, see Konrad et al. 2008).

Submodel photosynthesis

Assimilation of C_3 plants consumes CO_2 molecules according to the Farquhar model of photosynthesis (q, Γ, K, R_d depend on T):

$$A = q\, \frac{C_i - \Gamma}{C_i + K} - R_d \tag{3}$$

where q= asymptotic assimilation rate, Γ = CO_2-compensation point, R_d = daylight mitochondrial respiration rate, K= Michaelis-Menten-constant. Expression (3) represents a very compact description of the Farquhar model. For details (such as the temperature dependence of photosynthesis parameters), consult Farquhar et al. (1980) and Konrad et al. (2008).

Submodel optimisation

Combining (2) and (3), A and E can be expressed in terms of the stomatal conductance g:

$$A[g] = \frac{1}{2g}\left\{g\,(C_a + K) + (q - R_d) - \sqrt{\left[g\,(C_a - K) - (q - R_d)\right]^2 + 4g\,(gKC_a + q\Gamma + KR_d)}\right\} \tag{4}$$

$$E[g] = (w_i - w_a)\ ag \tag{5}$$

Optimisation according to "Variation subject to constraints" (weighing carbon gain $\int_{\Delta t} A[g]\,dt =$ max. by assimilation versus water loss $\int_{\Delta t} E[g]\,dt = W_0$ by transpiration) produces the (fictitious) optimum stomatal conductivity

$$g_{opt} = \frac{1}{(C_a + K)^2} \left\{ \sqrt{\frac{q\,(K+\Gamma)\,[C_a\,(q - R_d) - (q\Gamma + KR_d)]}{\left[C_a + K - \lambda a\left(w_i - w_a\right)\right]\lambda a\left(w_i - w_a\right)}}\,[C_a + K - 2\lambda a\,(w_i - w_a)] \right.$$
$$\left. + (q - R_d)\;C_a - (q\Gamma + KR_d) - q\,(K+\Gamma) \right\} \tag{6}$$

The optimisation procedure introduces the Lagrangian multiplier λ, which is constant during Δt and can be understood within the present context as "cost of water". Once g_{opt} is known, insertion into (4) and (5) produces A and E.

Plant regulation of gas exchange

Plants adjust the "real" stomatal conductance g to g_{opt} by varying the stomatal cross section a_{st} (short-term regulation) or the stomatal density ν (long-term regulation). Fick's Law of diffusion allows to express g in terms of leaf the anatomical parameters stomatal density ν, pore size a_{st} and pore depth d_{st}. d_{as}, τ_{as} and n_{as} denote thickness, tortuosity and porosity of the assimilating tissue, respectively (Parlange & Waggoner 1970):

$$g = \frac{D_{\mathrm{CO_2}}}{\left[\left(d_{bl} + d_{as}\frac{\tau_{as}^2}{n_{as}}\right) + \frac{d_{st}}{\nu a_{st}}\right]} \tag{7}$$

The relation $\nu(C_a)$ is obtained from first solving (7) for ν

$$\nu = \frac{1}{a_{st}} \left(\frac{\left[d_{st} + \sqrt{\frac{a_{st}}{\pi}}\right] g}{D_{\mathrm{CO_2}} - \left[d_{bl} + d_{as}\frac{\tau_{as}^2}{n_{as}}\right] g} \right) \tag{8}$$

and then replacing g by g_{opt} from expression (6). The resulting equation can, in principle, be solved for $C_a(\nu)$. Since it represents, however, a polynomial of fifth degree with respect to C_a, this last step can be performed only numerically.

Additional information on input parameters

Stomatal parameters

As the stomatal frequency changes significantly over a single leaf (Poole et al. 1996, 2000) cuticle preparations were taken from defined regions of each individual leaf: base, center and apex. Tissue samples were cut out of the leaf blade and subsequently put in Schulze Solution (crystalline potassium chlorate and nitric acid). After maceration, samples were neutralized in ammonia solution. As soon as the cuticles were removed from the mesophyll, they were washed thoroughly with clear water and subsequently stained with safranin. Cuticles were embedded in glycerine jelly, mounted on microscope slides and the microscopic images digitalized. For

determination of stomatal density of the fossil cuticles, the method of the cumulative mean was applied in order to determine the number of leaves per taxon that are required to obtain a stable signal (Beerling & Royer, 2002). In total, 28 leaves of *Laurophyllum lanigeroides* (336 counts) and 24 leaves of *Rhodomyrtophyllum sinuatum* (332 counts) were investigated with at least 12 counts per leaf. Only almost complete leaves were used for analysis. Results of stomatal density calculations are presented in Table 1.

Table 1: RESULTS OF STOMATAL DENSITY CALCULATIONS

Species	Leaf ID	ν	sd	Leaf ID	ν	sd
Laurophyllum lanigeroides	ME 02744	384	10	ME 23640	315	18
	ME 03857	382	39	ME 23641	372	61
	ME 11550	450	61	ME 23642	408	53
	ME 12529	419	46	ME 23643	463	48
	ME 12668	398	62	ME 23644	333	41
	ME 13488	509	22	ME 23645	424	31
	ME 13507	502	23	ME 23646	471	73
	ME 13581	378	19	ME 23647	405	50
	ME 13581	327	4	ME 23648	315	33
	ME 15704	516	58	ME 23649	571	18
	ME 19092	371	43	ME 23651	366	89
	ME 23630	364	40	ME 23719	375	22
	ME 23631	374	15	ME 23720	486	98
	ME 23632	399	28	ME 23731	399	31
Rhodomyrtophyllum sinuatum	ME 02746	254	31	ME 23634	360	30
	ME 03994	330	71	ME 23635	361	48
	ME 09531	337	78	ME 23636	315	13
	ME 09659	207	15	ME 23637	230	46
	ME 09681	248	41	ME 23712	223	28
	ME 09951	336	26	ME 23718	200	14
	ME 09955	270	16	ME 23733	198	16
	ME 10803	293	13	ME 23819	271	18
	ME 13454	417	48	ME 23835	247	33
	ME 13525	256	9	ME 23837	262	17
	ME 16694	270	32	ME 23841	368	39
	ME 23633	241	31	ME 23848	280	30

ν = stomatal density in $1/mm^2$, sd = standard deviation in $1/mm^2$;
Leaf ID is equivalent to "SM-B. Number" (which is an identification number in the palaeobotanical collection of the Senckenberg Forschungsinstitut und Naturmuseum (Frankfurt am Main)

Other leaf anatomical data

Other anatomical parameters that are needed by the model, such as mesophyll porosity, but which cannot be obtained by fossil material had to be determined by using extant taxa. Recent

plant material was provided by the Botanical Gardens of Tübingen, Berlin-Dahlem, Munich and Heidelberg (all Germany). We selected representatives of the Lauraceae and Myrtaceae showing anatomical, morphological and/or ecological similarities to the fossil species as provided by various species of the generae *Laurus*, *Cinnamomum*, *Cryptocarya*, *Ocotea* (all Lauraceae), *Psidium*, *Syzygium* and *Eugenia* (all Myrtaceae). For anatomical analysis, leaf cross sections were produced and analyzed.

Environmental data

For the model, Mean Annual Temperature (MAT) and Mean Relative Humidity (MRH) are of relevance. MAT affects photosynthesis (Bernacchi et al. 2003) whereas transpiration is dependent on relative humidity under a given g. Quantitative data for mean annual temperature (MAT) and relative air humidity (RH) for Messel during the middle Eocene, were determined by using two approaches for paleoclimate reconstruction.

The first one is the *Coexistence approach (CA)* after Mosbrugger & Uteschер (1997) which is based on the assumption that the climatic requirements of a fossil taxon is similar to that of its nearest living relatives (NLR). After defining the intervals of all NLRs known for a fossil taphocoenosis, the overlap for a certain climate parameter is identified. Finally, an interval is derived in which all these taxa could potentially coexist (Mosbrugger & Uteschер 1997). Climatic tolerances were extracted from the PALAEOFLORA database (Uteschер & Mosbrugger 2010) and imported as ASCII file into ClimStat (V1.02), a FORTRAN program used to determine the coexistence interval for climate parameters.

For Eocene species, the meaningful identification of a nearest living relative species may be quite difficult (Wilde 1989) and, thus, comparisons and interpretations for Messel were mostly based on the family level (e. g. Wilde 1989, 2004). Although the CA is commonly recommended to be ideally performed on the species level, in the case of a middle Eocene plant taphocoenosis like the one from Messel, identification on family level seems to be much more reliable than on genus or species level. The analysis is based on the most recent summary of the plant taphocoenosis from the middle Eocene oilshale of Messel (Wilde 2004) which lists 111 families of pteridophytes, lycophytes, gymnosperms and angiosperms. After excluding insecure taxa, cosmopolitans with no available climate data and monotypic families, the CA was applied to the remaining 55 families.

The second method is the *Leaf Margin Analysis (LMA)* using the fact that MAT increases with increasing proportion of taxa with entire-margined leaves (Wilf 1997; Traiser et al. 2005). This proportion is used in linear equations, derived from extant floras, to calculate the MAT. Application of LMA was based on the monograph of Wilde (1989) providing an overview of the Messel leaf assemblage containing systematic descriptions of 60 dicotyledonous angiosperm leaf types. 53 of them were regarded as woody and were used for LMA. Aquatic plants, plants with insecure leaf margin type and herbs were excluded. Leaf margins were determined according to descriptions and images of Wilde (1989) and Sturm (1971).

Three equations which were already tested on extant floras were used:

$$MAT = 1.141 + 0.306\, p_{entire} \quad \text{(LMA1)}$$

$$MAT = 2.240 + 0.286\, p_{entire} \quad \text{(LMA2)}$$

$$MAT = 0.512 + 0.314\, p_{entire} \quad \text{(LMA3)}$$

where p_{entire} denotes the percentage of leaves with entire leaf margin ($0 \leq p_{entire} \leq 100$). Equations (LMA1) and (LMA2) were obtained with extant floras from N-, M- and S-America (Wilf 1997) and East Asia (Wing & Greenwood 1993). Equation (LMA3) was obtained by Traiser et al. (2005) for European floras.

Biochemical parameters

Biochemical parameters of photosynthesis were mostly taken from literature dealing with species that are related to the fossil taxa. Furthermore, gas exchange measurements were performed on plants in the Botanical Garden of Tübingen using a portable gas analyzer (LCi Ultra Compact Photosynthesis Measurement System, ADC BioScientific Ltd.). Measurements on stomatal conductance were carried out between 8 and 11 a.m. on fully expanded leaves under ambient conditions. Ongoing FACE experiments (Free Air Carbon Dioxide Enrichment) in which plants are exposed to elevated C_a under outdoor conditions reveal that photosynthesis parameters can be influenced by C_a (Ainsworth & Rogers 2007). Therefore, C_a-driven variation of photosynthesis has to be taken into account and q was varied within the range that can be expected according to the recent results of FACE experiments.

Isotope analysis

In order to obtain the C_i/C_a-value, the C-isotopic composition of the fossil leaf material was measured with a NC 2500 connected to a Thermo Quest Delta+XL mass spectrometer (Department of Geochemistry, Institute for Geosciences, University of Tübingen).

References

Ainsworth, E. A. & Rogers, A. (2007): The response of photosynthesis and stomatal conductance to rising [CO_2]: mechanisms and environmental interactions. - Plant, Cell and Environment, **30**: 258-270.

Beerling, D. J. & Royer, D. L. (2002): Reading a CO_2 signal from fossil stomata. - New Phytologist, **153**: 387-397.

Bernacchi, C. J., Pimentel, C. & Long, S. P. (2003): In vivo temperature response functions of parameters required to model RuBP-limited photosynthesis. - Plant, Cell and Environment, **26**: 1419-1430.

Farquhar, G. D., Von Caemmerer, S. & Berry, J. A. (1980): A biochemical model of photosynthetic CO_2 assimilation in leaves of C_3 species. - Planta, **149**: 78-90.

Konrad, W., Roth-Nebelsick, A. & Grein, M. (2008): Modelling of stomatal density response to atmospheric CO_2. - Journal of Theoretical Biology, **253**: 638-658.

Mosbrugger, V. & Utescher, T. (1997): The coexistence approach - a method for quantitative reconstructions of Tertiary terrestrial paleoclimate data using plant fossils. - Palaeogeography, Palaeoclimatology, Palaeoecology, **134**: 61-86.

Parlange, J.-Y. & Waggoner, P. E. (1970): Stomatal dimensions and resistance to diffusion. - Plant Physiology, **46**: 337-342.

Poole, I., Lawson, T., Weyers, J. D. B. & Raven, J. A. (2000): Effect of elevated CO_2 on the stomatal distribution and leaf physiology of *Alnus glutinosa*. - New Phytologist, **145**: 511-521.

Poole, I., Weyers, J. D. B., Lawson, T. & Raven, J. A. (1996): Variations in stomatal density and index: Implications for paleoclimatic reconstructions. - Plant, Cell and Environment, **19**: 705-712.

Sturm, M. (1971): Die eozäne Flora von Messel bei Darmstadt. I. Lauraceae. - Palaeontographica B, **134**: 1-60.

Traiser, C., Klotz, S., Uhl, D. & Mosbrugger, V. (2005): Environmental signals from leaves - a physiognomic analysis of European vegetation. - New Phytologist, **166**: 465-484.

Utescher, T. & Mosbrugger, V. (2010): Palaeoflora - Data base for palaeoclimate reconstructions using the Coexistence Approach; www.palaeoflora.de.

Wilde, V. (1989): Untersuchungen zur Systematik der Blattreste aus dem Mitteleozän der Grube Messel bei Darmstadt (Hessen, Bundesrepublik Deutschland). - Courier Forschungsinstitut Senckenberg, **115**: 1-213.

— (2004): Aktuelle Übersicht zur Flora aus dem mitteleozänen "Ölschiefer" der Grube Messel bei Darmstadt (Hessen, Deutschland): Courier Forschungsinstitut Senckenberg, **252**: 109-114.

Wilf, P. (1997): When are leaves good thermometers? A new case for Leaf Margin Analysis. - Paleobiology, **23**: 373-390.

Wing, S. L. & Greenwood, D. R. (1993): Fossils and fossil climate: the case for equable continental interiors in the Eocene. - Philosophical Transactions of the Royal Society of London B, **341**: 243-252.

3.5 Addresses of the Authors

(in alphabetical order)

Michaela Grein
University of Tübingen, Institute for Geosciences
Sigwartstr. 10
72076 Tübingen, Germany
Email: michaela.grein@uni-tuebingen.de

and

State Museum of Natural History Stuttgart
Section Palaeontology
Rosenstein 1
70191 Stuttgart, Germany
Email: michaela.grein@smns-bw.de

Wilfried Konrad
University of Tübingen, Institute for Geosciences
Sigwartstr. 10
72076 Tübingen, Germany
Email: wilfried.konrad@uni-tuebingen.de

Anita Roth-Nebelsick
State Museum of Natural History Stuttgart
Section Palaeontology
Rosenstein 1
70191 Stuttgart, Germany
Email: anita.rothnebelsick@smns-bw.de

Torsten Utescher
Bonn University, Steinmann Institute
Geological Department
Nussallee 8
53115 Bonn, Germany
Email: utescher@geo.uni-bonn.de

Volker Wilde
Senckenberg Forschungsinstitut und Naturmuseum
Sektion Paläobotanik
Senckenberganlage 25
60325 Frankfurt am Main, Germany
Email: volker.wilde@senckenberg.de

4 Plates

Plate 1:

fossil *Laurophyllum lanigeroides* (ENGELHARDT 1922) WILDE 1989 & extant Lauraceae

1. *Laurophyllum lanigeroides* (fossil): Leaf with feeding damage and sample area for cuticle preparations in the basal region. SM.B.-Me 23847. - Scale: 1 cm
2. *Laurophyllum lanigeroides* (fossil): Interior view on the lower cuticle (SEM). SM.B.-Me 12668. - Scale: 10 μm
3. *Laurophyllum lanigeroides* (fossil): Cuticle slide preparation from the lower epidermis with stomata (Light microscope). SM.B.-Me 23643. - Scale: 50 μm
4. *Laurus nobilis* (extant): Cuticle slide preparation from the lower epidermis with stomata (Light microscope). - Scale: 50 μm
5. *Laurus azorica* (extant): Lower cuticle with stomata (SEM). - Scale: 10 μm
6. *Cryptocarya* sp. (extant): Cuticle slide preparation from the lower epidermis with stomata (Light microscope). - Scale: 100 μm

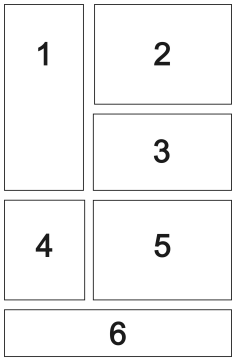

Plate 1

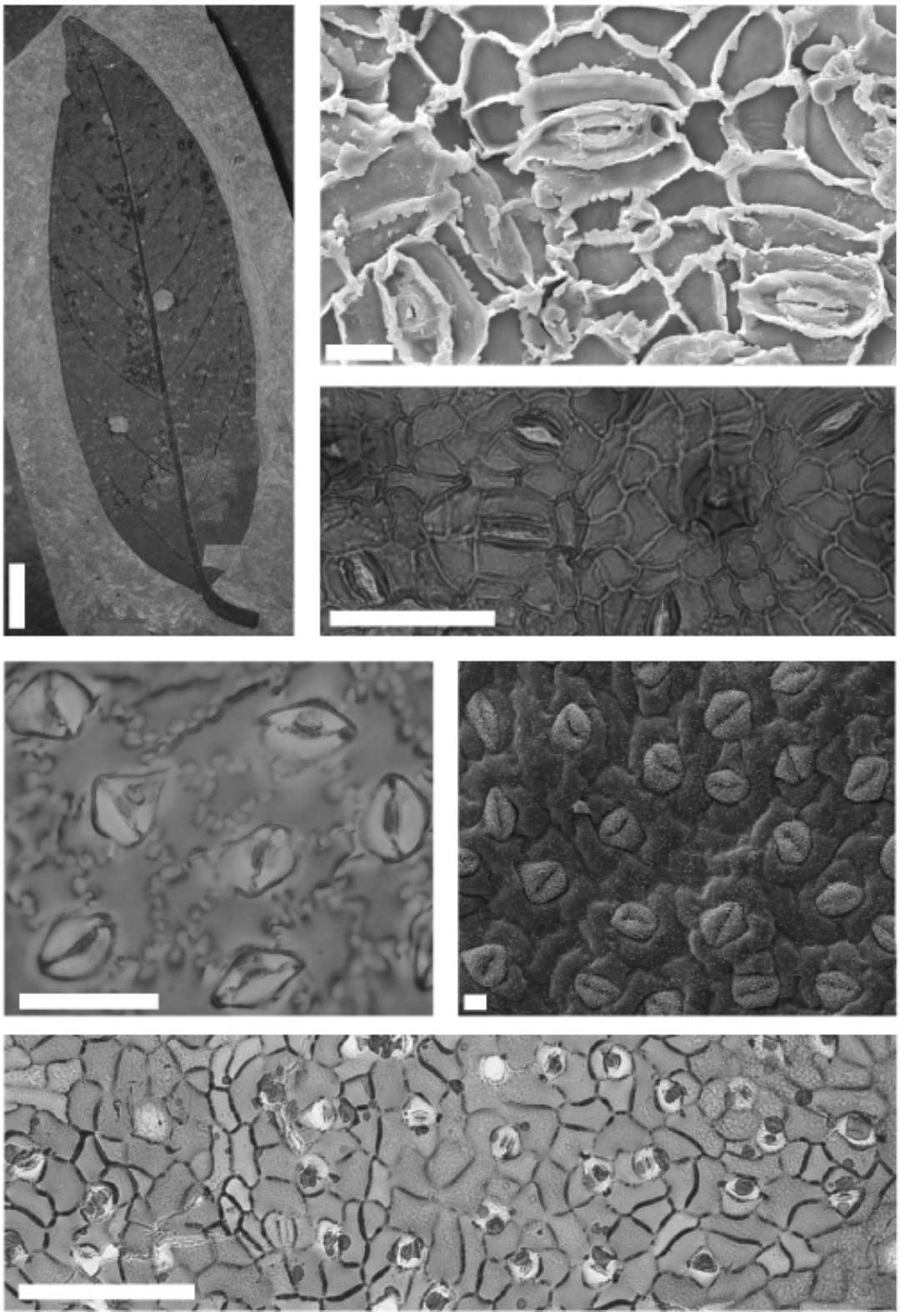

Plate 2:

fossil *Daphnogene crebrigranosa* (STURM 1971) WILDE 1989 & extant Lauraceae

1. *Daphnogene crebrigranosa* (fossil): Leaf with sample area for cuticle preparations in the apical region. SM.B.-Me 23832. - Scale: 1 cm
2. *Daphnogene crebrigranosa* (fossil): Interior view on the lower cuticle (SEM). SM.B.-Me 9611. - Scale: 10 μm
3. *Daphnogene crebrigranosa* (fossil): Cuticle slide preparation from the lower epidermis (Light microscope). SM.B.-Me 17165. - Scale: 100 μm
4. *Cinnamomum camphora* (extant): Cuticle slide preparation from the lower epidermis (Light microscope). - Scale: 50 μm
5. *Cinnamomum camphora* (extant): Lower cuticle with stomata (SEM). - Scale: 10 μm
6. *Ocotea foetens* (herbarium material from 2001): Epidermal impression of the lower epidermis (produced with Marabu-Fixogum) (Light microscope). - Scale: 100 μm

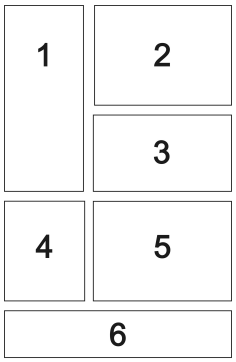

Plate 2

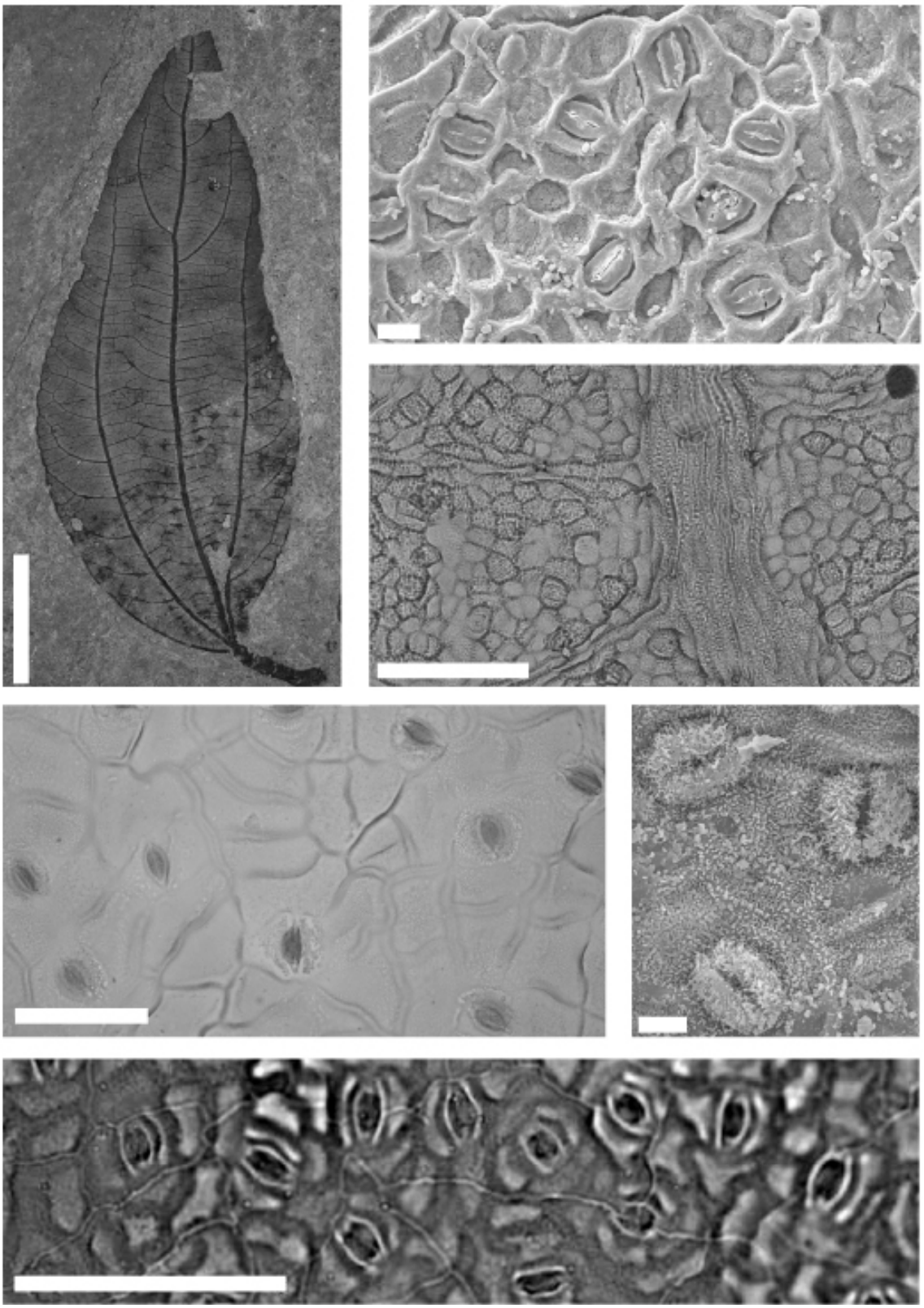

Plate 3:

fossil *Rhodomyrtophyllum sinuatum* (BANDULSKA 1923) WALTHER ex MAI & WALTHER 1985 & extant Myrtaceae

1. *Rhodomyrtophyllum sinuatum* (fossil): Leaf with sample areas for cuticle preparations in the basal, central and apical region. SM.B.-Me 23633. - Scale: 1 cm
2. *Rhodomyrtophyllum sinuatum* (fossil): Interior view on the lower cuticle (SEM). SM.B.-Me 23835. - Scale: 10 μm
3. *Rhodomyrtophyllum sinuatum* (fossil): Cuticle slide preparation from the lower epidermis (Light microscope). SM.B.-Me 23637. - Scale: 50 μm
4. *Syzygium jambos* (extant): Cuticle slide preparation from the lower epidermis (Light microscope). - Scale: 50 μm
5. *Psidium littorale* (extant): Lower cuticle with stomata (SEM). - Scale: 10 μm
6. *Syzygium paniculatum* (extant): Cuticle slide preparation from the lower epidermis (Light microscope). - Scale: 100 μm

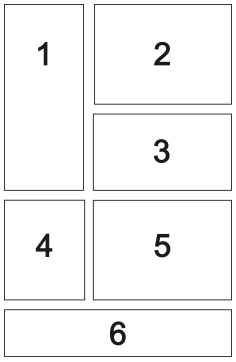

Plate 3

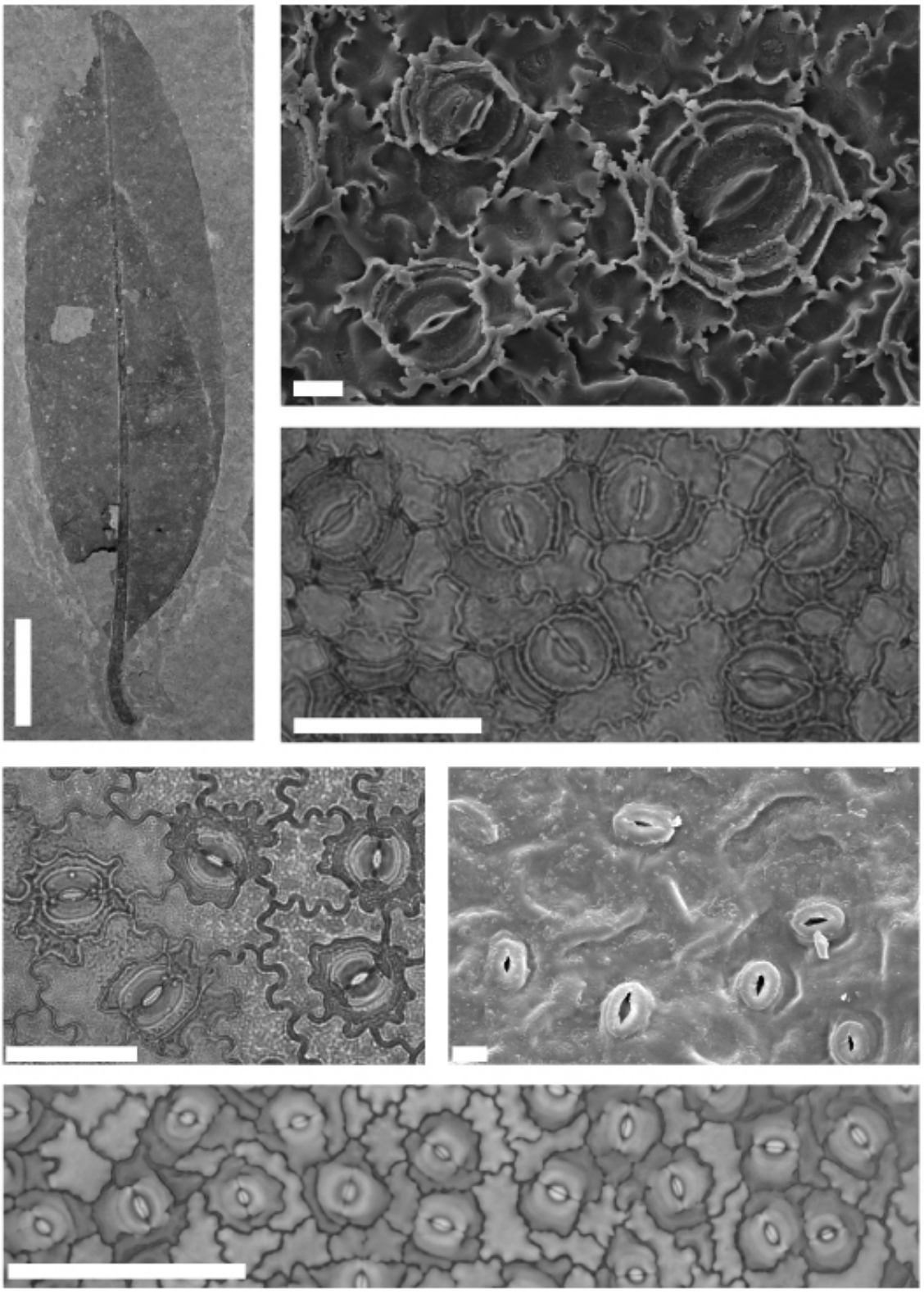

5 Danksagungen

An dieser Stelle möchte ich mich zuerst sehr herzlich bei meiner Betreuerin Anita Roth-Nebelsick (Staatliches Museum für Naturkunde Stuttgart) bedanken, die mit ihrem Fachwissen, ihrer konstruktiven Kritik und ihrer Begeisterung für dieses Thema sehr viel zum Gelingen dieser Arbeit beigetragen hat. Auch Volker Wilde (Senckenberg Forschungsinstitut und Naturmuseum, Frankfurt am Main) danke ich sehr herzlich für seine wertvolle Unterstützung insbesondere bei der Bestimmung und Bearbeitung der fossilen Blätter aus der Grube Messel und für die freundliche Übernahme des Koreferats.

Ganz besonders möchte ich mich bei Torsten Utescher (Universität Bonn) und Wilfried Konrad (Universität Tübingen) für ihre tatkräftige Unterstützung bei den paläoklimatischen Rekonstruktionen und den CO_2-Modellierungen bedanken.

Ein Wort des Dankes richte ich auch an die Leiterin der Forschungstation Grube Messel, Sonja Wedmann, die mir während meiner "Laboraufenthalte" in Frankfurt eine Unterkunft im "Messelhaus" gewährte, was meine Arbeit sehr viel angenehmer und effizienter machte. Darüberhinaus bedanke ich mich sehr herzlich beim gesamten Team der Forschungsstation, insbesondere bei Uta Kiel, Michael Ackermann, Marion Groppo und Bruno Behr, die mir während der Grabung im Sommer 2007 eine beeindruckende Einsicht in ihre Arbeit und den Grabungsalltag in der Grube Messel gewährten.

Ein herzliches Dankeschön richte ich auch an die technischen Assistenten vom Senckenberg Forschungsinstitut und Naturmuseum (Frankfurt a. M.) Karin Schmidt, die mich in die Präparation von fossilen Blattkutikeln im Allgemeinen und in den sicheren Umgang mit Flusssäure und anderen "netten" Chemikalien im Besonderen einführte und Martin Müller, der die fossilen Blätter für diese Arbeit freipräparierte und mir so eine zügige Weiterbearbeitung und Auswertung ermöglichte.

Auch Johanna Eder, Mike Thiv und Thomas Jossberger danke ich sehr herzlich für ihre Unterstützung und dafür, dass sie mir unkomplizierten Zugang zu den Sammlungen im Herbarium des Staatlichen Museums für Naturkunde Stuttgart ermöglichten.

Ich danke Rüdiger Hampp, Maren Babbick sowie dem gesamten Team des Botanischen Gartens Tübingen für ihre Unterstützung und auch bei den Mitarbeitern der botanischen Gärten von München, Heidelberg und Berlin-Dahlem möchte ich mich an dieser Stelle herzlich für ihre Kooperation bedanken.

Bernd Steinhilber vom Geochemischen Zentrallabor (Lehrstuhl für Geochemie, Universität Tübingen) danke ich für die zahlreichen Kohlenstoffisotopenmessungen.

Darüberhinaus hatten viele weitere Menschen mit ihren Anregungen und Ideen Anteil am Gelingen dieser Arbeit: Zu ihnen gehören James “Jimmy” Nebelsick, Hartmut Schulz, Christopher Traiser (alle Universität Tübingen), Thomas Tütken (Universität Bonn), Thomas Bach (Urweltmuseum Geoskop) sowie meine (nicht nur) Kollegen Jasmin Schöneberger, Juliane Hinz, Birgit & David Storz, Tatiana Miranda und Martin Ebner.

Der Landesgraduiertenförderung Baden-Württemberg sowie Anita Roth-Nebelsick danke ich für die Finanzierung dieses Projekts.

Abschließend möchte ich mich noch aus tiefstem Herzen bei meiner Familie bedanken ohne deren Liebe, Geduld und Unterstützung mein Studium und diese Arbeit nicht möglich gewesen wären. Ein ganz besonderer Dank geht dabei an meine Eltern und Schwestern, die mich stets aufbauten und mir den Rücken frei hielten, wenn es mal nicht so gut lief. Vielen Dank für euer Vertrauen!

Native laurel forest on Tenerife (Canary Islands, Spain): Anaga massif (top left) and Teno massif (top right). Leaves and flowers of the Lauraceae *Laurus novocanariensis* (bottom). Photos by M. Grein.

6 Bildungsgang

26.12.1980	geboren in Tübingen
1987 - 2000	Bästenhardt-Grundschule und Quenstedt-Gymnasium in Mössingen
2000 - 2006	Studium der Geowissenschaften an der Eberhard-Karls Universität in Tübingen und Abschluss als Diplom-Geologin mit Vertiefungsrichtung Biogeologie/Paläontologie
	Studienarbeit: *Palynologische Untersuchung eines Fließgewässers (Steinlach) im Kreis Tübingen* am Institut für Geowissenschaften der Universität Tübingen betreut von Prof. Dr. Dr. h. c. Volker Mosbrugger
	Diplomarbeit: *Erprobung eines mechanistischen Modells zur Rekonstruktion des atmosphärischen CO_2-Gehalts mit den Stomatadichten von vier Fagaceen-Arten* am Institut für Geowissenschaften der Universität Tübingen betreut von PD Dr. Anita Roth-Nebelsick
2006 - 2010	Dissertation zum Thema *Reconstruction of atmospheric CO_2 and climate of the middle Eocene based on fossil plants from the Messel Formation* am Institut für Geowissenschaften der Universität Tübingen bei PD Dr. Anita Roth-Nebelsick